

Crystals for quartz resonators

J. C. Brice

Philips Research Laboratories, Redhill, Surrey RH1 5HA, England

This paper briefly describes the hydrothermal growth process and then discusses the important defects in quartz (twins, inclusions, dislocations, and impurities) and the correlations among them. The properties of quartz are reviewed and tabulated under the headings of intrinsic properties and defect-related properties. Resonator theory and fabrication techniques are outlined, with particular reference to aspects related to defects in the crystals. At this stage, it is possible to list the circuit design factors which must be taken into account when the application calls for very high performance. The paper then looks at the approach of a device maker faced with problems caused by impurities, inclusions, dislocations, and other nonideal properties of real crystals. This question leads to a specification of the crystals suitable for device use. The major parameter of this specification is the infrared Q , which must exceed about 1.8 million for satisfactory performance and yield. Acceptance test procedures are discussed, and finally the present state of the subject and the future prospects are briefly described.

CONTENTS

I. Introduction	105	VIII. Conclusions	144
II. The Growth of Quartz Crystals	106	Acknowledgments	145
A. The hydrothermal growth process	106	References	145
B. Relevant growth theory	107		
III. Defects in Quartz Crystals	108		
A. Gross defects	108		
B. Dislocations	109		
C. Impurities	109		
D. Relations between defects	111		
1. Dislocation densities and inclusions	111		
2. Dislocation densities and hydrogen content or Q	112		
3. Impurity concentrations and Q	114		
4. Strength and Q	114		
5. Hardness and Q or dislocation density	115		
6. Uniformity and Q	115		
7. Summary	116		
IV. The Properties of Quartz	116		
A. Intrinsic properties	117		
1. Structural and thermodynamic data	117		
2. Elastic constants	119		
3. Piezoelectric constants	121		
4. Dielectric constants	123		
B. Defect-related properties	124		
1. Lattice parameters and related properties	124		
2. Optical properties	125		
V. Basic Device Theory	125		
A. General aspects	125		
B. The AT cut	127		
C. Other cuts	129		
VI. Device Construction	130		
A. Blank preparation	130		
1. X-ray orientation	130		
2. Cutting	132		
3. Lapping	132		
4. Etching	134		
B. Electrodes	135		
C. Mounting and encapsulation	135		
D. Manufacturer's and user's responsibilities	135		
VII. The Results Obtained Using Real Crystals	138		
A. The measurement of infrared Q	138		
B. Device properties affected by Q	140		
C. The effect of impurities	142		
D. The effect of inclusions	142		
E. The effect of dislocations	142		
F. Other parameters affecting devices	143		
G. The selection of suitable material	143		

I. INTRODUCTION

Quartz resonators are widely used in timing devices and in circuits which generate or filter radio frequency signals. The high electrical quality factor, Q_e ,¹ and great stability of such resonators make them almost irreplaceable. Without them the widespread use of mobile radio and high-quality color television would not be possible, telephone systems would be more cumbersome, and accurate clocks and watches would be much more expensive. By current standards these applications in general call for easily met specifications: single devices or monolithic arrays of devices with fractional frequency deviations of ± 5 to 20 parts in 10^6 (ppm) over a temperature range of -20°C to $+70^\circ\text{C}$ and device Q_e 's of $< 10^5$ are usually adequate. Broadcasting and professional telecommunications (particularly in military applications) generate much more onerous specifications: maximum frequency deviations of much less than 1 ppm are commonly requested. For some applications, e.g., satellite navigation, deviations of < 0.01 ppm are called for, and measurement systems need even greater accuracy, e.g., frequency deviations of < 1 in 10^9 (1 ppb) or even < 1 in 10^{10} .

¹I use Q_e here for the electrical quality factor, because in the field of quartz for piezoelectric devices the symbol Q is universally used to denote the infrared quality factor which is the value of Q_e for a carefully specified and fabricated device operating in a particular way (see Sec. VII.A). For almost all devices Q_e is less than the Q of the material. There is, of course, a third quality factor, Q_m , which describes the mechanical performance of a device. Q_m is small compared to the other quality factors: quartz has a significant elastic viscosity (see Sec. IV.B, Table XXVI).

It is still not easy to meet all these specifications, and there is a gap between what can be achieved occasionally in research and what is regularly available commercially at a reasonable price.

Cady (1922) gives the first published data about quartz resonators. For further historical information, see Hol-lom (1981) and Heising (1946).

This paper looks at the problems caused by the imperfect character of available crystals and reveals why device makers have pressed crystal producers to make more nearly ideal crystals. In order to develop these ideas in a coherent manner, it is necessary to give a considerable amount of background information. Thus the next sections consider in turn crystal growth (both practically and as far as necessary theoretically), the defects that can exist in quartz, the properties of quartz (some of which depend on defects), device theory (in outline only), and device construction, and then in more detail looks at the results of using real crystals. Finally, in the conclusions section, the present state and future prospects are summarized.

The aim is to give a readable account of a complex subject. Some aspects have not yet been explored as thoroughly as is desirable. Since device properties can be correlated with several variables which are themselves interdependent, time may reveal defects in some of the conclusions. However, the current state is one in which we can say with confidence that quartz to the specification suggested in Sec. VII.F will make high-quality devices with excellent yields, so that even if some of the arguments are found to be false, the conclusions given should have some lasting value.

II. THE GROWTH OF QUARTZ CRYSTALS

A. The hydrothermal growth process

The hydrothermal growth process is a technique for growing crystals from a solution near or above its critical temperature. Essentially, the method involves dissolving a nutrient of natural quartz chips at a high temperature. The saturated solution so produced moves by convection to a cooler region where it is supersaturated. To relieve this supersaturation the solution deposits quartz onto seed crystals. High temperatures ($> 300^{\circ}\text{C}$) are necessary to ensure adequate solubility even when mineralizers are added to increase the solubility. Typical solutions for the growth of quartz are between about $0.5M$ and $1M$ (i.e., they contain between 0.5 and 1 mole per liter) NaOH or Na_2CO_3 . It is believed that natural quartz also grows from aqueous solution but at much smaller rates.

Crystal growth occurs only when the growth solution is supersaturated. For natural quartz, this supersaturation is probably created by cooling over geological time intervals. For the growth of synthetic quartz, the necessary conditions are produced in a steel autoclave. See Fig. 1. Small (5- to 6-mm) chips of quartz are placed in a basket filling the lower 40% of the autoclave, and suitably oriented seed crystals are held in clips in the upper por-

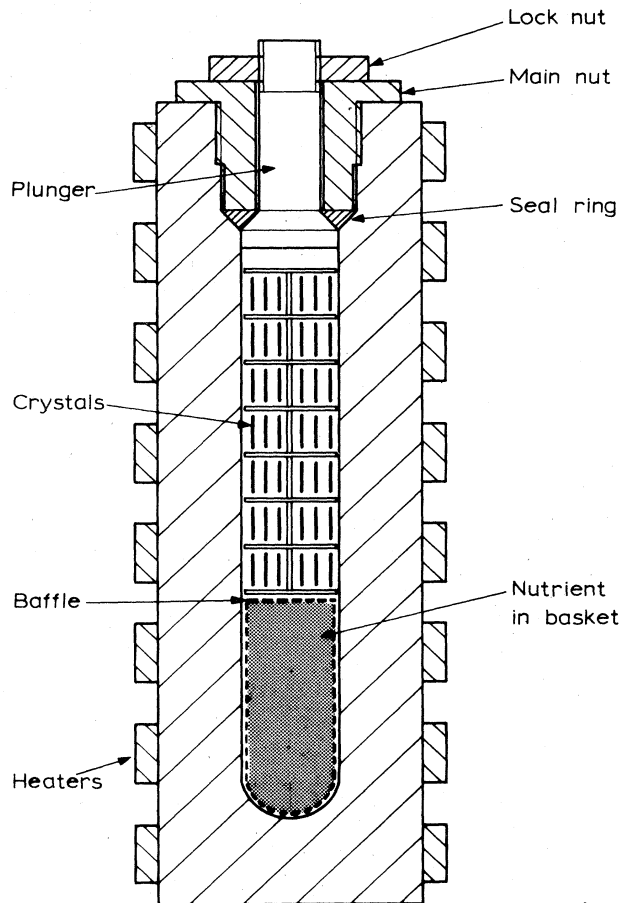


FIG. 1. A schematic drawing of an autoclave for the hydrothermal growth of quartz. Note that different vertical and horizontal scales have been used: typically the height of a system is 18 times its internal diameter. In the most recent autoclaves heights can be up to 8 m.

tion. The autoclave is filled with water so that roughly 80% of the volume is filled and the system is sealed. Power is supplied to the heaters so that the lower portion of the vessel reaches about 400°C and the upper portion about 350°C . A baffle with 5–10% opening helps to maintain the temperature difference.

As the temperature is raised, the liquid expands to fill the autoclave at some temperature below the critical point (375°C for pure water). At the temperatures mentioned previously, the pressure often exceeds 1000 bars. (The pressure depends on the actual temperature and fraction filled with water.) When NaOH is used as the mineralizer, pressures up to 2000 bars are used. When Na_2CO_3 is the mineralizer, lower pressures are adequate.

Apparatus for growth is usually bought from specialist suppliers who produce autoclaves of up to about 50 cm internal diameter. External diameters are usually 1.8–2.5 times the internal diameter, and the length is usually 10–20 times the internal diameter.

Apparatus for growth is discussed by Laudise and Nielsen (1961). Rudd and Lias (1967) discuss production

equipment. For a survey of recent equipment see Lias *et al.* (1973) and Key *et al.* (1974) (both these papers discuss problems with constructional materials). A series of reports by Nagai and Asahara (Toyo 1977,1979,1980) gives a fascinating account of the development and performance of large autoclaves.

One practical point worth mentioning is that all commercial autoclaves are constructed of steel, which is protected from attack by a self-renewing layer possibly of acmite ($\text{Na}_2\text{O}\cdot\text{Fe}_3\text{O}_4\cdot 4\text{SiO}_2$). Inclusions of silicates are occasionally found in synthetic quartz but as shown in the next section the iron content of synthetic quartz is usually negligible. Systematic studies of impurity effects have been made by Flickstein and Schieber (1971,1974) and Yamashita *et al.* (1975), concluding in general that almost all impurities are undesirable. Thus V, Ga, Mg, Ge, and Zn slow down the growth. Fe, Al, and Mg cause inclusion formation. Zn, K, and Rb increase the considerations of undesired impurities and Al and Fe degrade the properties of the crystals. From the data in Secs. III.C and VII.B it seems that avoiding significant amounts of these impurities is not especially difficult, but some research workers use small autoclaves with noble-metal liners and for some critical applications swept quartz (which has been subjected to solid-state electrolysis) is used. See, for example, Young *et al.* (1978), Euler *et al.* (1978), and the references they quote.

B. Relevant growth theory

There exists a considerable body of literature providing at least a semiquantitative understanding of the processes involved in crystal growth—see, for example, Brice (1973,1977), Wilke (1973), Rosenberger (1979), and Pampalin (1980). Studies of the growth of quartz are described or reviewed by Laudise and Nielsen (1961), Ballman and Laudise (1963), Rudd and Lias (1967), Laudise (1970), and James and Kell (1975). For the purposes of this paper we need only a qualitative understanding of the processes involved. The main theoretical conclusions relevant to our purpose can be stated as follows.

(a) It is possible to distinguish two main types of faces on crystals. Singular faces are usually the natural faces of a crystal and correspond to sharp (cusp-shaped) minima in a plot of surface free energy against crystallographic direction. For quartz the main singular faces are usually labeled z , y , m , X^+ , and X^- , corresponding to (1011), (1011), (1010), (2110), and (2110) in the conventional labeling [see the recommended conventions (IRE, 1949)]. Singular faces can be subdivided into two classes: perfect and imperfect. Imperfect faces are those intersected by a screw dislocation or, if we are loose in our definition of a crystal, by a twin plane. All faces which are not singular are called rough, because on an atomic scale they are not flat. Singular faces are atomically smooth (if we neglect the occasional steps which occur on real crystals). The important rough face is Z (0001).

(b) For growth to occur the growth medium must be supersaturated with respect to the material being grown.

For hydrothermal growth at a temperature T with the nutrient zone at a temperature $T + \Delta T$, the supersaturation is essentially a linear function of ΔT for any given T . Under all likely conditions for hydrothermal growth the growth rate f is a monotonically increasing function of ΔT . (Increasing T , the pressure, or in some cases the opening in the baffle, increases f .)

(c) Rough faces grow by the random addition of atoms or molecules at any suitable site. This gives a linear growth law with $f \sim \Delta T$ when other conditions are constant. On imperfect singular faces growth proceeds by the addition of atoms or molecules at the step created by the screw dislocation or twin plane. These steps are self-renewing. The resulting growth rate is slower than growth on a rough face. On a perfect singular face, growth requires the deposition of a nucleus which expands either to cover the face or until it meets the growth originating at another nucleation site. The growth rate on a perfect singular face is usually extremely small. See Table I. The Z face is the only rough face. The y and m faces are usually dislocation free and are therefore likely to be perfect singular faces. The other faces are usually imperfect singular faces. At very large growth rates the rate-limiting process is diffusion in the fluid phase. Large concentration gradients can be established at the growth face with the result that any projection on the face grows more rapidly than the rest of the face. This makes the growth unstable and solution can become trapped between projections. The halo of inclusions around the seed crystal in some crystals (see Sec. III.A) is usually attributed to unstable rapid growth at the beginning of a growth run.

(d) While growth normal to a singular face is slower than on a rough face, the rate of step advance across a singular face is very rapid. Thus while on a rough face an impurity atom on the growth face can be desorbed, one on a singular face is much less likely to be desorbed. Thus impurity segregation coefficients on singular faces are larger than on rough faces. Segregation coefficients are the ratios of impurity concentration in the crystal to that in the growth fluid. Thus material grown on the X^+ face contains about 3 times as much hydrogen, 10 times as much aluminum, and 15 times as much germanium as

TABLE I. Typical relative rates of growth. Here growth on the Z face is assumed to occur at unit rate. Note that growth from NaOH is several times faster than from Na_2CO_3 . Changing growth parameters (ΔT , T , pressure, mineralizer concentration, etc.) can result in up to 50% variations from these ratios. The data used to construct this table can mostly be found in the references quoted in Sec. II.A.

Face	Mineralizer	
	Na_2CO_3	NaOH
$Z(0001)$	1	1
$z(1011)$	0.4	0.6
$r(1011)$	0.05	0.03
$X^+(2110)$	0.6	0.3
$X^-(2110)$	0.4	0.1
$m(1010)$	0	0.04

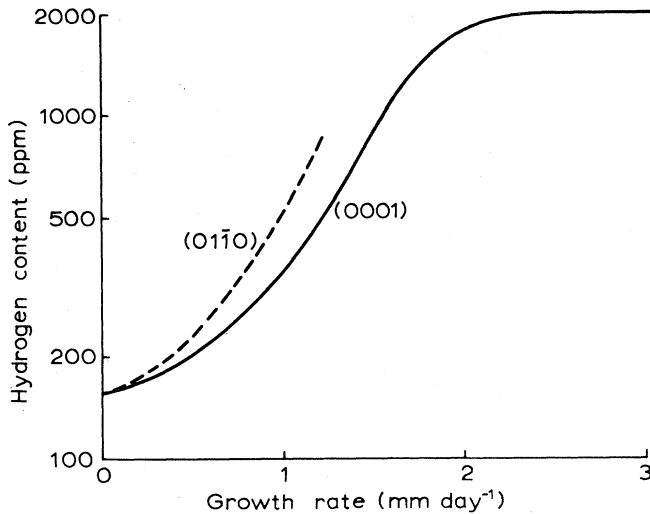


FIG. 2. Hydrogen content (in atomic ppm relative to silicon) as a function of growth rate on a rough face (0001) and a singular face (0110). Most other impurities should behave in the same way. The data given are typical for growth at 350 °C.

material grown on *Z* faces of the same crystal. Therefore, in any critical application only material grown on the *Z* faces is used. (Further data are given in Sec. III.D.)

(e) Most segregation coefficients are less than 1: incorporating an impurity almost always involves distorting either the bonding or the lattice positions and the energy of distortion increases the free energy of the crystal with respect to unstrained material [see Brice (1975) for a quantitative description]. Since segregation coefficients are usually less than 1, the growth face rejects impurity and the fluid at the growth face becomes enriched by an amount which increases with the growth rate. Thus with a constant impurity concentration in the bulk of the fluid, faster growth causes an increase in the impurity concentration in the crystal.

From the data presented later, it will become clear that hydrogen (probably incorporated as hydroxyl ions) is the major impurity in quartz. Thus from the arguments given above, we expect the hydrogen content to increase with growth rate. Figure 2 demonstrates this effect and also shows that growth on a rough face [(0001)] results in less incorporation than growth on a singular face [(0110)]. Note that we can take hydrogen as a typical impurity and can expect other impurities to behave in the same qualitative way. Thus if the growth conditions yield a large hydrogen content, we expect large contents of other impurities. We shall see that on a statistical basis this occurs.

III. DEFECTS IN QUARTZ CRYSTALS

A. Gross defects

Two- and three-dimensional defects are discussed in this section. In synthetic quartz these defects are usually

obvious to the naked eye.

Almost all crystals have a veil of inclusions around the seed crystal. In some cases this veil is very prominent and the seed portion may fall out of slices cut from such crystals. Normally the seed portion of a slice is not used to make devices, and it is reasonable to recommend that this region should never be used. However, as discussed in Sec. III.B, a prominent seed veil can imply a high dislocation density and brittleness. The inclusions around the seed are the results of rapid initial growth and were probably originally full of solvent.

Outside the seed veil occasional inclusions are found. These can be of the original solvent-filled type, or the inclusion can be a speck of acmite (from the autoclave wall). Very occasionally other solids are found, presumably insoluble matter introduced with the nutrient when the autoclave was loaded. Work within Philips and elsewhere (Toyo, 1975) suggests that inclusions in the *Z* zone (i.e., material grown on the *Z* face) have a roughly constant size distribution. See Table II. If there are N inclusions of a given size in unit volume, then simplistic arguments suggest that in a volume V (for example, the active region of a device), the probability of finding no inclusions is $1 - NV$. However, a more refined argument shows that of all the possible volumes of size V , some contain more than one inclusion, so that in a set of volumes cut from a crystal, the yield of inclusion-free samples is actually $\exp(-NV)$. For NV about unity, the difference in yield is important. Similarly, we can evaluate the yield of samples with surface area A in which no inclusions intersect the surface. This yield is $\exp(-A \int ND dD)$, where the integral is taken over the size range of interest and N is the volume concentration of inclusions with size D . This relation has uses in surface-wave devices which have transducers composed of interlaced sets of fingers. In these devices the pit left by an inclusion might cause a break in the finger (with a width of perhaps a few μm). In this case the lower limit of the integral could be, say, half the finger width.

Two types of sheet defects occur commonly in natural quartz. Boundaries between left- and right-handed quartz are often seen. The defect, called a Brazil twin, corresponds to a reflection across a $\{1120\}$ face. The other

TABLE II. Relative concentrations of inclusions of various sizes. Relative concentrations vary by $\pm 30\%$. A typical useful crystal contains 30 inclusions in the 1- to 10- μm range, 6 in the 10- to 30- μm range, and perhaps 1 with dimensions over 30 μm in each cubic centimeter.

Size (μm)	Relative concentration
> 100	1
70–100	5
30–70	12
10–30	60
1–10	300

twin type, a Dauphiné twin, corresponds to a rotation of 180° about the c axis. Such twins can be created and moved by mechanical and thermal stresses (Anderson *et al.*, 1976). The other sheet-type defect is caused by the intergrowth of two crystals forming one or more grain boundaries. In synthetic quartz, homogeneous nucleation or nucleation on insoluble particles in the growth solution can result in the presence of small crystallites which can come to rest on the face of a growing crystal.

All these sheet-type defects are uncommon in synthetic quartz. Certainly, less than 1% of boules sold show them. They are usually revealed by the presence of grooves on the natural faces of the crystal. (Remember in this context that the Z face, which is usually grooved and which may have a cobblestone structure, is not a natural face.) Crystals with sheet defects should not be used, and the possibility of Dauphiné twinning caused by mechanical and thermal stresses should be remembered when designing production processes.

Examination of the internal structure of synthetic crystals frequently shows sector boundaries between material grown on different faces. See Fig. 3. Such boundaries should not cross the active region of any device, and as shown elsewhere the zones other than Z tend to be dirty and the sector boundaries are appreciably strained. Normal practice is to use only material grown on a Z face.

B. Dislocations

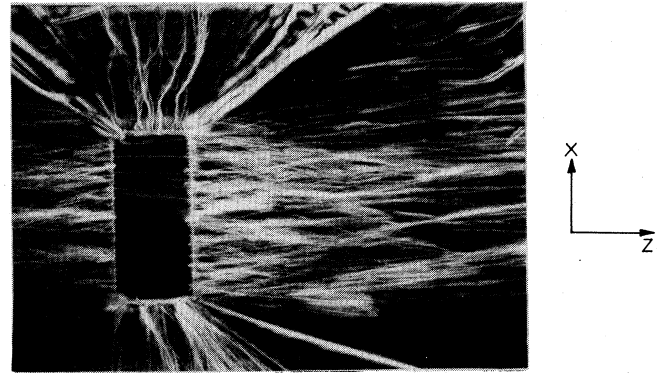
X-ray topographic studies by Takagi *et al.* (1974), Lang and Miuscov (1967), Homma and Iwata (1973), and others show that dislocations exist in α quartz and mostly lie normal to the growth face of the zone being examined. Klapper (1972,1975) shows that this orientation is in general favored, since it minimizes the elastic energy of the dislocation. McLaren *et al.* (1971) show that three types of dislocations are common:

screw dislocations: $b = c[0001]$, i.e., with axes perpendicular to c ;

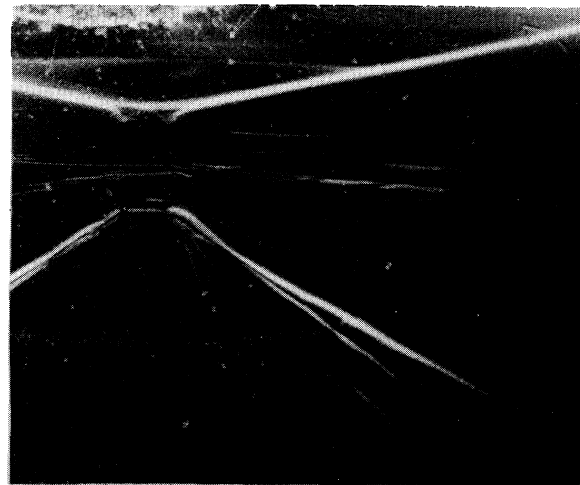
edge dislocations: $b = \langle 1210 \rangle$, i.e., with axes parallel to c ;

mixed dislocations: $b = (a + c)\langle 1123 \rangle$.

Here b is the Burgers vector. Since we are primarily interested in Z zone material, the dislocations of major importance are the edge type. Figure 3 shows x-ray topographs of sections perpendicular to Y in typical bad [Fig. 3(a)] and good [Fig. 3(b)] crystals. The crystal shown in Fig. 3(a) had an obvious seed veil, and it is clear that the dislocations originate mostly from the inclusions forming this veil. The crystal shown in Fig. 3(b) had a nearly invisible veil, and it is obvious that most dislocations are continuations of those in the seed. Other topographs, not reproduced here, show that both these effects are general and that in crystals without prominent veils the dislocation density depends almost entirely on the dislocation density in the seed. Thus with selected seeds,



(a)



(b)

FIG. 3. X-ray topographs of sections from two crystals. Note in (a) that the dislocations (white lines) originate from the included area around the seed.

dislocation-free crystals can be grown, as has been demonstrated by workers in the Bell organization and elsewhere.

McLaren *et al.* (1971) suggest a correlation between dislocation density and hydrogen content. Griggs (1974) has shown that the presence of hydrogen makes the dislocations mobile and able to multiply. Data given in Sec. III.D confirm the dislocation density correlation with hydrogen content.

C. Impurities

Table III gives typical ranges of impurity concentrations found in quartz. The table is based on analyses of about 50 natural quartz samples and 70 synthetic samples. Only the purest of these samples would be suitable for device use. Sections III.D, VII.B, and VII.F discuss actual results on crystals offered for device use and indicate which should be accepted.

TABLE III. Impurities in quartz (values in atomic ppm relative to Si). The concentration ranges given include roughly the central 67% of reported values. The maximum values are lowest estimates of the solid solubilities. Brown and Thomas (1960) suggest that 390 ppm is the maximum solid solubility for Na. Further data are given in Sec. III.D. The table is based on data from many sources, including unpublished analyses by G. Grainger and D. Hilton (Philips, Redhill).

Impurity	Typical concentration		Maximum concentration
	Synthetic	Natural	
H	250–2500	200–1200	15 000
Li	0.5–35	200–2000	8 000
Al	1–30	1000–4000	20 000
Na	0.1–15	100–300	390
Ca	0.1–2	30–100	1 000
K	0.03–2	<1	4
Fe	0.01–1	100–900	1 000
Ge	<0.1	100–900	1 000
Mg	<0.6	50–200	8 000

Impurities can either substitute for the main constituents or sit in interstitial sites. Interstitial atoms are particularly likely in quartz because of its open structure (see Sec. IV.A). Table IV gives what is known (or perhaps more accurately, inferred) about the position of various impurities in the lattice. Armed with these results, the ionic radii in oxides (Shannon and Prewitt, 1969), and a knowledge that the interstitial sites have radii of about 1.4 Å, one can construct Table V and deduce that most of the listed impurities could be interstitial. Indeed, the ionic radii marked (—) probably exclude substitutional sites which for anions and cations have radii of, respectively, 1.35 and 0.26 Å.

One reason for the interest in the sites occupied by impurities is that the position influences electrical and mechanical losses at high frequencies. The other reason is that interstitial species move more rapidly than substitutional ones. Both diffusion and electromigration are of interest. Table VI gives the activation energies for various species and directions which apply to electromigration and Table VII gives the same data for diffusion. Studies of electromigration have shown that in an electric field of 400–1000 V cm⁻¹ at 400°C to 500°C many im-

purities can migrate at rates of several mm h⁻¹. Migration of Na, Al, and Fe has been studied by Lushnikov and Khadzi (1967), of Ag by White (1968), and of Cu and Ag by Mortley (1969). Because quartz resonators have very large resistances (of order 10¹⁰ Ω is usual), they can—even with blocking capacitors (resistances of which can be 10⁹ Ω or less)—be exposed to significant fields (of order 100 V per cm of quartz). Thus electromigration which might change the mass distribution in the long term is a real possibility and electromigration effects are known (Filler *et al.*, 1984). Similarly, diffusion from electrodes or caused by strains must be considered. There are plausible suggestions that migration is quicker along dislocations which must also therefore be considered.

It should be noted that the rate of diffusion of hydrogen at room temperature appears to be large enough for significant out-diffusion to occur from relatively thick slices. Table VIII shows the values of the extinction coefficient at 3500 cm⁻¹ (which is proportional to hydrogen content) measured immediately after cutting (1972) and six years later (1978). Between measurements the slices were stored in a desk drawer.

TABLE IV. The positions of impurities in quartz. For further data see Dodd and Fraser (1965), King (1959), Passaret and Regreny (1974), Weil (1973), and papers given at the Symposium on Defect Structure of Quartz and Glassy Silica [J. Phys. Chem. Solids 13, 271 (1960)].

Impurity	Location
H	Probably present as OH on O sites but behaving as if it were interstitial, i.e., diffusing rapidly parallel to the <i>c</i> or <i>Z</i> axis.
Li, Na, K	Interstitial.
Al, Fe, Ga	For material grown on the <i>Z</i> face may be interstitial. For material grown on other faces (including natural crystals) may also be substitutional.
Ge	Substitutional to 5400 ppm. At higher concentrations probably also interstitial.

TABLE V. Effective ion sizes (Å).

Ion	Substitutional ^a	Interstitial ^b
O ²⁻	1.35	1.38
Si ⁴⁺	0.26	0.40
(OH) ¹⁻	1.48	1.52
Ge ⁴⁺	0.40	0.54
Al ³⁺	0.39	0.53
Fe ³⁺	0.49	0.55
Ga ³⁺	0.47	0.62
Mg ²⁺	0.49	0.72
Ca ²⁺	0.95(-)	1.00
Li ¹⁺	0.59(-)	0.74
Na ¹⁺	0.99(-)	1.02
K ¹⁺	1.33(-)	1.38
Cu ¹⁺	0.46	0.96
Ag ¹⁺	0.67(-)	1.15
Au ¹⁺	1.33(-)	1.37
Pt ⁴⁺		0.65
F ¹⁻	1.285	1.31

^aSubstitutional sites are twofold coordinated for anions and fourfold coordinated for cations.

^bInterstitial sites are fourfold coordinated for anions and sixfold coordinated for cations.

D. Relations between defects

1. Dislocation densities and inclusions

The topographs in Fig. 3 and many similar ones make it clear that inclusions act as nuclei for dislocations. Thus we expect and find that as the inclusion density rises the dislocation density also rises, and it is reasonable to suggest that most inclusions nucleate at least one dislocation. The inverse correlation does not hold: crystals can have low inclusion contents and large dislocation densities if the seeds are highly dislocated.

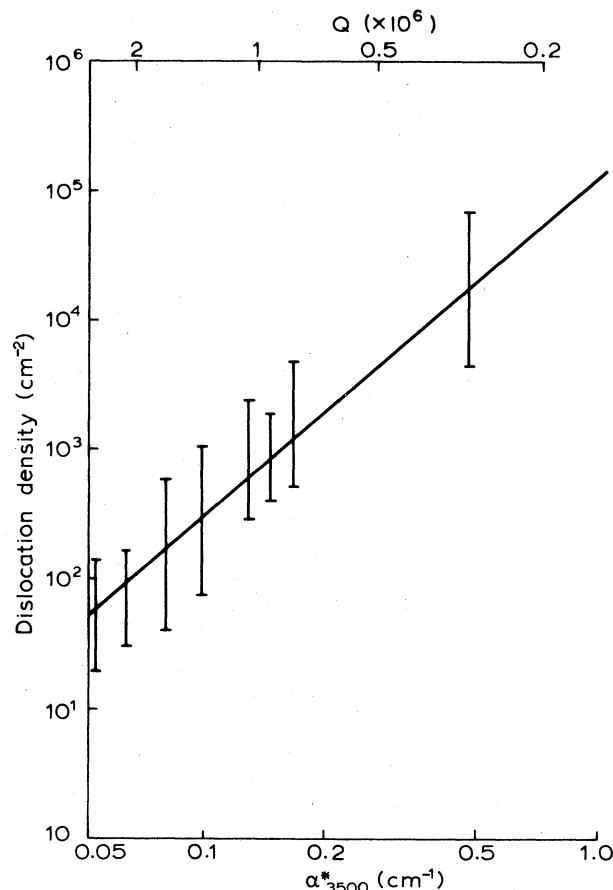


FIG. 4. The correlation between dislocation density and extinction coefficient α .

TABLE VI. Activation energies for electromigration. Column A is the total energy involved. Column B is the same less the energy of activation between the crystal and the source film.

Solute	Direction	Energy (kJ mol ⁻¹)	
		A	B
Li	c	82, ^a 81, ^b 78 ^d	67 ^c
Li	a		129 ^c
Na	c	96, ^a 94, ^b 98 ^d	75 ^d
Na	a		129 ^c
K	c	125 ^a	
Ag	c	80 ^c	92 ^d
native interstitial	c	150 ^f	
O or Si	a	171 ^f	
Au	c	145 ^g	
Pt	c	160 ^g	

^aVerhoogen (1952).

^bGibson and Vogel (1950).

^cSnow and Gibbs (1964).

^dMilne and Gibbs (1964).

^eWhite (1968).

^fVanfleet *et al.* (1963).

^gWenden (1957).

TABLE VII. Diffusion in quartz. We assume $D = D_0 \exp(-Q/kT)$.

Solute	Direction	D_0 (cm ² sec ⁻¹)	Q (kJ mol ⁻¹)
H ^a	<i>c</i>	7×10^{-2}	24
Na ^b	<i>c</i>	1.64×10^{-1}	72
Ca ^{2+b}	<i>c</i>	1×10^5	273
Na ^{+b}	<i>a</i>	2×10^2	165
Ag ^c	<i>c</i>		97
Cu ^c	<i>c</i>		113
O ^{2-d}		<i>c</i> $D = (3.0 \pm 1.5) \times 10^{-10}$ at 345°C	

^aSosin (1973).^bFrischat (1970).^cJ. C. Brice (unpublished).^dSawyer (1976).

2. Dislocation densities and hydrogen content or Q

The infrared absorption at various infrared frequencies including 3500 cm^{-1} is used to measure hydrogen content. Thus Fig. 4 suggests a correlation between hydrogen content and dislocation density (determined from x-ray topographs). The error bars indicate the range between the upper and lower quartiles. At any α value the logarithm of the dislocation density has a Gaussian distribution (see Fig. 5). The line on Fig. 4 can be represented by

$$\log_{10} N_D = 5.00 \pm 0.48 + 2.5 \log_{10} \alpha, \quad (1)$$

where N_D is the dislocation density (cm⁻²) and α is the absorption coefficient at 3500 cm^{-1} (in units of cm⁻¹).

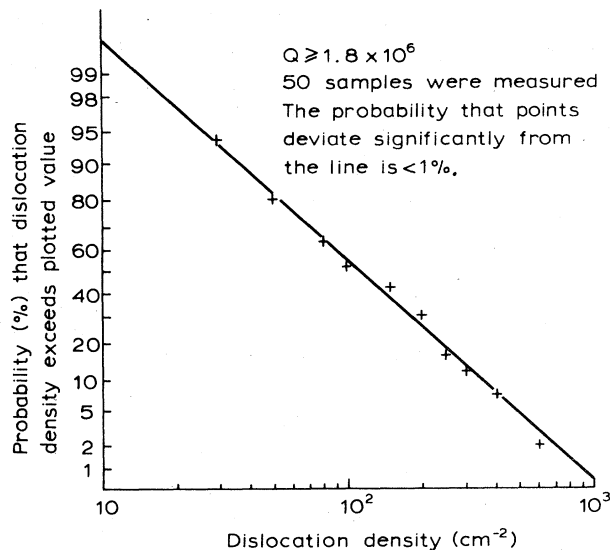


FIG. 5. A cumulative frequency diagram for dislocation densities of crystals from one supplier plotted on log-probability paper. The diagram proves that with 99% confidence the logarithm of the dislocation density has a normal (Gaussian) distribution. The data refer to samples with $\alpha = 0.043 \pm 0.007 \text{ cm}^{-1}$ ($Q = 2.0 \pm 0.2$ million).

However, this line represents the population of all the samples examined by my colleagues. If we look at similar plots for individual suppliers, we find that we can draw different lines, e.g.,

$$\log_{10} N_D = 4.75 \pm 0.26 + 2.5 \log_{10} \alpha \quad (2)$$

and

$$\log_{10} N_D = 5.36 \pm 0.20 + 2.5 \log_{10} \alpha \quad (3)$$

for two suppliers. Again at any Q value, $\log_{10} N_D$ has a Gaussian distribution, but these lines and the distributions that they represent are in a statistical sense significantly different from one another and from the overall distribution. Thus while for each supplier we can say that N_D increases with α in a way which allows us to predict N_D from α within a factor of about 2,² there is no unique relation between α and N_D . At a given α value, the dislocation densities for the two suppliers differ by a factor of 7.4 on average. Thus to explain the result we cannot invoke McLaren's (1971) suggestion of a direct relation between N_D and hydrogen content and instead must look at the suggestion by Griggs (1974) of easier dislocation movement as the hydrogen content rises and postulate that the conditions employed by the various suppliers involve different amounts of strain and hence different amounts of dislocation climb and multiplication. However, it is not easy to think of a process which gives

$$N_D \sim [\text{H}]^{2.5}, \quad (4)$$

where $[\text{H}]$ is the hydrogen content.

We shall later discuss the relation between α , and a commonly used quantity Q (the infrared quality factor of the quartz). For the present we can assume an empirical relation in which $Q \geq 2$ million implies $\alpha_{3500} \leq 0.06 \text{ cm}^{-1}$ or $[\text{H}] \leq 300$ ppm relative to silicon and a Q of 1 million corresponds to $\alpha_{3500} = 0.12$ or $[\text{H}] = 600$ ppm. Using this notation, we can, however, use our data inversely to say

²The estimates of dislocation densities probably involve errors of this magnitude. For further data see Brice (1984).

TABLE VIII. A variance ratio (F) test shows that we can be 95% confident that the variation of ϕt^2 is less than that of ϕ . Thus we can assume that the fractional decrease is inversely proportional to the square of the slice thickness which is consistent with loss by diffusion. Unpublished data from Philips Research Laboratories.

Slice thickness (t , cm)	α (cm^{-1})		% decrease	
	1972	1978	ϕ	ϕt^2
0.70	0.215	0.082	62	30
0.75	0.225	0.095	58	32
0.80	0.059	0.034	42	27
0.90	0.124	0.075	40	32
0.90	0.080	0.052	28	23
0.95	0.071	0.051	28	25
			43 ± 14	28 ± 4

TABLE IX. Median impurity concentrations as a function of Q . The distribution of results is skewed. A few samples have very large impurity concentrations, but the results are much more consistent than those for minor impurities given in Table X: for Na, Al, and Li, 90% of samples contain less than 2.5 times the median values given. The logarithms of the concentrations of Na, Al, and Li have roughly Gaussian distributions with a standard deviation of 0.3. Note that these results apply in the Z zone. In the X zones impurity concentrations are much larger. For all impurities except H and Li the values are 10–30 times higher than the values in this table and Table X. For H and Li the concentrations are about a factor of 3 higher.

$Q \times 10^{-6}$	Concentrations (atomic ppm) ^a			
	H	Na	Al	Li
2.5	250	0.5 ± 0.4	2 ± 1	1 ± 0.5
2.0	300	1.0 ± 0.5	2 ± 1	2 ± 1
1.5	400	3 ± 2	3 ± 2	20 ± 10
1.0	600	10 ± 5	10 ± 5	30 ± 10
0.5	1200	10 ± 5	20 ± 10	25 ± 10

^aErrors are half the interquartile ranges—i.e., for $x \pm \Delta x$, half the values found lie between $x - \Delta x$ and $x + \Delta x$.

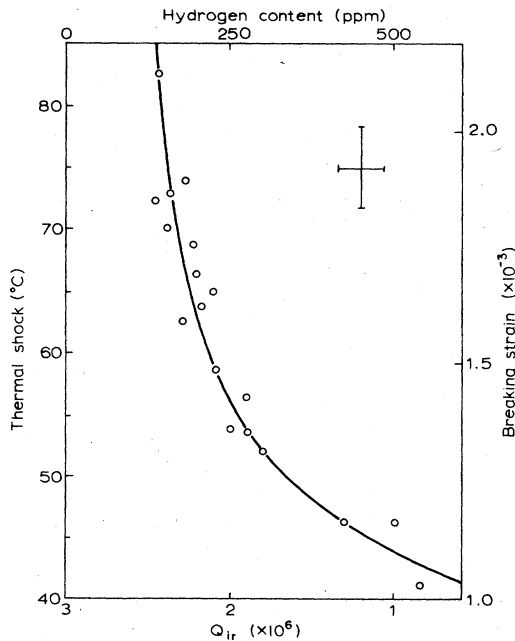


FIG. 6. The correlation between thermal shock to fracture the crystals and infrared Q (Brice *et al.*, 1981).

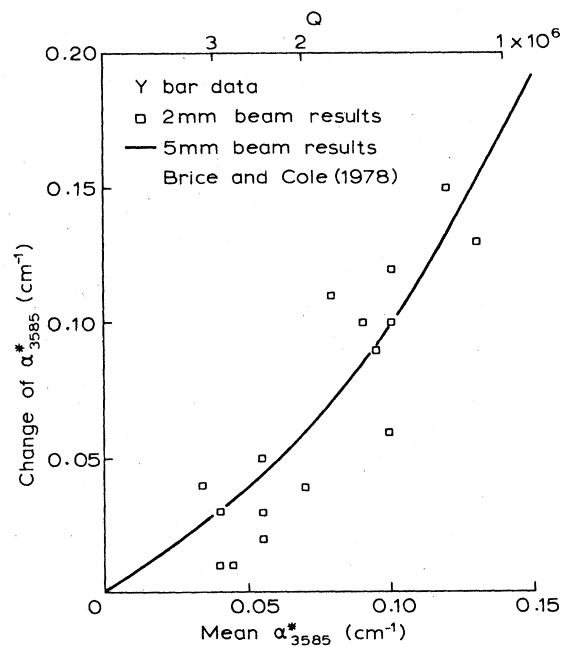


FIG. 7. The change of α with mean α for a 1-cm displacement in the z direction.

TABLE X. Median impurity concentrations (atomic ppm relative to silicon). The logarithms of the concentrations have roughly Gaussian distributions with standard deviations of about 0.5, i.e., the equivalent of a factor of 3. Thus 90% of samples tested have concentrations of less than four times the median values given. These results apply to Z zones only. See footnote to Table IX.

Impurity	Samples with	
	$Q = (2.0 \pm 0.4) \times 10^6$	$Q = (1.0 \pm 0.4) \times 10^6$
C ^a	24	70
C ^b	4	15
S	0.6	2
F	0.5	2
Cl	0.5	1
Ca	0.3	0.6
K	0.1	0.6
Br	0.1	0.2
Zn	0.1	0.2
Co	0.03	0.1
Fe	0.03	0.3

^aGrown from Na₂CO₃.

^bGrown from NaOH.

that for $Q \lesssim 2$ million the dislocation density is most unlikely to exceed 10^3 cm^{-2} (see Fig. 5).

3. Impurity concentrations and Q

When we come to consider impurities, there are fewer data available. Dislocation densities were measured on about 200 samples by x-ray topography. Solid-source mass spectrometric measurements of impurities were performed on about 60 samples. The results now discussed apply to the Z zone only. (In the X zones impurity concentrations are typically 10–30 times larger for impurities other than Li or H, both of which have concentrations in the X zone of about three times the level in the Z zone.)

The rather smaller amount of data makes it difficult to be certain what occurs. From the data in Tables IX and X, it is clear that there is a general tendency for all impurity concentrations to rise as Q falls. The results from different suppliers suggest that some suppliers' material is consistently purer than the average. This would be expected from the use of different raw materials, but we cannot prove it from our data. The differences of suppliers averaged values were less than the standard deviations. The only certainty was that, as might be expected, the carbon content of material grown by the carbonate process was much higher than the concentrations found when NaOH was the mineralizer. Thus again we have an overall trend but individual suppliers probably differ. Inverting the data gives the result that we can be 90% confident that the impurity concentrations will not exceed the tabulated values by more than a factor of 2.5 in Table IX or a factor of 4 for Table X.

TABLE XI. Thermal shock data. The tabulated quantities are the mean shock \pm its standard deviation together with the sample size in parenthesis.

Batch	Shock to break	
	Seed veil prominent	Seed veil nearly invisible
1	58.4 \pm 9.8 (13)	55.4 \pm 5.4 (14)
2	55.8 \pm 6.0 (10)	57.0 \pm 1.6 (6)

4. Strength and Q

The thermal shock required to break a crystal is a measure of the breaking strain. The general correlation with Q is shown in Fig. 6. There is no doubt that as Q falls, the boules become more fragile. A somewhat unexpected result was that the results obtained appeared to be independent of damage. Thus, for example, from a given batch³ selecting an apparently undamaged sample of specimens and comparing the result with a sample of obviously chipped boules gives the result that the undamaged sample of 18 boules broke with a mean shock of $56.1 \pm 7.4^\circ\text{C}$ and the sample of 9 chipped boules broke with a mean shock of $57.3 \pm 8.9^\circ\text{C}$. The median shocks to break both samples were 57.5°C . Thus we can conclude that all boules have sufficient crack nuclei in the as-received state, but note that the standard deviation of the damaged sample is larger at a 95% confidence level. In any batch the distribution of shock to break has an approximately Gaussian distribution. Different batches even from the same suppliers had significantly different means and standard deviations. If samples were selected from a given batch on the basis of the density of the seed veil, we obtain the results in Table XI. Clearly, the means do not differ in any significant manner but the standard deviations of the samples with prominent seed veils are larger at least at a 95% confidence level. Thus batches with prominent seed veils contain a greater proportion of easily broken crystals than batches with nearly invisible seed veils. Note that in a given batch (i.e., crystals grown in the same autoclave at the same time) a sample selected to have prominent seed veils has a lower Q than a sample selected to have a nearly invisible veil. However, the prominence of the veil is difficult to quantify in a reproducible way.

Note that from the thermal shock data it is possible to deduce the maximum strain to which the surface is subjected. This strain is a reasonable estimate of the breaking strain of the sample.

For further discussion of thermal shock testing see Brice (1984), who shows that a 50°C shock breaks a fraction of boules in a batch which falls rapidly with the

³Some of the batch had broken free of their packing.

TABLE XII. Cutting forces. The X force is the load needed to maintain a constant rate of cut. In this case 0.25 mm sec^{-1} . The Y force is the drag on the wheel. This force multiplied by the rate of peripheral movement of the blade (1676 cm sec^{-1}) is the energy dissipated in the sample. The lubricant was Shell Fusus A. The data were obtained by I. S. Baldwin (Mullard, Southampton), using a modified Capco Q35/M12 machine.

Q (in millions)	Dislocation density (cm^{-2})	X force (N)	Y force (N)
1.8	10^2	176	5
1.2	10^3	191	16
1.0	10^4	430	24
0.8	10^5	446	46

batch mean Q (typically 5% at $Q=2.0$ million to 0.1% at $Q=2.7$ million).

5. Hardness and Q or dislocation density

A quantity related to the breaking strain is the hardness of the material. It is not easy to measure the hardness of a brittle material like quartz. The usually quoted values of Mohs hardness are about 7 corresponding to a microhardness of about 800 kg mm^{-2} . Most values fall in the range $700\text{--}850 \text{ kg mm}^{-2}$, but there is a wide variation. Even on one sample the hardness varies with position and not all of this variation is attributable to the material's being in a different growth zone (X -zone material is harder than that of the Z -zone, for example). Data relating to the related quantity—cutting forces—are given in Table XII. Clearly more force is needed to cut low- Q material.

6. Uniformity and Q

The uniformity of crystals is of great interest. Marked nonuniformity might result in some parts of the crystal being useful for device fabrication and other parts yielding poor devices. We have already noted that the seed region is not suitable for use in devices and that material grown on faces other than Z is also usually too impure and strained to yield good devices. In this section we

TABLE XIII. The range of Q values found when varying x coordinate with z constant^a for large crystals.

Mean $Q \times 10^{-6}$	Range ^b $\times 10^{-7}$	Fractional change % cm^{-1}	Number of samples
2.6–2.9	3.0 ± 1.3	4	8
2.1–2.5	3.1 ± 1.1	4	8
1.5–2.0	3.0 ± 1.5	5	8
0.9–1.4	2.6 ± 0.9	8	6

^aThese data are for $z=8$ or 10 mm .

^bThe range is the difference between the maximum and minimum values found.

shall therefore examine effects in material grown only on Z faces. Since almost all the properties of potential interest are correlated with the hydrogen content, we can limit attention to how either the hydrogen content or some parameter (α or Q) immediately relatable to the hydrogen content varies.

We are interested in two types of uniformity. We need to know about the uniformity of material in one crystal and how far crystals grown in the same batch differ from one another.

Looking first at the uniformity of one crystal, let us consider a coordinate system with the origin at the geometric center of the crystal and with an x axis parallel to the a crystallographic axis and z parallel to c . In Fig. 7 the solid line represents the data gathered by Brice and Cole (1978) for relatively small crystals grown on bar-shaped seeds with their long axes parallel to y . The solid-line results were obtained with a 5-mm-diam beam. The individual points we obtained with a 2-mm-diam beam. From this figure it is clear that $d\alpha/dz$ tends to increase with α —i.e., on the average crystals with large α are less uniform in the z direction than ones with low α . At a constant value of z changes with x and y in the Z zone are small. For large crystals grown on platelike seeds, the results of varying the z coordinate are similar to those shown in Fig. 7, but show a larger spread—e.g., for $\alpha=0.07 \text{ cm}^{-1}$ the changes found range from 0.012 to 0.030 cm^{-1} per cm and for $\alpha=0.12 \text{ cm}^{-1}$ the range was $0.006\text{--}0.015 \text{ cm}^{-1}$ per cm . In terms of infrared Q these correspond to 20–50% changes for $Q=1$ million and 10–25% for $Q=2$ million. At constant z , the variations found by changing y were small. Table XIII shows data for constant z with x varying.

In order to discuss sensibly the uniformity of Q (or α) in a batch we need to define a mean Q (or α) in a boule. Since it is useful to think about only large batches (>100 boules), we can restrict our attention to small crystals, i.e., to ones with bar seeds. From the preceding discussion it is clear that the only important parameter is the z coordinate of the measurement and we have therefore somewhat arbitrarily selected a point for the measurement which is halfway from the seed to the outside of the crystal.⁴ Without knowing the form of the distribution we can use the standard deviation as a measure of dispersion (i.e., the inverse of uniformity), but with an appreciably skewed distribution some other measure may be better. Brice and Cole (1978) implicitly assumed that Q was distributed in a Gaussian form. There is evidence for this at $Q \geq 2$ million. Figure 8 shows the cumulative frequency curves for two batches, and analysis of the data shows that for these batches the probabilities that the distributions are not Gaussian is $<10\%$ in one case and 5% in the other. However, there is some evidence that for lower Q , Q is described by a skewed distribution. Q is inversely related

⁴This is usually the location of the active region of a device.

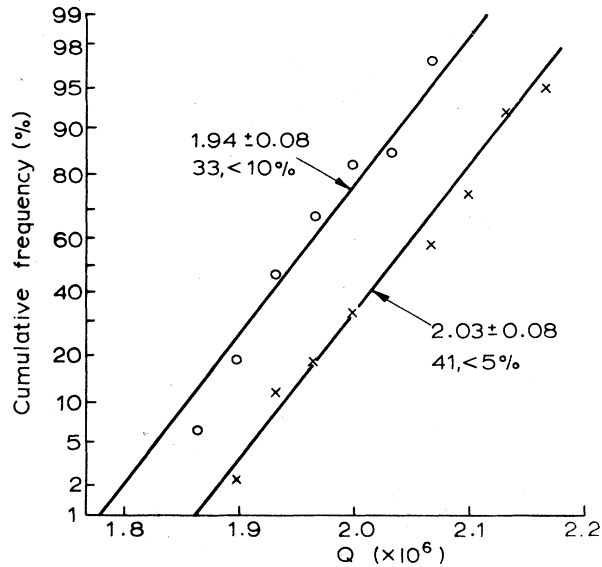


FIG. 8. Cumulative frequency curves for Q in two batches of quartz. The parameters given are the mean Q and its standard deviation in millions, the sample size, and the probability that the points deviate significantly from the lines.

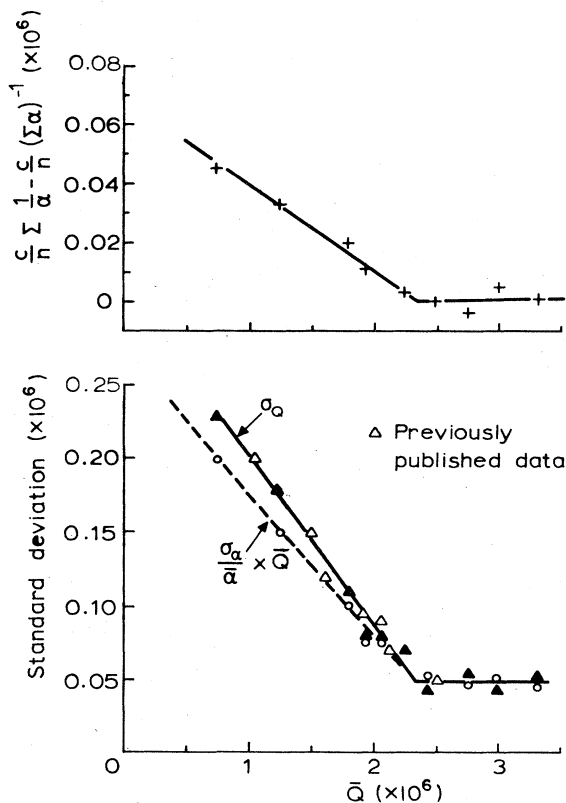


FIG. 9. Mean Q derived from individual α values minus mean Q derived from mean α values (upper part). The lower part shows the standard deviations σ of Q and α (normalized to the Q scale). Since $\sigma_\alpha < \sigma_Q$, α is more likely to be distributed normally.

to α and on general grounds we might expect α to be randomly distributed. At $Q \approx 2$ million the standard deviations of Q and α are both about 5% and we would not expect to be able to distinguish which is a Gaussian distribution. However, at $Q = 1$ million the standard deviation of Q is about 20% of the mean. At this level the evidence favors α 's being the variable with a Gaussian distribution. The upper portion of Fig. 9 shows the difference between mean Q values calculated in the two possible ways and makes it clear that Q calculated individually from the α values gives a higher mean value than calculating the mean value of α and then deriving Q . The lower part of the figure shows that expressed as a fraction of the mean the standard deviation of α is less than the standard deviation of Q . This shows that α is a better measure of dispersion than Q and that for small Q , Q has a skewed distribution. For $Q > 1.8$ million, the differences are negligible. Figure 9 gives the standard deviation of Q (σ_Q), and the standard deviation of α can be deduced from the dashed line. The break in the curve of $Q \approx 2.3$ million, and the constant values of the standard deviations for higher Q are artificial, illustrating the fact that our techniques introduced a random error equivalent to a variation of 0.05 million. Note that each point is a mean of several batches.

Results are given later (Sec. IV.B) for the variation of lattice constants with Q . There it is shown that not only the parameters change as the Q falls but the spread of values found also increases.

7. Summary

To summarize we can say the following.

- (a) For a given Q value, in general we find that the logarithms of the dislocation densities and impurity concentrations have Gaussian distributions.
- (b) For a given batch, the extinction coefficients and the breaking strains have Gaussian distributions. The presence of inclusions increases dislocation densities and the fraction of crystals with low breaking strains.
- (c) As the measured mean Q of a batch falls, the dislocation densities and impurity concentrations rise, but materials from different suppliers follow curves with different intercepts. Also, as the mean Q falls, the batches become less uniform and have lower breaking strains. Again, different suppliers' materials behave differently.
- (d) In cases where the supplier affects the relation found, we can expect that the best supplier's material will be at most a factor of only about 3 better than the average for a given Q .

IV. THE PROPERTIES OF QUARTZ

Quartz has been studied for a long time because it was and indeed still is of geological interest. Its optical properties were exploited before the discovery of piezoelectricity by Pierre and Jacques Curie in 1880. This long history has created many property data, not all of which are reli-

able by modern standards. Thus some handbook data need to be viewed critically. The best handbook data sources are Frondel (1962) and Landolt-Bornstein (1966,1979), who cover some properties in depth, and Gray (1972), who gives carefully selected values of some properties. Up-to-date files on the properties of quartz are maintained by the Electronic Materials Information Service (EMIS).⁵ The values given in this section are selected on the basis that they are widely accepted and their use gives reasonable agreement with experiment.

Where possible the spread of apparently reasonable values is indicated. The data are treated under two headings: intrinsic properties and defect related properties. It may well be that some properties are placed in the first category simply because the work necessary to establish the effect of defects has not yet been done. Thus it may eventually be found that some properties here called intrinsic may vary slightly with purity or perfection [see Ward (1984)].

A. Intrinsic properties

1. Structural and thermodynamic data

The material of interest to us is α -quartz, which is the thermodynamically stable form of SiO_2 at temperatures up to 573°C . At higher temperatures and atmospheric pressure, β -quartz or β -tridymite is stable to 867°C , α -tridymite is the stable form between 867°C and 1470°C , and the cristoballite phases are the stable structures from 1470°C to the melting point at 1723°C . These other forms of SiO_2 exist metastably at room temperature.

Unless otherwise specified, we shall now be concerned only with α -quartz. The crystal structure is discussed by Wyckoff (1960) and Evans (1966). The bonding is about 60% covalent and 40% ionic. The structure has class 32 symmetry, a space group $D_3^4-P3_12$, with atoms at the positions given in Table XIV. Conventionally (IRE, 1949), the Z or c axis is parallel to the threefold axis and the X or a axes are parallel to the three twofold axes. In a right-hand set of rectangular axes, Y is at right angles to Z and X . (In a right-hand set of axes, Z is the thumb, X is the first finger, and Y is the second finger.) Quartz can exist in two forms—right- or left-handed. Most but not all synthetic quartz is right-handed. The rule for determining the type is given (IRE, 1949) as follows: “on extension, the positive ends of the a axes, and therefore the X axes, become negatively charged with right quartz, positively charged with left quartz” (IRE, 1949, p. 1385). Note that a right-hand set of axes is used to describe both right- and left-handed quartz. This has the following consequences: for all quartz, s_{14} is positive, c_{14} is nega-

TABLE XIV. Coordinates of atoms in the unit cell. x_1 is a distance along one a axis and x_2 a distance along the other a axis used to define the cell edges. z is a distance parallel to the c axis.

	x_1/a	x_2/a	z/c
silicon	0.535	0.535	0.333
	0.465	0	0
	0	0.465	0.666
oxygen	0.415	0.272	0.120
	0.857	0.585	0.453
	0.143	0.728	0.880
	0.272	0.415	0.547
	0.585	0.857	0.213
	0.728	0.143	0.787

tive, $d_{11} = -d_{12} = d_{26}/2$, $e_{11} = e_{12} = -e_{26}$, $d_{14} = -d_{25}$, and $e_{14} = -e_{25}$; for right quartz d_{11} , d_{14} , and e_{11} are negative and e_{14} is positive; for left quartz d_{11} , d_{14} , and e_{11} are positive and e_{14} is negative. These parameters are defined and discussed later.

The structure of quartz leaves a tunnel shown in Fig. 10, where the small circles are Si atoms and the large ones O atoms. Neutral particles with radii less than 0.5 \AA can pass easily along the pipe; ones with radii between 0.5 and 0.8 \AA , have to follow a zigzag path; and particles with radii up to 1.4 \AA can be accommodated without significant lattice distortion. For particles with radii over 0.8 \AA ,

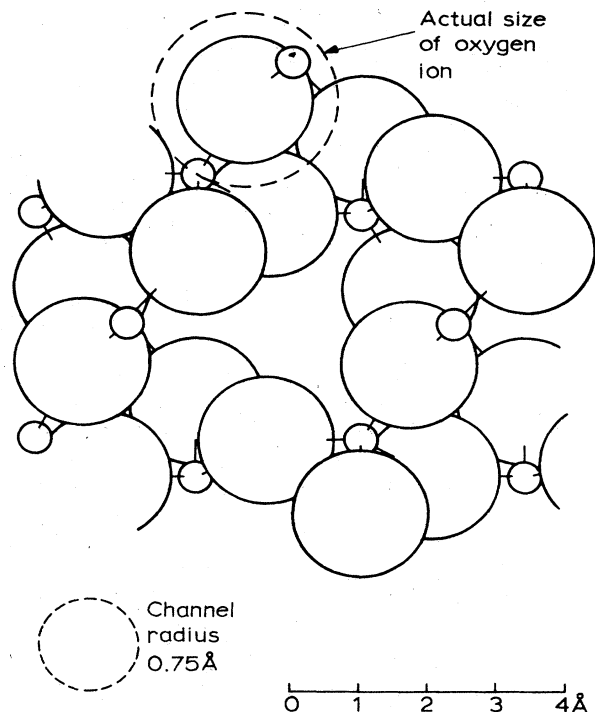


FIG. 10. A vertical projection of the α -quartz structure. The c axis is normal to the plane of the diagram. The edges of the unit cell are parallel to a axes. The small ions are silicon and the large ones oxygen. The numbers are the vertical positions of the ions as a percentage of the c -lattice parameter (5.404 \AA).

⁵For information about the EMIS computer data bank, which can be accessed in most countries, contact EMIS, The Institution of Electrical Engineers, Station House, Nightingale Road, Hitchin, Herts SG5 1RJ, England.

however, movement requires cooperative movement of other atoms. Si—O bonds occur in pairs with lengths of about 1.598 and 1.616 Å. Each silicon is coordinated by four oxygens and each oxygen lies slightly off a line joining two silicons. Both the axial ratio and the lattice constants depend on purity; a discussion of their values is given in Sec. IV.B. Bond energies are about 468 kJ mol⁻¹.

Thermodynamically quartz is very stable: the enthalpy of formation at 25°C is 860 kJ mol⁻¹ and the free energy of formation is 805 kJ mol⁻¹. (Here we consider the reaction Si + O₂ → SiO₂.) Thus of the possible electrode materials, only Al, Cr, and Ti are likely to reduce quartz: all the other likely electrode materials (Ta, Ni, Cu, Pt, Ag, and Au) have oxides with lower free energies of formation [see, for example, Samsonov (1973) and Weast (1964)].

The vapor pressure of α-quartz has not been determined. The vapor pressures of β-tridymite and vitreous silica are quoted by Samsonov (1973). From these data we can infer that the vapor pressure of α-quartz should not exceed 10⁻⁹², 10⁻⁴⁸, 10⁻³⁰, or 10⁻²⁰ Pa at, respectively, 0°C, 200°C, 400°C, and 600°C (1 bar = 10⁵ Pa). Thus, for example, the rate of evaporation at 500°C should be less than about 10¹¹ atoms cm⁻² yr⁻¹ or less than 10⁻⁴ monolayers per year.

Figure 11 gives specific-heat data and is based on the data given by Weast (1964) and Touloukian (1967). Samsonov (1973) gives a molar specific heat of

$$C_p = 47.0118 + 3.4358 \times 10^{-2} T - 1.131 \times 10^6 T^{-2}, \quad (5)$$

where T is the absolute temperature. Since the molar weight is 60.085 g, this agrees well with the data in Fig. 11. Gray (1972) quotes a Debye temperature of 470 K, and other higher values are mentioned, but taking $C_p - C_v = 0.075 \text{ J(g atom } ^\circ\text{C)}^{-1}$ and using Fig. 11 with the

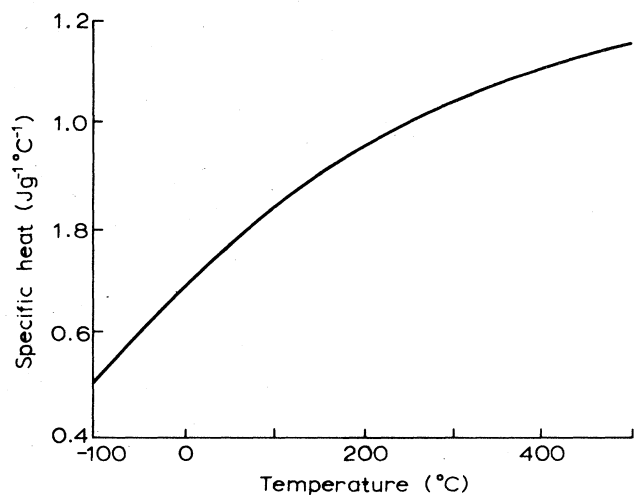


FIG. 11. The specific heat of α-quartz as a function of temperature.

tables given by Gray for the Debye function suggest that a Debye temperature of 700 ± 50 K is more appropriate for the temperature range in which devices are fabricated and used.

Figure 12 gives the thermal expansion data quoted by Gray (1972) from a critical study. Ackerman and Sorrell (1974) give very similar values. McSkimin *et al.* (1965) give data for $77 < T < 300$ K in the form of a polynomial

$$l = l_0(1 + \alpha_1\theta + \alpha_2\theta^2 + \alpha_3\theta^3 + \alpha_4\theta^4), \quad (6)$$

where l is a dimension at $\theta^\circ\text{C}$ and l_0 is the dimension at 0°C . Values of α_1 , α_2 , α_3 , and α_4 are 7.030×10^{-6} , 10.25×10^{-9} , 6.58×10^{-12} , and 48.5×10^{-15} , respectively, when l is parallel to the c axis and for l parallel to a , the values are 13.20×10^{-6} , 22.85×10^{-9} , 86.36×10^{-12} , and 276×10^{-15} , respectively. Equation (6) essentially gives the integral of the thermal expansion over the tempera-

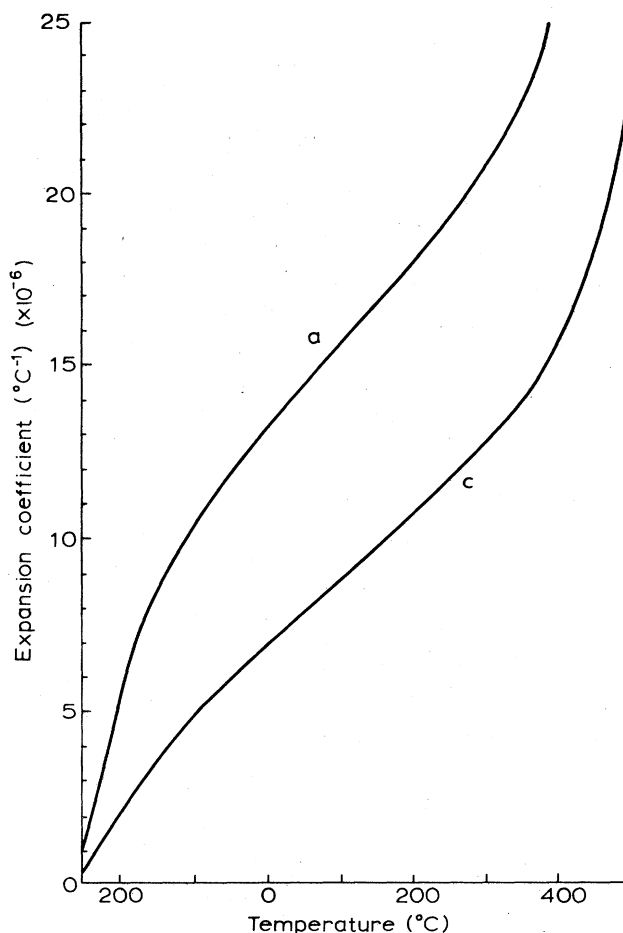


FIG. 12. The thermal expansion of α-quartz. The curve marked a is for the direction parallel to $a(x)$, and the curve marked c is for the direction parallel to $c(z)$. Actual values at -100°C , -50°C , 0°C , 25°C , 100°C , and 200°C are 4.9 , 6.0 , 7.0 , 7.5 , 8.8 , and $10.4 \times 10^{-6} \text{ } ^\circ\text{C}^{-1}$ in the c direction and 10.3 , 11.8 , 13.1 , 13.7 , 15.6 , and $17.9 \times 10^{-6} \text{ } ^\circ\text{C}^{-1}$ in the a direction. Errors should not exceed 2%.

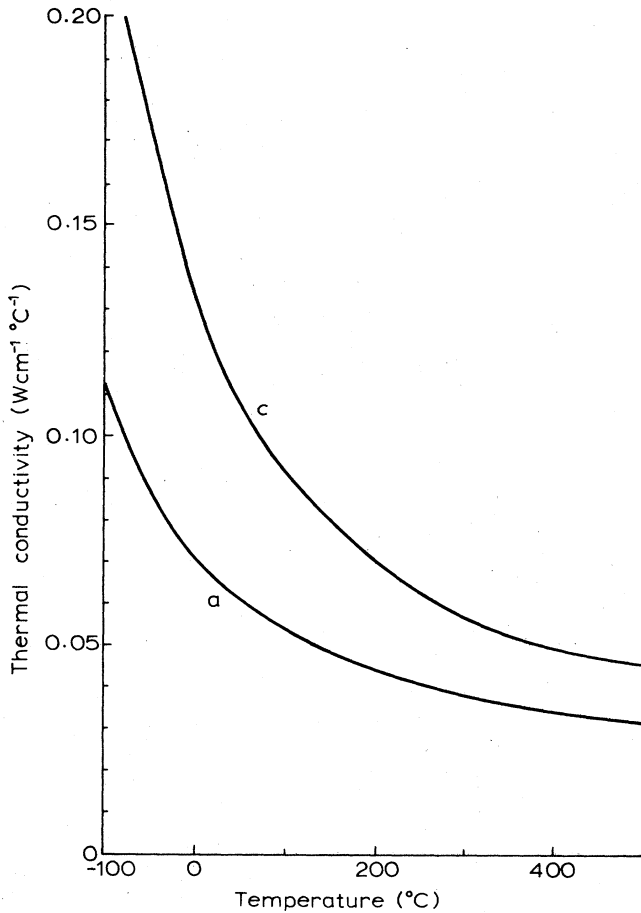


FIG. 13. The thermal conductivity of α -quartz parallel to the a and c crystallographic axes.

ture interval 0 to θ . The agreement between these data and Fig. 12 is excellent.

The density of quartz varies with purity and is discussed in Sec. IV.B with the data on the lattice parameters.

Figure 13 gives the thermal conductivities as a function of temperature. The curves are smoothed values through a variety of handbook data. The scatter of data suggests that the curves are unlikely to be in error by more than 5%, but it is not clear whether purity and perfection cause variations at this level of accuracy.

The symmetry of quartz does not permit any pyroelectric phenomena. However, nonuniform heating reduces the symmetry so that an apparent pyroelectric effect can sometimes be observed. (This phenomenon is often called a tertiary pyroelectric effect.) Similarly a mechanical or

electric strain could reduce the symmetry and make pyroelectric effects possible. No problems with pyroelectric origins seem to have been reported.

2. Elastic constants

The elastic constants of prime interest for resonator design are the elastic stiffnesses. The constant c_{ij} is used for the tensor which written fully would be c_{lmnp} . The rules for obtaining i and j from lm and np are given in Table XV.

The elastic constants of quartz have been determined many times. See Koga *et al.* (1958) and Bechmann (1958) for references to early work. The values of c_{ij} and their temperature coefficients usually used are those given by Bechmann *et al.* (1962) or the very similar values given by Mason (1951). The calculated quantities given in Sec. V are based on the first of these sets of values and give excellent agreement with experiment. However, it must be remembered that the values are deduced from measurements on resonators so that any set of data based on a representative set of samples should produce reasonable results, but it is not advisable to use part of one set and part of another. In particular, this applies to temperature coefficients. Thus in Tables XVI–XXIV we give all the relevant data quoted by Bechmann *et al.* Using other sets of temperature coefficients, e.g., those due to Koga *et al.* (1958) and Mason (1951), also gives good results.

For comparison in Table XVI, I also give the mean and the standard deviation of the values of c_{ij} given by Bechmann (1958), Koga *et al.* (1958), McSkimin *et al.* (1965), Ludanov *et al.* (1976), and Shevel'ko and Yakovlev (1977). These mean values could be regarded as unbiased estimates of the c_{ij} values. The standard errors of the various means could then be taken as half the standard deviations quoted. The final column of this table gives the deviations found by Ludanov *et al.* (1976), who found systematic changes in c_{ij} when they irradiated their samples with α rays. These results suggest that the c_{ij} may depend on the sample, so that some of the spread of values may be real, and it would be advisable to assume that the standard error of each mean is the same as the standard deviation of the distribution of means.

The c_{ij} values quoted in Table XVI are the values of the elastic stiffnesses at constant field and under adiabatic conditions (constant entropy). These are usually labeled c_{ij}^{ES} . Three other stiffness coefficients exist: c_{ij}^{DS} (constant displacement and entropy), c_{ij}^{ET} (constant field and temperature—i.e., isothermal values), and c_{ij}^{DT} (constant displacement and temperature). These other values differ by small amounts from the values quoted (see Table XVII).

TABLE XV. The convention for compressing tensor notation. For quartz only terms up to i or $j=6$ are needed, because the symmetry of the lattice ensures that $C_{22}=C_{11}$, $C_{55}=C_{44}$, $-C_{24}=C_{36}=C_{14}$, $C_{23}=C_{13}$, and $C_{66}=\frac{1}{2}(C_{11}-C_{12})$.

lm or np	11	22	33	23	31	12	32	13	21
i or j	1	2	3	4	5	6	7	8	9

TABLE XVI. Elastic stiffnesses of quartz at 25 °C.

	Bechmann (1958) ^a	GN m ⁻²	
		All values	Change when irradiated
c ₁₁	86.74	86.80±0.04	+ 0.02
c ₃₃	107.2	106.2±0.8	+ 0.006
c ₁₂	6.97	7.10±0.09	-0.02
c ₁₃	11.90	11.91±0.01	
c ₄₄	57.93	58.17±0.13	-0.006
c ₆₆	39.89	39.85±0.03	+ 0.02
c ₁₄	-17.91	-18.02±0.07	

^aBechmann's data were for 20 °C. They have been corrected here to 25 °C. All values are c_{ij}^{ES}. Kahan (1982) gives very similar values except for c₁₁, c₁₃, and c₃₃, for which he obtains 83.63, -0.88, and 77.60, respectively.

From a device designer's point of view, small errors in c_{ij} are not usually important. It is often possible to correct the frequency during manufacture (see Secs. V and VI).

For completeness Table XVIII gives the values of elastic compliances s_{ij} and Table XIX gives the changes in values for different conditions.

While the data for c_{ij} and s_{ij} are reasonably consistent, the published values of the temperature coefficients are less homogeneous. The notation used to describe the various parameters is unusual. Consider a parameter which has a value ρ₀ at some reference temperature T₀ (usually 25 °C). Then its value at some other temperature T = T₀ + ΔT is ρ and this is given by

$$\rho = \rho_0(1 + T_\rho^{(1)} \Delta T + T_\rho^{(2)} \Delta T^2 + T_\rho^{(3)} \Delta T^3), \quad (7)$$

so that

$$T_\rho^{(n)} = \frac{1}{n! \rho_0} \left. \frac{\partial^n \rho}{\partial T^n} \right|_{T=T_0} \quad (8)$$

Most workers fit data to only a cubic approximation, and the values of T_ρ⁽ⁿ⁾ give very poor estimates of (∂ⁿρ/∂Tⁿ) as n increases. This is why one should use sets of temperature coefficients as sets rather than attempting to determine the "best" value of each coefficient by looking at several determinations. However, T_{c_{ij}}⁽¹⁾ should be the least affected by the fitting routine. Table XX gives the available data. The first column gives Bechmann's data.

TABLE XVII. Differences in elastic stiffnesses. The data are from Bechmann (1958) except for values in parenthesis which are from McSkimin *et al.* (1965), marked with a superscript a, or from Ludanov *et al.* (1976), marked with a superscript b.

ij	c _{ij} ^{DS} - c _{ij} ^{ES} or c _{ij} ^{DT} - c _{ij} ^{ET}	c _{ij} ^{DT} - c _{ij} ^{ET} or c _{ij} ^{DS} - c _{ij} ^{ES}
11	0.746 (0.770) ^b	0.288 (0.32) ^a
33	0	0.193 (0.20) ^a
12	-0.746	0.288 (0.32) ^a
13	0	0.236 (0.25) ^a
44	0.0415	0
66	0.746 (0.800) ^b	0
14	-0.177	0

The second column gives the mean values of other available data deduced in the same way. The final column gives the data of Sinha and Tiersten (1978,1979), which were deduced differently. The only coefficients determined by Sinha and Tiersten's method appear to be first-order ones. Note that the two types of data have to be used differently. Either used correctly gives good results.

In most cases we are interested in T_{c_{ij}}⁽ⁿ⁾, and the coefficients of c_{ij} under other conditions should be very similar. There are, however, minor differences. See Table XXII, which also gives data for the first-order coefficients of s_{ij}. Values of T_{s_{ij}}⁽¹⁾ are given in Table XXI.

Tables XXIII-XXV give the data available about second- and third-order temperature coefficients of c_{ij} and s_{ij}. As expected, individual sets of data show considerable divergence.

The basic temperature coefficient data used by Bechmann *et al.* (1962) have been reappraised by Kahan (1982), Hruska (1983) (see the footnote to Table XX), and Lee and Yong (1983). Looking at all the data suggests that since the temperature coefficients given by Bechmann *et al.* are a representative set which work in practice for quartz with a Q of two million or over, this set should therefore be recommended. However, the possibility that the temperature coefficients of different samples may vary must not be forgotten, and variations of, say, 10% cannot be excluded.

So far, I have treated only the real portions of stiffness tensor c and the compliance tensor s. A rigorous treatment attributes imaginary parts to these tensors to allow for losses. Lamb and Richter (1966) and Ballato (1978)

TABLE XVIII. Elastic compliances of quartz at 25 °C.

	In units of 10 ⁻¹² m ² N ⁻¹	
	Bechmann (1958)	McSkimin <i>et al.</i> (1965)
s ₁₁	12.77	12.777
s ₃₃	9.60	9.735
s ₁₂	-1.79	-1.807
s ₁₃	-1.22	-1.235
s ₄₄	20.04	19.985
s ₆₆	29.12	29.167
s ₁₄	4.50	4.521

TABLE XIX. Differences in elastic compliances. Data in parenthesis are from McSkimin *et al.* (1965); other data from Bechmann (1958).

	In units of $10^{-12} \text{ m}^2 \text{ N}^{-1}$ $s_{ij}^{DS} - s_{ij}^{ES}$ or $s_{ij}^{DT} - s_{ij}^{ET}$	$s_{ij}^{ES} - s_{ij}^{ET}$ or $s_{ij}^{DS} - s_{ij}^{DT}$
s_{11}	-0.134	-0.028 (-0.032)
s_{33}	0	-0.008 (-0.008)
s_{12}	0.134	-0.028 (-0.032)
s_{13}	0	-0.016 (-0.017)
s_{44}	-0.0132	0
s_{66}	-0.536	0
s_{14}	-0.042	0

have done this for quartz. Essentially in this approach we write Hooke's law in the form

$$t_1 = \left[c + \eta \frac{\partial}{\partial t} \right] s_1 \tag{9}$$

and

$$e = \left[s - \xi \frac{\partial}{\partial t} \right] t_1, \tag{10}$$

where t is time, t_1 is stress, s is strain, η is viscosity, and ξ is called fluency. Lamb and Richter (1966) measured the viscosity of quartz in the range 0.5–5 GHz but did not characterize their samples. Ballato (1978) used their data to evaluate the fluency, and the two sets of data are given in Table XXVI. Ballato shows that at an angular frequency ω

$$S = (c - \omega^2 \eta^2 c^{-1})^{-1} \tag{11}$$

and

$$\xi = c^{-1} \eta s, \tag{12}$$

and in the limiting case $\omega \rightarrow 0$

$$S = c^{-1} \tag{13}$$

and

$$\xi = S^2 \eta. \tag{14}$$

Clearly, the rewritten forms of Hooke's law will lead to resonant frequencies which depend on the fluency and viscosity. In Sec. V we shall deal with this problem by using an equivalent circuit parameter R_1 , which takes into account losses additional to those in the quartz. Both the viscosity and fluency would be expected to depend on the purity (particularly the hydrogen content) of the quartz, so that the data in Table XXVI should be treated with caution.

McSkimin *et al.* (1965) give what are essentially compressibility data. They express a length l in the form

$$l = l_0(1 + aP), \tag{15}$$

where P is the pressure and l_0 is the length when $P \rightarrow 0$. When l is parallel to the c axis, $a = s_{33} + 2s_{13} = 7.3063$ in units of $10^{-12} \text{ m}^2 \text{ N}^{-1}$, and when l is parallel to the a axis, $a = s_{11} + s_{12} + s_{13} = 0.8156$. Here the values for 25°C and values at -195.8°C are, respectively, 6.9307 and 9.3779 in units of $10^{-12} \text{ m}^2 \text{ N}^{-1}$. The numerical values are those quoted in the paper. Using the values of s_{ij} tabulated here gives slightly different values.

McSkimin *et al.* (1965) give pressure derivatives for c_{ij} , and the same team later gives the third-order elastic constants needed for calculating the effects of strain on device frequencies (Thurston *et al.*, 1966). See Table XXVII.

3. Piezoelectric constants

Quartz has eight independent piezoelectric constants. The values due to Bechmann (1962) are given in Table XXVIII. Koga *et al.* (1958) give values of d_{11} and d_{14} of $2.37 \times 10^{-12} \text{ C N}^{-1}$ and $0.77 \times 10^{-12} \text{ C N}^{-1}$, respectively. Koga *et al.* give $e_{11} = -0.175 \text{ C m}^{-2}$ and $e_{14} = 0.00407 \text{ C m}^{-2}$. Shevel'ko and Yakovlev (1977) give $e_{11} = -0.171 \text{ C m}^{-2}$ and $e_{14} = 0.04 \text{ C m}^{-2}$ and give the temperature coefficients listed in Table XXIX. Ludanov *et al.* (1976)

TABLE XX. First-order temperature coefficients of c_{ij}^{ES} at 25°C.

	Temperature coefficient in units of $\text{ppm}^\circ\text{C}^{-1}$		
	Bechmann (1958) ^a	Literature	Sinha and Tiersten (1978,1979)
c_{11}	-48.5	-46.4 ± 2.1	18.16
c_{33}	-160	-172 ± 24	-66.60
c_{12}	-3000	-2901 ± 183	-1222
c_{13}	-550	-476 ± 111	-178.6
c_{44}	-177	-170 ± 13	-89.72
c_{66}	178	177 ± 8	126.7
c_{14}	101	105 ± 8	-149.2

^aHruska (1983) has reappraised the data on which these values were based and obtains slightly different values for some coefficients. Thus he suggests that values of -2635, -736 ± 35, -232 ± 15, and -174 $\text{ppm}^\circ\text{C}^{-1}$ would be appropriate for the coefficients of c_{12} , c_{13} , c_{33} , and c_{44} , respectively.

TABLE XXI. The first order coefficients of s_{ij}^{ES} at 25 °C.

ij	Temperature coefficient in ppm °C ⁻¹		
	Bechmann (1958)	Zelenka and Lee (1971)	Mason (1951)
11	15.5	8.5	13.6
33	140	139.7	127.3
12	-1370	-1296.5	-1241
13	-166	-168.8	-573
44	210	211.1	191
66	-145	-151.9	137
14	134	140	137.5

TABLE XXII. The variation of first-order coefficients of c_{ij}^{XY} and s_{ij}^{XY} (in units of ppm °C⁻¹). The data are from Zelenka and Lee (1971).

ij	$T_{c_{ij}}^{(1)DS} - T_{c_{ij}}^{(1)ES}$	$T_{s_{ij}}^{(1)DS} - T_{s_{ij}}^{(1)ES}$
11	-2.5	5.3
33	0	0
12	-285	-61.2
13	0	0
44	-2	-1.5
66	-9.9	7.6
14	17	-0.9

TABLE XXIII. Second-order temperature coefficients of c_{ij} at 25 °C (in units of 10⁻⁹ °C⁻²). The values due to Mason (1950) and Koga *et al.* (1958) were determined at 50 °C and 20 °C, respectively. They have been adjusted to 25 °C using the values of $T_{c_{ij}}^{(3)}$.

ij	Bechmann <i>et al.</i> (1962)	Mason (1950)	Koga <i>et al.</i> (1958)	Shevel'ko and Yakovlev (1977)
11	-107	-73	-418	-104
33	-275	-243	-1419	-106
12	-3050	-1787	-7119	
13	-1150	-2090	-763	3000
44	-216	-180	-231	-209
66	118	20	178	96
14	-48	-175	-32	-80

TABLE XXIV. Third-order temperature coefficients of c_{ij} (in units of 10⁻¹² °C⁻³). The temperatures at which the values were measured is given at the top of each column.

ij	Bechmann <i>et al.</i> (1962) (25 °C)	Mason (1950) (50 °C)	Koga <i>et al.</i> (1958) (20 °C)	Shevel'ko and Yakovlev (1977) (25 °C)
11	-70	-15	-371	-17
33	-250	410	-243	650
12	-1260	1910	4195	
13	-750	600	-5559	
44	-216	-65	-190	390
66	21	-167	-777	-850
14	-590	-630	-625	-1400

TABLE XXV. Second- and third-order temperature coefficients of s_{ij} .

ij	$T_{s_{ij}}^{(2)}$ (in units of 10 ⁻⁹ °C ⁻²)		$T_{s_{ij}}^{(3)}$ (in units of 10 ⁻¹² °C ⁻³)	
	Bechmann <i>et al.</i> (1962) (25 °C)	Mason (1950) (50 °C)	Bechmann <i>et al.</i> (1962) (25 °C)	Mason (1950) (50 °C)
11	85.3	58.5	147	33
33	247	144	300	570
12	-1385	-575	-2287	-215
13	-718	-2100	-823	610
44	262	200	162	-26
66	-85	-18	-135	3
14	93	40	-465	-54

TABLE XXVI. The fluency and viscosity matrices of quartz. The matrices have the same symmetry as c_{ij} and s_{ij} . Note that these values are based on one set of data and that the values are expected to be sample dependent.

ij	Fluency (in units of 10^{-26} sec Pa $^{-1}$)	Viscosity (in units of cP)
11	18.56	1.37
33	6.21	0.96
12	3.21	0.73
13	3.80	0.71
44	17.65	0.36
66	30.70	0.32
14	7.87	0.01

give $e_{11} = -0.174$ C m $^{-2}$ and record that after irradiation with x rays the value fell by 1.5% (dose greater than 10^7 rad). Thus the piezoelectric constants may be sample dependent.

If t_1 is the stress, s_1 is the strain, E is the electric field, and D is the electric displacement, then the parameters d , g , e , and h are related as follows:

$$d = \left[\frac{\partial s_1}{\partial E} \right]_{t_1} = \left[\frac{\partial D}{\partial t_1} \right]_E, \tag{16}$$

$$g = - \left[\frac{\partial E}{\partial t_1} \right]_D = \left[\frac{\partial s_1}{\partial D} \right]_{t_1}, \tag{17}$$

$$e = - \left[\frac{\partial t_1}{\partial E} \right]_{s_1} = \left[\frac{\partial D}{\partial s_1} \right]_E, \tag{18}$$

$$h = - \left[\frac{\partial t_1}{\partial D} \right]_{s_1} = - \left[\frac{\partial E}{\partial s_1} \right]_D, \tag{19}$$

and if ϵ_{11} is the dielectric constant, then

$$\frac{d_{ij}}{g_{ij}} = \epsilon_{11} \tag{20}$$

and

TABLE XXVII. Third-order elastic coefficients (in units of GN m $^{-2}$).

c_{111}	-210
c_{112}	-345
c_{113}	+12
c_{114}	-163
c_{123}	-294
c_{124}	-15
c_{133}	-312
c_{134}	+2
c_{144}	-134
c_{155}	-200
c_{222}	-332
c_{333}	-815
c_{344}	-110
c_{444}	276

TABLE XXVIII. The piezoelectric constants at 25°C. Note that the signs of d_{ij} , etc., are those conventionally given for right-handed quartz. The other components of the matrix can be found by using the relations $d_{11} = -d_{12} = \frac{1}{2}d_{26}$, $d_{14} = -d_{25} - e_{12} = e_{11}$, $-e_{25} = e_{14}$, and $-e_{26} = e_{11}$. Note that the existence of the twofold symmetry axis in the X or a direction ensures that there is no piezoelectric effect along any axis perpendicular to a . Landolt-Bornstein (1966) gives temperature coefficients of -200 to -350 ppm °C $^{-1}$ and 1290 to 1770 ppm °C $^{-1}$ for d_{11} and d_{14} , respectively.

Strain	Stress
$d_{11} = -2.31 \times 10^{-12}$ CN $^{-1}$	$e_{11} = -0.171$ C m $^{-2}$
$d_{14} = -0.727 \times 10^{-12}$ CN $^{-1}$	$e_{14} = +0.0406$ C m $^{-2}$
$g_{11} = -0.0578$ m 2 C $^{-1}$	$h_{11} = -4.36 \times 10^9$ NC $^{-1}$
$g_{14} = -0.0182$ m 2 C $^{-1}$	$h_{14} = +1.04 \times 10^9$ NC $^{-1}$

$$\frac{e_{ij}}{h_{ij}} = \epsilon_{11}. \tag{21}$$

The notes to Table XXVIII give the relations between listed and unlisted components of the piezoelectric matrix. These data with the above relations enable us to work out most of the desired values.

4. Dielectric constants

Bechmann *et al.* (1962) give values of the dielectric constants as follows:

$$\epsilon_{11}^T = \epsilon_{22}^T = 39.97,$$

$$\epsilon_{33}^T = 41.03,$$

$$\epsilon_{11}^s - \epsilon_{11}^T = -0.76,$$

$$\epsilon_{33}^s - \epsilon_{11}^T = 0,$$

where the units are 10^{-12} F m $^{-1}$. Other authors quote values differing by up to 1.5% for ϵ_{11}^T and 0.7% for ϵ_{33}^T [see Landolt-Bornstein (1966)]. Bottom (1972) measured the dielectric constants and found $\epsilon_{11} = 39.93$ and

TABLE XXIX. The temperature coefficients of e_{11} and e_{14} at 25°C. Landolt-Bornstein (1966) gives $T_{e_{11}}^{(1)} = -160$ ppm °C $^{-1}$ and $T_{e_{14}}^{(1)} = -1440$ ppm °C $^{-1}$.

$T_{e_{11}}^{(1)}$	-300×10^{-6} °C $^{-1}$
$T_{e_{11}}^{(2)}$	-3600×10^{-9} °C $^{-2}$
$T_{e_{11}}^{(3)}$	-21000×10^{-12} °C $^{-3}$
$T_{e_{14}}^{(1)}$	-2450×10^{-6} °C $^{-1}$
$T_{e_{14}}^{(2)}$	-15600×10^{-9} °C $^{-2}$
$T_{e_{14}}^{(3)}$	-95000×10^{-12} °C $^{-3}$

TABLE XXX. Recommended lattice parameters at 25°C. Over small temperature ranges values can be calculated by taking $(da/dT)=6.7\times 10^{-5}\text{ \AA}^\circ\text{C}^{-1}$ and $[d(c/a)/dT]=-6.9\times 10^{-6}\text{ }^\circ\text{C}^{-1}$ and the rate of decrease of density with temperature as $9.2\times 10^{-5}\text{ K}^{-1}$.

Grade of quartz	Type	a (Å) ^a	c/a ^a	Cell volume (Å ³)	X-ray density (g cm ⁻³)
pure	natural	4.9127±2	1.100 13±4	112.96	2.6497
	synthetic	4.9134±1	1.100 13±2	113.01	2.6486
premium ($Q < 2$ million)	natural	4.9129±2	1.100 10±6	112.97	2.6495
	synthetic	4.9134±2	1.100 12±4	113.01	2.6486
medium ($Q \approx 1$ million)	natural	4.9132±3	1.100 04±9	112.99	2.6488
	synthetic	4.9136±3	1.100 08±6	113.02	2.6484
low ($Q < 1$ million)	natural	4.9138±5	1.099 92±12	113.02	2.6484
	synthetic	4.9138±5	1.100 04±10	113.03	2.6482

^aThe uncertainties quoted are in the last digit.

$\epsilon_{33}=40.73$ at 20°C with errors of ± 0.09 . These are probably the best available estimates of values at constant temperature. The variations of ϵ values with temperature are usually justifiably ignored in the calculation of resonator properties, but Landolt-Bornstein quotes temperature coefficients of 28 and 39 ppm $^\circ\text{C}^{-1}$ in the range 25°C to 100°C for ϵ_{11} and ϵ_{33} , respectively.

B. Defect-related properties

In this section, the presence of impurity atoms is regarded as a defect. The discussions in Secs. III.C and III.D showed that dislocation densities and the concentrations of impurities other than hydrogen both tend to increase with hydrogen content. Thus we can concentrate our attention on what happens to properties when the hydrogen content changes. However, it must be borne in mind when we do this that hydrogen may not be the direct cause of the effects reported: the causes could be other impurities or dislocations. Since quartz is usually specified in terms of infrared Q which is inversely proportional to the hydrogen content, we tend to use this parameter.

TABLE XXXI. The values of b_i in $a = a_0 + \sum b_i C_i$.

Impurity	b_i ($\mu\text{Å}$ per atomic ppm)
Fe	1
Cr	1
Ca	0.3
Mg ^a	0.2
Al ^a	0.2
Na	0.2
Ge	0.1
H	0.09
Ti	0.05
Li	0.01

^aThese values are applicable only to 2000 ppm. At higher concentrations these elements have small or even negative effects. Cohen and Summer (1958) suggest that at high concentrations some impurities sit on interstitial sites, which because of the channel in the quartz crystal structure does not necessarily involve much lattice dilation.

1. Lattice parameters and related properties

Brice (1980) has given a critical review of lattice parameter data and recommends the values given in columns 3 and 4 of Table XXX as being appropriate to various types of quartz. Note that here "pure" quartz is a hypothetical material (the data related to it are the result of extrapolation to zero impurity). It is believed that the spreads (shown as variations in the last digit) are real. Thus we expect the a values of premium synthetic quartz samples to vary over the range 4.9132–4.9136 Å and the c/a value to vary from 1.100 08 to 1.100 16. The calculated cell volume (column 5) varies very little and therefore the x-ray density in column 6 also varies very little. Reliable measured density values lie in the range 2.648–2.650 g cm⁻³ at 25°C. Frondel (1962) quotes an absolute density (i.e., value determined in vacuum in 2.6484 g cm⁻³ with an uncertainty of 5 in the last digit. He also gives a rate of decrease with increasing temperature of $(9.4\pm 0.3)\times 10^{-5}\text{ g cm}^{-3}\text{ }^\circ\text{C}^{-1}$ over the range 0°C to 35°C. The expansion coefficient data given in Sec. IV.A give a value of $(9.1\pm 0.3)\times 10^{-5}\text{ g cm}^{-3}\text{ }^\circ\text{C}^{-1}$.

Brice (1980) determined the coefficients a_0 and b_i in the relation

$$a = a_0 + \sum b_i C_i, \quad (22)$$

which gives the lattice parameter a as a function of the lattice constant a_0 of "pure" quartz and the concentration C_i of impurity i (measured relative to silicon). Values of a_0 are 4.912 69 Å for natural quartz and 4.913 37 Å for synthetic quartz. The values of b_i are given in Table XXXI. To calculate the effect of an impurity on c or c/a , it should be remembered that $d(c/a)/da$ is $-(0.20\pm 0.03)\text{ \AA}^{-1}$.

The fact that natural and synthetic quartz behave dif-

TABLE XXXII. Ranges of strains resulting from changes of a and c between zones in the same crystal.

j^*	$[(a_j - a_z)/a_z] \times 10^4$	$[(c_j - c_z)/c_z] \times 10^4$
r	0.6 to 1.4	-0.2 to +1.2
X	0.2 to 1.2	-1.4 to -0.4

TABLE XXXIII. Optical properties.

λ (μm)	0.4	0.6	1.0	3.0
refractive n_0	1.558	1.534	1.535	1.499
indices n_e	1.568	1.543	1.544	
$n_0 - n_e$	-9.6×10^{-3}	-8.8×10^{-3}	-8.8×10^{-3}	
$(dn_0/dT) \times 10^5$ ($^\circ\text{C}^{-1}$)	-0.477	-0.541		
$(dn_e/dT) \times 10^5$ ($^\circ\text{C}^{-1}$)	-0.557	-0.644		
$(dn_0/d\lambda)$ (μm^{-1})	-0.113	-0.029	-0.014	-0.028
$(dn_e/d\lambda)$ (μm^{-1})	-0.117	-0.030	-0.014	

ferently can be explained in two ways. First, synthetic quartz is typically grown at 350°C and natural quartz at a lower temperature (possibly 200°C to 250°C), so that the equilibrium defect densities will be different. Brice (1980) points out the difference in infrared spectra. The second possible mechanism is the difference in the growth mode. The synthetic quartz used is grown relatively quickly on rough faces. Natural quartz grew slowly on singular faces. In this context it is worth noting that synthetic quartz grown on singular faces has appreciably different lattice constants from material grown on the rough Z faces of the same crystal. Table XXXII gives some typical ranges of differences expressed as strains.

2. Optical properties

The optical properties of quartz are of little relevance to piezoelectric resonators. Table XXXIII gives the data which might be needed for polarizing microscope or infrared examination. Gray (1972, pp. 6-26 and 6-248) gives comprehensive tabulations, but there are significant differences between measured values, and I have measured significant changes in the birefringence due to the hydrogen content: if λ is the wavelength in μm and Q is the infrared quality factor in millions, the birefringence changes roughly as $4(\lambda^2/Q) \times 10^{-4}$, so that $n_0 - n_e$ changes by $2\lambda^2 \times 10^{-4}$ when Q changes from one million to two million. Here the wavelength λ is in μm .

V. BASIC DEVICE THEORY

A. General aspects

Much of the theory of quartz resonator design is based on the work of Christoffel (1877), who formalized the treatment of plane acoustic waves in anisotropic linear media. [Here *linear* means that the material properties do not vary with wave amplitude. For most quartz resonators it is reasonable to assume linearity at power levels up to about 100 μW , but some of the losses at surfaces are nonlinear even at these power levels, giving rise to drive level dependence (DLD).] Christoffel's work was extended by Lawson (1941) to include piezoelectricity, giving a theoretical base which could describe many cases in which single vibration modes were excited. Tiersten (1963) pro-

duced the exact solution showing that the three bulk waves were piezoelectrically coupled at the device surface. Tiersten (1969) gives a comprehensive review of the theory and Bottom (1982) gives a simpler one.

A general description of device theory lies outside the scope of this paper. Indeed, it is possible to "design" perfectly adequate resonators at least at high frequencies (above 10 MHz for fundamental mode devices) on the basis of very simple theory and tabulated data [e.g., those given by Ballato (1977)], and lower frequency devices can be designed on an empirical basis. The design of monolithic filters (several acoustically coupled resonators on one quartz blank) is best done with recourse to reasonably complete theory, but again an experienced semiempirical approach works. Many formerly theoretically naive small firms exist in the industry and their customers have only recently started to demand device performance which calls for near optimum design. In this paper I only outline the theory. Readers who wish to go further could usefully consult Mason (1950), Tiersten (1969), Holland and EerNisse (1969), Ballato (1977), Bottom (1982), and the many excellent reviews in the Academic Press (New York) series *Physical Acoustics*, edited in early years by W. P. Mason and in recent years by Mason and R. N. Thurston, and then move on to selected papers appearing in the *Proceedings of the Annual Symposium on Frequency Control* (which contains about half the relevant papers each year). For guidance to the more recent literature see Gerber (1979), Ballato *et al.* (1982), and Besson *et al.* (1982). Brice (1981) gives a simple outline of the theory as applied to simple structures and Ballato (1977) gives a more complete one. Both authors essentially assume an infinite quartz plate with electrodes of negligible weight and then look at the modifications that are produced by adding electrodes which have mass but which do not cause any viscous damping. This type of theory is quite useful provided that the lateral dimensions of the plate exceed its thickness by a large factor.

In an infinite solid it is possible to excite three types of waves. These can be approximately described as one longitudinal mode (with particle motion parallel to the propagation direction) and two shear modes (with particle motion normal to the propagation direction). In an anisotropic material like quartz in most propagating directions the modes are mixed—i.e., there may be three distinguishable waves but each has longitudinal and shear components. In a finite solid other vibration modes are

possible—e.g., plates can both flex and twist and waves can propagate on surfaces, but in the majority of commercial devices we use a slow shear mode.

The essential theoretical problem is to find the conditions under which standing waves exist and then to determine the way in which the resonant frequencies change with temperature. It is, of course, also necessary to be able to couple to the waves piezoelectrically. The approach used is to determine a wave velocity usually given by $(c_i/\rho)^{1/2}$, where c_i is an elastic stiffness appropriate to the wave⁶ and ρ is the density. We then look at the dimension h of the device in the appropriate propagation direction and find that there is a resonance condition when h is an odd number of half wavelengths. If this number is m , then we say that for $m=1$ we have the fundamental mode, $m=3$ is the third overtone, and so on. Ballato (1977) tabulates all the properties needed to describe bulk wave devices in this sort of theory and gives their variations with temperature. Thus we can easily calculate the resonant frequencies of a plate in the longitudinal mode or in either of the shear modes. In general, we are interested in a slow shear mode with small temperature coefficient of resonant frequency.

When we add electrodes to our plate, the theory becomes more complex. The resonant frequency falls (because the mass to be vibrated increases) and the temperature coefficient changes. However, these problems are familiar and we can draw on tabulated data to predict what effects the electrodes will have and with somewhat less reliability what will happen if we use a plate which is not a plane paralleliped. Particularly, at low resonant frequencies, say, less than 8 MHz, it is an advantage to have a device with curved faces [see Bennett (1960)]. Both convex surfaces and electrodes in the center of the face serve to concentrate the vibration in the center of the device. This energy trapping is important, since if energy leaks to the mounting devices, the resonator becomes lossy and its electrical Q_e falls. Energy loss to the electrodes and to the gas in the envelope enclosing the quartz can also occur. There are a number of semiempirical rules for minimizing the losses—e.g., there are preferred locations for mounting clips (at the nodes of possible spurious vibration modes), the use of polished surfaces (to give less energy scatter to spurious modes), the choice of electrode material, etc.

Even with perfect construction, real devices have some losses and these (as in all damped oscillators) cause a frequency change. The easiest way to look at the effect of losses is to consider the electrical equivalent circuit. Figure 14(a) shows an isolated device and Figs. 14(b) and

⁶Mason (1950) gives the method for calculating the value of c_i appropriate for the cut and mode of vibration. For cuts with $\phi=0$ (see Fig. 15 below) working in the slow shear mode (e.g., an AT-cut device) $c_i = c_{66}\cos^2\theta + C_{44}\sin^2\theta - 2C_{14}\sin\theta\cos\theta$, where θ is as defined in Fig. 15.

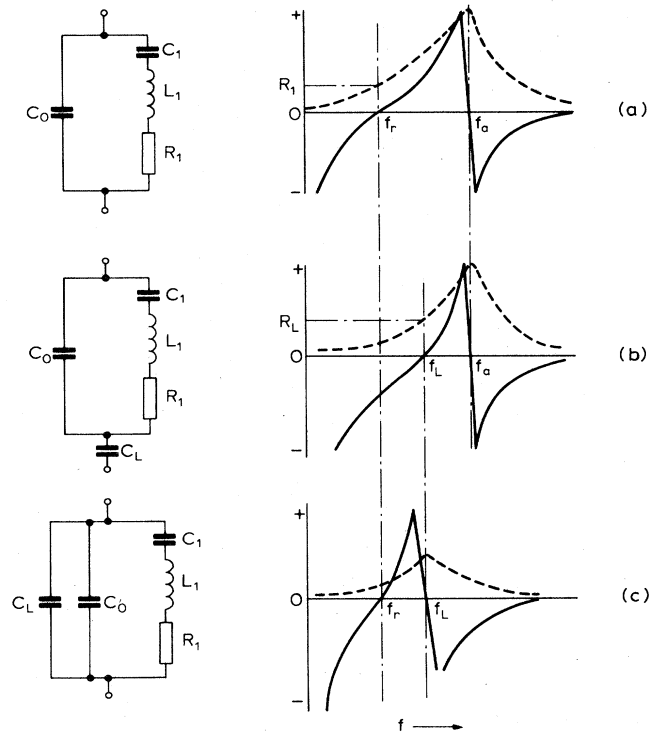


FIG. 14. The equivalent circuit of a quartz resonator and its behavior near to resonance is shown in (a). (b) The same for a device with a series-load capacitor C_L . (c) The same for a device with a parallel-load capacitor. In the right-hand diagrams the solid lines give the reactance and the dashed lines the resistance as functions of frequency. Typical equivalent component values are C_0 , 3–30 pF; L_1 , 2–20 fF; L_1 , 6–60 mH; R_1 , 5–50 Ω ; C_L , 5–60 pF. The use of the circuit in (c) is rare.

14(c) show more realistic circuits in which there is a load capacitor C_L . Table XXXIV relates the various quantities. In these circuits C_0 represents the static capacity of the device and L_1 and C_1 are related to the kinetic and potential energies of the resonating quartz. R_1 is com-

TABLE XXXIV. Relations between circuit parameters. Formulas (a)–(c) assume that R_1 is zero. The presence of a finite series resistance R_1 decreases f_r by an amount which is approximately $f_r C_0 R_1^2 / 2L_1$, which is typically a few parts per million of f_r . This is of importance only if R_1 varies, which can happen in devices with loose particles (dust, chips of quartz, etc.) on the plate surface.

$$f_r = \frac{1}{2\pi(L_1 C_1)^{1/2}} \quad (a)$$

$$f_a = \frac{1}{2\pi[L_1 C_1 C_0 / (C_1 + C_0)]^{1/2}} \quad (b)$$

$$f_L = \frac{1}{2\pi[L_1 C_1 (C_0 + C_L) / (C_1 + C_L)]} \quad (c)$$

$$R_L = R_1 (1 + C_0 / C_L)^2 \quad (d)$$

$$f_L - f_r \approx \frac{f_a C_1}{2(C_0 + C_L)} \quad (e)$$

$$Q_e = \frac{1}{2\pi f_r R_1 C_1} \quad (f)$$

posed of two components: the first and usually smallest is R_M^1 , the losses due to motion in the quartz which has a finite viscosity. The residue of R_1 represents all the other losses. These losses include significant components involving energy transfer to the electrodes, mounts, and gas ambient. Ballato (1977) justifies the use of these equivalent circuits near the resonant frequencies and derives the following values for a plate:

$$L_1 = h^2 / 8C_0 k^2 v_i^2, \quad (23)$$

$$C_1 = 8C_0 k^2 / \pi^2 m^2, \quad (24)$$

and

$$R_M^1 = \pi^2 m^2 \eta h / 8e^2 A, \quad (25)$$

where h is the plate thickness, k is the coupling constant (discussed later), v_i is the wave velocity, η is the viscosity of quartz, e is the piezoelectric coefficient, and A is the effective area of the electrode which is bigger than its physical area because there are significant fringing fields. The ranges of the various parameters can be very large, but typical values are 3–30 pF for C_0 , 2–20 fF for C_1 , 6–60 mH for L_1 , and 5–50 Ω for R_1 for $m=1$ at 10 MHz, are 1–10 pF for C_0 , 2–20 fF for C_1 , 10–20 mH for L_i , and 4–30 Ω for R_1 . Load capacitors are often in the range 5–60 pF.

The electrical quality factor of a device is

$$Q_e = (2\pi f R_1 C_1)^{-1}, \quad (26)$$

and typical devices have Q_e in the range 10^4 – 10^5 .

The coupling constant k is a function of the cut and the mode of vibration. It can be calculated from the elastic, piezoelectric, and dielectric constants [see Mason (1950)]. (Figure 17 below gives some calculated values.)

In a simple theory if the mass of one electrode is μ times the mass of the quartz between the electrodes, then a pair of electrodes of this weight changes the frequency of the device by a fraction equal to μ . This is a reasonable approximation for fundamental mode devices. For overtone modes the effect is much larger (e.g., a factor of 10 for a seventh overtone) [see Ballato (1977) and Ballato *et al.* (1982)]. The effect of mass loading on the temperature coefficient is that $\mu \approx 0.01$ produces a change by one or two parts in 10^7 . A more complete theory [Mindlin (1961, 1963), Tiersten and Mindlin (1962), and Suchanek (1982)] shows that for large values of μ and for large electrode to plate area ratios there are significant deviations from these simple ideas. See Ballato *et al.* (1982) for some examples.

The effect of electrode masses on resonant frequency is significant when we are interested in long-term stability. One monolayer of extra atoms produces an easily measurable frequency change. (In a typical case the change can be 0.1–1 ppm.) Thus if the electrodes outgas or become contaminated by material left in the sealed device, the device frequency will change with time. In this context material interchanged between the electrodes and the quartz can change the mass distribution and hence the resonant

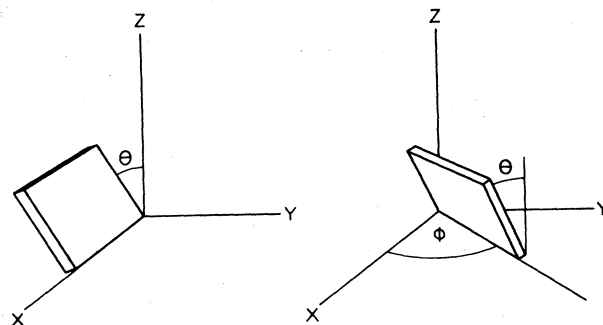


FIG. 15. The angles θ and ϕ used to define the cut of a crystal plate.

frequency. We have already mentioned that electromigration is a serious possibility.

In general, the metal electrodes are deposited by evaporation. This can result in significant strain in the electrodes which in turn can modify the elastic constants of the quartz and so change the resonant frequency. Thus strain relaxation has often been implicated in the aging of devices.

Finally, it is worth noting that the temperature coefficient of frequency is not a completely independent parameter. Differentiating the equations in Table XXXIV shows that the value of C_L is important. Thus trimming the frequency by varying C_L can push the equipment outside the hoped-for specification. Ballato (1979b) explores this aspect. Note also that C_L is temperature dependent: its temperature coefficient can easily be 100 ppm $^{\circ}\text{C}^{-1}$.

B. The AT cut

The cut of a crystal refers to the orientation of its faces with respect to the crystallographic axes. Most platelike crystals can be described conveniently in the θ, ϕ notation given in Fig. 15. For the AT cut, ϕ is nominally zero and small departures ($< 1^{\circ}$) from this condition have negligible effect on the temperature coefficient of frequency. If this coefficient is f_T , then $df_T/d\phi$ is zero at $\phi=0$ and the second differential is small. The value of θ has been a matter of some dispute. Depending on how you do the calculations, the theoretical value for an unelectroded plate is between about 35.25° and 35.33° . Practical values depend, as we have seen, on the electrode thickness,⁷ but for most purposes we can take a value in the range

⁷The experimental data suggest that the angle change as a function of mass loading is within a factor of 2 of what would be expected, which is for the required value of θ to increase by 0.1° for a mass loading of 3%. However, it should be noted that some materials, e.g., chromium, create strains which themselves change the required angle.

35.22°–35.27° for fundamental plane parallel devices with diameter to thickness ratios of 25 or more. For similar devices with smaller diameter to thickness ratios, the value of θ falls as the ratio decreases and is about 34.90°, for example, for a ratio of 10. Contouring the blank (i.e., making it lens shaped) increases θ for a fundamental crystal with a large diameter-to-thickness ratio to about 35.30°–35.35°. Contoured crystals with small diameter-to-thickness ratios can have much smaller θ values, say, about 35.0 for a ratio of 10. Overtone crystals with large diameter-to-thickness ratios need θ in the range of about 35.42°–35.48°, and those with small ratios require smaller angles. Here the θ values are those required to give zero first- and second-order temperature coefficients which occur at 27°C. Other angles mentioned in the literature correspond to obtaining zero first-order temperature coefficient at a different temperature. Figure 16 gives the frequency temperature characteristics; each curve is labeled

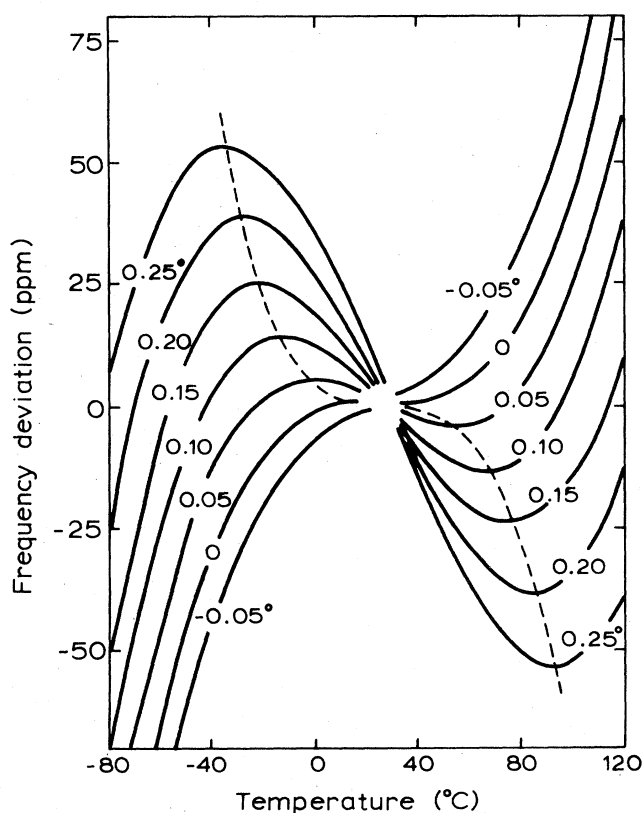


FIG. 16. The fractional deviation of frequency from the value at 25°C as a function of temperature for *AT*-cut devices. The parameter marked is the angle deviation in degrees from the value giving the curve marked 0. Note that the curves are drawn as if $d^2f/dT^2=0$ at 26°C. This is correct to $\pm 1^\circ\text{C}$ for flat or bevelled plates in their fundamental modes. Approximate temperatures for $d^2f/dF^2=0$ for the devices are 28°C (plates in overtone modes), 32°C (planoconvex devices), and 35°C (biconvex devices). The temperature scale can be moved horizontally to describe these devices (data supplied by W. S. Metcalf, Cathodeon Crystals, Linton, U.K.).

with the deviation from the values discussed here. Thus, for example, a plane parallel device with a large diameter-to-thickness ratio would follow the curve marked +0.25 if its θ angle were about 35.40°. This device would have a zero first-order temperature coefficient at about 90°C and if it were maintained in an oven at that temperature would perform well. However, many users do not wish to use ovens, because their products have to be inexpensive, for example, or because the power drain is not acceptable.⁸ If we look at the curve for +0.1°, we see that by making a device which follows this curve we can help such customers because in the range -55°C to $+105^\circ\text{C}$ the frequency change by only ± 15 ppm. Over smaller ranges we can do even better. Thus the curve for +0.05° deviates by only ± 5 ppm over a range from -30°C to $+80^\circ\text{C}$. Until recently most crystals sold were *AT* cut.⁹ In part this was because of the very desirable temperature characteristics just discussed. However, the other reason was connected with the coupling coefficient k , which is a variable in the relation for the equivalent circuit parameters. The coupling coefficient for a given mode of oscillation is defined in either mechanical or electrical terms so that

$$k^2 = \frac{\text{electrical energy converted to mechanical energy}}{\text{input electrical energy}}$$

or

$$k^2 = \frac{\text{mechanical energy converted to electrical energy}}{\text{input mechanical energy}}$$

Obviously, $k^2 < 1$ and for the cuts usually considered, $k^2 < 10\%$ for all modes. For the *AT* cut, k^2 for both the *a* and *b* modes is zero (see Fig. 17), producing a very significant advantage: the response frequency plot contains responses for only the fundamental *c* mode and its overtones. Thus there is very little chance of a spurious resonance's being established. However, while the *AT*-cut family of devices is and will continue to be very useful, these devices do have some disadvantages. In particular, they are very sensitive to strains due to mechanical and thermal stresses. Vibration, acceleration, temperature gradients, and temperature changes, as well as construction faults (electrode and mounting strains which can change with time), all produce very easily discernible frequency changes. Designers have worked very hard to minimize these problems, but except under unrealistically favorable conditions, frequency variations of order 0.01 ppm are almost unavoidable. Also, it is not possible to

⁸Note that it is possible to design circuits in which a varactor diode is used to compensate for temperature variations.

⁹Until the sales of digital watches became significant, 90% of crystals sold were *AT* cut. The residue were mostly low-frequency devices, e.g., *NT*-cut devices.

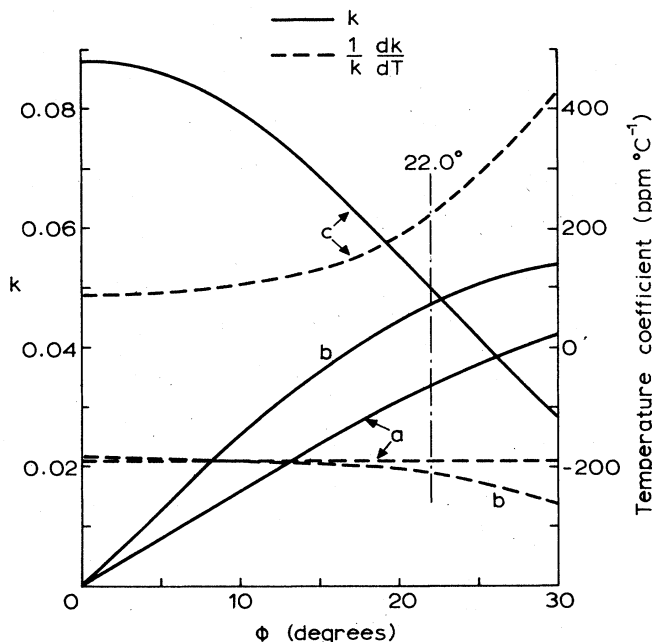


FIG. 17. The coupling coefficient k and its temperature coefficient as a function of φ along the AT -to- SC locus. Figure 18 gives the corresponding θ values.

make small low-frequency devices,¹⁰ and although k^2 is not large for the AT c mode, there is still a large effect of circuit conditions on the resonant frequency. Thus we have to look at other cuts.

C. Other cuts

Only a limited number of cuts have zero (or very small) temperature coefficients, and further restrictions on the choice of cuts can be imposed by stating that the zero coefficient must occur at a reasonable working temperature. Here let us impose an even greater restriction: we shall look only at platelike devices using a slow shear mode. We shall then be limited to the AT to SC locus defined in Figs. 17 and 18 (and its extension to higher φ values), but the negative θ loci involving the BT cuts (with θ, φ values of about $-49.20, 0$) and the RT cuts (near to $-34.50, 15$) should also be mentioned. See Ballato (1977) for more detail about these cuts.

¹⁰This is a slight overstatement and is correct only for plate-type resonators. Using the AT cut in a bar-type resonator allows much smaller dimensions, and such devices can have excellent frequency-temperature characteristics. Okano *et al.* (1981) show frequency changes of ± 1 ppm in the range -20°C to $+70^\circ\text{C}$. However, such resonators have many possible vibration modes and designing them is not easy.

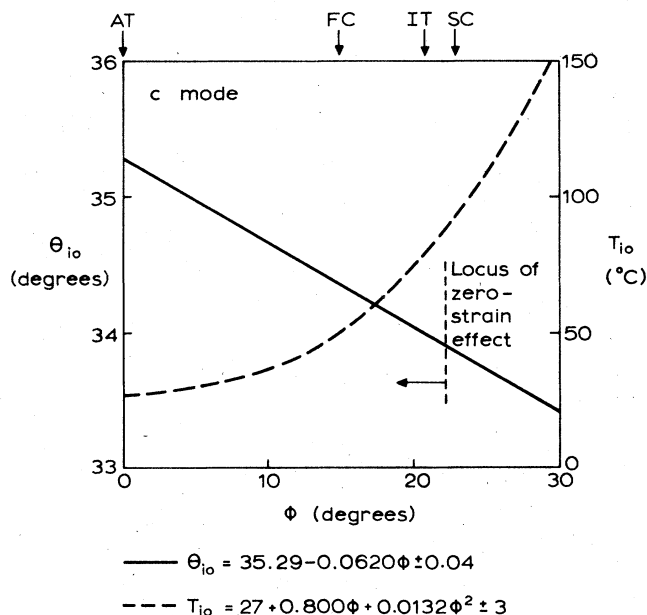


FIG. 18. The value of θ_{10} is the value of θ to give zero first- and second-order temperature coefficients of frequency, and T_{10} is the temperature at which this point of inflection occurs. The spreads of values indicated are the deviations between calculations carried out in different ways by Ballato (1977) and G. Simpson and R. F. Milsom (Phillips, Redhill, unpublished). The results strictly apply only to large plane-parallel devices without electrodes. Data obtained with 10-MHz devices with very thin electrodes show the same spreads, possibly because of the difficulty of measuring both θ and φ accurately, but there are indications that some of the spreads may be real, i.e., be caused by technological factors—electrode and mounting strains, for example. The dashed line in this figure represents the locus of orientations (in θ, φ coordinates) for which there is no effect of strain. At larger values of φ , θ_{10} is not single valued. See Hruska (1983).

As Fig. 18 shows, moving along the AT to SC locus away from the AT cut to the FC , IT , and SC cuts raises the temperature of the inflection point. Even with devices in ovens it is an advantage to work at the inflection point rather than a minimum in the frequency-temperature curve. (The fact that both the first- and second-order temperature coefficients are zero gives a much longer range of temperatures in which the frequency does not change appreciably.) A bigger advantage, however, is that in the region of the SC cut, strain in the device does not affect the frequency. The locus of zero strain effect is shown as a dashed line in Fig. 18. Strain can arise from bad technology (electrode strains, mounting strains), from unfavorable environments (vibration and acceleration), or from thermal stresses (temperature gradients or temperature variations which create gradients as heat flows in and out of the quartz). These effects are discussed by Keyes and Blair (1967), EerNisse (1976), Kusters and Leach (1977), Ballato *et al.* (1977), EerNisse *et al.* (1978), Balla-

to (1979), Fletcher and Douglas (1979), Brice and Metcalf (1982), and many others. The conclusions are that cuts near the *SC* cut have significantly better properties (good frequency stability in unfavorable situations, lower aging, etc.) but are more difficult to make (both θ and φ have to be closely controlled) and require better designed circuits (the *b*-mode frequency is near the *c*-mode frequency and it is possible to excite either or even both modes). There seems to be little doubt that in many critical applications the *SC* cut will replace the *AT* cut, but the *AT* cut will still be widely used in applications where cost is critical.

As reference to the various volumes of the *Proceedings of the Annual Symposium on Frequency Control* shows, many other cuts have been developed for various special purposes. In particular, many cuts using nonshear modes have been developed to give very small devices operating at low frequencies, e.g., the edge mode devices (Vangheluwe and Fletcher, 1981). It seems unlikely that any of these cuts will be widely used in the same way that the *AT* cut has been used for the last few decades.

VI. DEVICE CONSTRUCTION

In this section, as in Sec. V, we shall concentrate attention on plate resonators. Extension of the ideas to monolithic filters fabricated on plates is obvious. Much of the

discussion can also be made relevant to other resonators, e.g., bar types. Plate resonators and filters made on plates currently constitute about 90% of the market by value and probably by number. The only significant market for nonplatelike devices is for very small devices, e.g., watches.

A. Blank preparation

1. X-ray orientation

As noted in the theory section (V.B), it is necessary to have the face of a plate accurately parallel to a particular orientation. (The exact angles to be cut depend on details on the device design—size, mode, electrode mass, surface curvature, etc.) The accuracy needed varies with the type of resonator and its application but as an order of magnitude we can consider 0.01° , which is equivalent to an error of order $0.1 \text{ ppm } ^\circ\text{C}^{-1}$ in the device temperature coefficient or a change of 6°C in the position of the minimum in the frequency-temperature coefficient. For an *AT* cut we need only one accurate orientation angle. For a doubly rotated cut, we need two accurate angles. Methods exist which allow angles to be measured with precisions of about 0.002° (Darces and Merigoux, 1978; Clastre *et al.*, 1978; Kobayashi *et al.*, 1978). Bond (1976) and Heising

TABLE XXXV. Intense x-ray reflections from α -quartz.

Reflection <i>hk.l</i>	Intensity ^{a,b}		Bragg angle ^c (deg)	θ^d (deg)
	Positive <i>l</i>	Negative <i>l</i>		
01.0	24	24	10.4297	0
01.1	100	41	13.3200	38.2103
01.2	2	14	19.7336	57.5781
01.3	5.5	3	27.6631	67.0506
02.0	18	18	21.2267	0
02.2	10	2	27.4375	38.2103
02.3	32	63	34.0719	49.7397
02.6	17	4	68.2081	67.0506
03.1	18	1	34.1575	14.7031
03.2	19	27	37.8306	27.6908
03.4	6	3	51.9358	46.3867
04.3	3	7	57.2378	30.5581
04.4	12	1	67.1550	38.2103
05.2	1	24	71.6142	17.4783
11.0	13	13	18.2733	0
11.1	4	4	20.1461	24.4417
11.2	17	17	25.0703	42.2706
12.2	9	3	33.8722	30.7558
12.3	6	1	39.9417	41.7525
22.0	1	1	38.8364	0
22.3	5	5	49.3731	34.2839
22.5	6	6	71.6569	48.6492
23.2	0.4	2	57.0325	19.8594
23.4	26	4	76.7728	35.8442

^aIntensities are expressed as percentages of 01.1.

^bReflections with intensities < 1 include 00.3, 00.6, 11.3, 11.4, 11.5, 11.6, 12.0, 12.1, 12.5, 12.6, 13.0, 13.1, 13.2, 13.3, 13.4, 13.5, 14.0, 14.1, 14.2, 14.3, 22.1, 22.2, 22.4, 23.0, 23.1, 23.3, 24.0, 24.1, 33.0, 33.1, and 33.2.

^cBragg angles are for Cu $K\alpha_1$ at 25°C .

^dThese are face angles in θ, φ notations. For values of φ see Table XXXVI.

TABLE XXXVI. Possible values of φ for various reflections.

φ^0	Reflection	Approximate θ values ^a
0	$0k.l$	0,15,17,28,31,38,46,49,58,67
19.1067	$12.l$	31,42
23.4133	$23.l$	20,36
30.000	$hh.l$	18,20,25
36.5867	$23.\bar{l}$	20,36
40.8933	$12.\bar{l}$	31,42
60.000	$0k.\bar{l}$	0,15,17,28,31,38,46,49,58,67
79.1067	$12.\bar{l}$	31,42
83.4133	$23.\bar{l}$	20,36
90.0000	$hh\bar{l}$	18,20,25

^aFor exact values see Table XXXV.

(1946) discuss the basic x-ray methods used and Bond and Kusters (1977) describe the basic method used to obtain the two accurate angles needed for doubly rotated cuts. For the AT cut, the strongest reflection in the lattice 0111 is usually employed. Tables XXXV and XXXVI give a list of possible reflections. The practical problems are severe: refraction effects are significant, variations in lattice constant (Brice, 1980) need to be considered, and exact alignment of equipment (Asanuma and Asahara, 1980) is necessary. Anyone thinking of getting involved with really accurate work should read these eight papers and some of the background references which they quote.

A crystallographic face in quartz can be written ($hkil$). Symmetry dictates that

$$h + k + i = 0. \tag{27}$$

Thus one index is redundant and usually i is omitted to give a face written ($hk.l$). A reflecting plane is usually written without parentheses, i.e., $hk.l$. The set of faces ($hkil$), ($ihkl$), and ($kihl$) are equivalent: they represent the effects of the threefold axis. The twofold axes produce a further three equivalent faces ($hkil$), ($hkil$), and ($hkil$). Finally, for x-ray purposes only, Friedel's law suggests that the reflections from one side of a plate are the same as those from the other, so that $hk.l$ is equivalent to $hk.l$. Friedel's law is an approximation in structures like that of quartz which have no center of symmetry. However, the effects are small: the intensities vary by only a few percent and the intensities are identical if the plane is parallel to a twofold axis. Thus one set of indices $hk.l$ represents up to twelve reflections. Note that there is one restriction: faces ($000l$) give reflections only if l is a multiple of three—i.e., 0003 and 0006 are the only planes of this type which will reflect the radiation. Tables XXXV and XXXVI give most of the possible reflections. In these tables, since $hk.l$ is equivalent to $kh.l$, the values listed are restricted so that $h \leq k$. These tables give the values of θ and φ (see Fig. 15) deduced from

$$\sin\varphi = \frac{h\sqrt{3}}{2(h^2 + k^2 + hk)^{1/2}} \tag{28}$$

and

$$\tan\theta = \frac{a\sqrt{3}}{2c(h^2 + k^2 + hk)^{1/2}}. \tag{29}$$

The lattice parameters a and c were chosen to give $a=4.9134 \text{ \AA}$ and $c/a=1.0012$ with errors in the last places of 2 and 4, respectively (i.e., they are values for high-grade quartz).

To a first approximation, Bragg's law may be written

$$\lambda = 2d \sin\theta_B, \tag{30}$$

where for $\text{Cu } K\alpha_1$, the wavelength λ is 1.5405974 \AA with an error usually assumed to be about 1 ppm; but, as Hart (1981) has pointed out, the wavelength scale for x rays is not consistent. The interplanar spacing d is given by

$$d = \frac{a}{[(\frac{4}{3})(h^2 + k^2 + hk) + l^2 / (c/a)^2]^{1/2}}. \tag{31}$$

Any solid has a refractive index for x rays given by $1 - \delta$, where

$$\delta = 2.71 \times 10^{-6} \rho \lambda^2 \sum Z / \sum A, \tag{32}$$

where ρ is the density, λ is the wavelength (in \AA), $\sum Z$ is the sum of the atomic numbers of all the atoms in a unit cell, and $\sum A$ is the equivalent sum of the atomic weights. For quartz

$$\delta = 1.44 \times 10^{-5} \lambda^2 \tag{33}$$

or for $\text{Cu } K\alpha_1$

$$\delta = 3.43 \times 10^{-5}. \tag{34}$$

Allowing for refraction changes Bragg's law to

$$\lambda = 2d \sin\theta_m (1 - \delta / \sin^2\theta_m) (1 - \delta) \tag{35}$$

or

$$\lambda = 2d \sin\theta_B (1 - \delta / \sin^2\theta_B), \tag{36}$$

where θ_m and θ_B are the apparent Bragg angle and its calculated value, respectively (see Fig. 19). For small values of Δ and Δ^1 (defined in the figure) and small δ , the following approximations for angles in radians are

$$\theta_m = \theta_B + \delta \cot(\theta_B + \alpha), \tag{37}$$

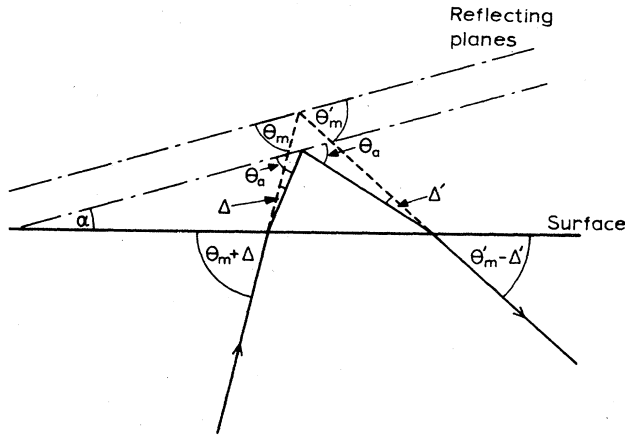


FIG. 19. Refraction effects in x-ray measurements.

$$\theta_m^1 = \theta_B + \delta \cot(\theta_B - \alpha) \tag{38}$$

These corrections are significant and the second one is larger than the first, so if we do one measurement we should choose the setup shown in the upper part of Fig. 20. However, we have the possibility of doing two measurements, i.e., measuring the angle change between the upper and lower parts of Fig. 20. If α is in degrees, the correction for the measured α to the real one is $6.94 \times 10^{-5} \alpha / \sin^2 \theta_B$. More generally, for angles in radians

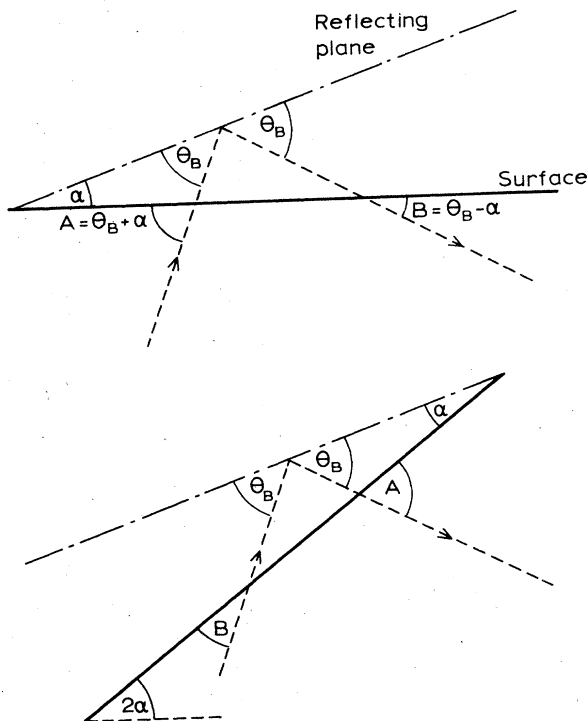


FIG. 20. X-ray reflections in quartz, ignoring refraction effects. Taking refraction into account makes $A = \theta_m + \alpha$ and $B = \theta'_m - \alpha$.

$$2\alpha 1 = 2\alpha \pm \delta [\cot(\theta_B + \alpha) - \cot(\theta_B - \alpha)] \tag{39}$$

where the positive sign is taken when we measure A before B . This type of double measurement has a number of advantages. For example, when only a single measurement is made, the value of θ_B needs to be known and it changes measurably with the purity of the quartz, the measurement temperature, and the amount of tilt. The tilt is the angle (t) which the plane being measured makes with the normal to the plane which is defined by the x-ray beams. A tilt t reduces θ_B by about $(1 - \cos t) \tan \theta_B$ radians (e.g., for $\theta_B = 45^\circ$ and $t = 2^\circ$ the change in θ_B is about 0.035°).

2. Cutting

Given an accurately oriented boule on a cutting jig, the next stage is to saw the boule into a set of oriented blanks. This is often done with a slurry saw, which is basically a set of reciprocating tensioned steel blades over which during cutting a slurry of silicon carbide or alumina abrasive in water is poured. The alternative cutting machines use rotating diamond wheels which cut either at the outside edge (peripheral wheels) or at an inside edge (annular wheels). In all cases, particularly when the saws have been in use for some time, the cuts are V shaped and the blanks are tapered. Clearly this causes the faces to be misoriented and can introduce errors in face orientation of up to, say, 0.03° . The amount of misorientation can be minimized by mounting the boule on a glass plate and continuing the cut into this "waster." However, it is in practice difficult to avoid errors of about 0.01° from this source. Table XXXVII gives cutting yields which show a pronounced dependence on the Q of the raw material.

3. Lapping

After cutting, one cuts or grinds the blanks to the desired lateral dimensions unless the boule was trimmed to size before cutting. The semifinished blanks are then lapped (or occasionally ground) to nearly the desired thickness. A typical lapping process involves upper and lower metal laps and the blanks are placed between the laps in a plastic carrier (i.e., a sheet of plastic with holes a little larger than the blanks and a thickness less than the final thickness needed). An abrasive slurry is fed between the laps and the thickness is often monitored by connecting a radio receiver between the upper and lower laps (which now have to be insulated appropriately). The action of the abrasive is sufficient to produce a piezoelectric signal at the resonant frequency of the blank. Manufacturers regard the details of the lapping process as trade secrets and most have empirically optimized their processes. Several factors are important. The process inevitably produces a further degradation of orientation which even with an optimized process varies with the material used. This effect does not appear to be correlated

TABLE XXXVII. Approximate^a cutting yields as a function of method, thickness, and Q .

$Q \times 10^{-6}$	Yield %			
	Slurry saw		Rotating saw	
	1 mm	0.5 mm	1 mm	0.5 mm
> 2.2	95-98	92-97	90-95	70-90
≈ 1.8	80-90	80-85	70-90	60-70
≈ 1.0	70-90	70-75	50-70	40-60
< 0.5	40-60	30-60	40-60	20-40

^aThese data represent the types of results obtained with a reasonably optimized process. The values given are approximately the upper and lower quartiles reported. The data come from many sources using different processes and yields, particularly with rotating saws, depend very strongly on the process

with Q . Different high- Q (greater than two million) batches produce different results. Possibly, dislocation density may be the important parameter. Typically the angle change is 0.01° – 0.02° and its direction is largely predictable: the spread of orientations increases only slightly but the mean orientation changes significantly. Inevitably the lapped blanks are not flat. The edges are thinner than the centers. Comparing a thickness 1 mm from the edge (which is usually appreciably rounded) with a thickness at the center usually reveals a few microns' difference. The difference is related to the mean abrasive size and is typically a small fraction (<0.2) of the abrasive particle diameter. A slightly curved surface is not usually a disadvantage. Deliberately curved surfaces are produced either by using curved laps (for small radii of curvature) or by tumbling (for radii of a few cm). Tumbling involves putting the blanks in a tube with an abrasive. The tube is then rotated about its axis and the axis is rocked slowly through an angle of, say, $\pm 10^\circ$ to $\pm 20^\circ$ from the horizontal. The process is slow, so that blanks can be removed every few hours to see if they are near the final thickness required. The radii of curvature

of the surfaces are both ultimately equal to the radius of the tube. Lapping processes damage the surface. Figure 21 gives the depths of damage found for a double-sided lapping process and a grinding process. The smaller amount of damage done by grinding is due to the fact that the abrasive is embedded in the wheel. The amount of damage depends slightly (say, $\pm 50\%$) on the pressure between the blank and the lap and on the abrasive used: silicon carbide does more damage than alumina. Surface damage is undesirable. Manufacturers remove the damage either by using successively finer abrasives finishing with a submicron abrasive (i.e., polishing) or by etching. With regard to polishing, the exact mechanisms involved are not well understood. It should be noted that polishing to a visually satisfactory finish does not guarantee removal of all surface strain. Figure 22 illustrates this point by giving the x-ray rocking curve widths of a set of samples

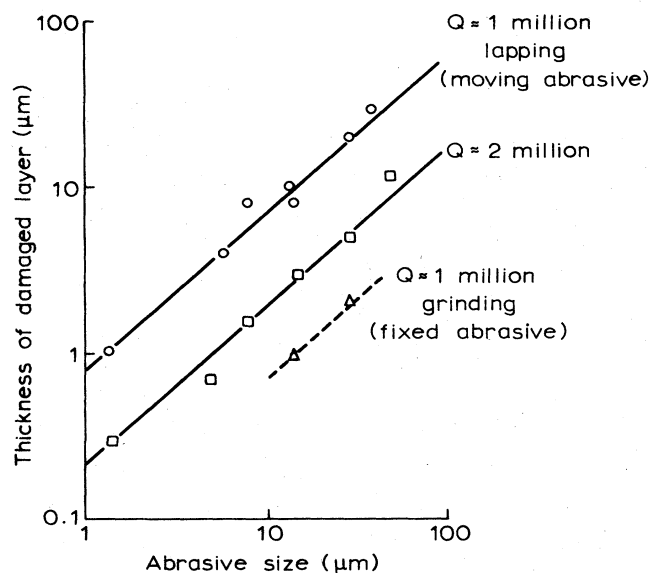


FIG. 21. Thickness of the damaged layer on quartz as a function of abrasive size.

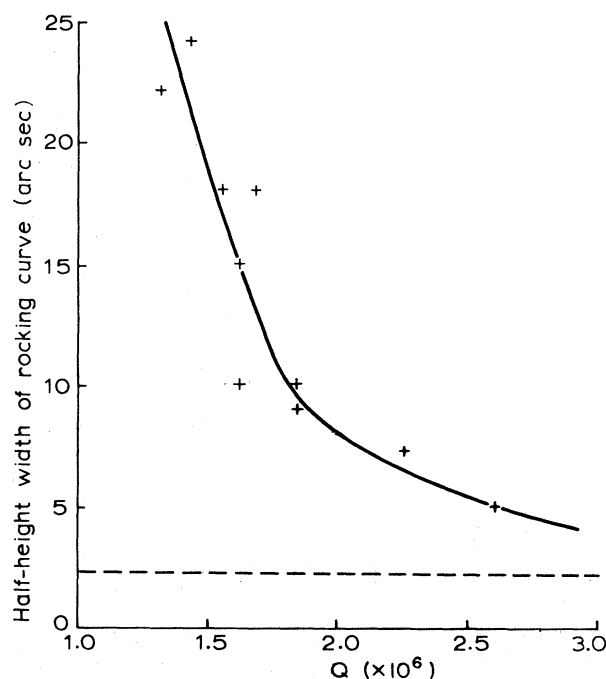


FIG. 22. The half-height widths of x-ray rocking curves as a function of Q for samples polished to a "mirror" finish, as judged by the eye.

(for infrared measurements) as a function of infrared Q . It can be seen that for low- Q samples very significant strains remain.

4. Etching

Etching is another complex technology. The final surface needed is smooth. Roughness with an amplitude or wavelength comparable to about one-tenth of the wavelength of the elastic waves in the quartz will cause appreciable scattering of the energy in the wave and will degrade the device performance (Q_e falls, R_1 rises). However, some manufacturers like a slightly rough surface to provide a "key" for the electrodes. Certainly it is necessary that in the final device there should be no loose particles of either quartz or the electrode materials. Failure to meet this condition results in drive level effects [R_1 and f vary with the input power; see Knowles (1975)]. However, with appropriate cleaning before the electrodes are applied a polished surface will retain its electrodes. Etching depends on many parameters.

(a) The nature of the etchant: fluorides—e.g., ammonium fluoride or ammonium bifluoride—are commonly used, but hydrofluoric acid and caustic soda have also been used successfully.

(b) The etchant concentration: the rate etching and the surface finish depend critically on this parameter. Typical concentrations are 0.5–10 moles per liter.

(c) The nature of the quartz: most etchants preferentially attack the quartz around dislocations, and it is possible to form a channel linking both faces of a blank (an "etch tunnel"). For this reason natural quartz with low or zero dislocation density is sometimes preferred. Certainly, low dislocation densities are desirable. Increasing the temperature changes the spread of etching rates in a batch of blanks. Typical spreads are 50% at 25°C and 25% at 55°C. The etches giving the most uniform rates give spreads of about 25% at 25°C and 12% at 55°C. The advantage of a high temperature is obvious. However, since we want to apply a constant (or as near as we can get to a constant) thickness of electrodes, the spread in the etch rates provides a problem. For example, to maintain the thickness of the quartz constant to 0.1% over the batch, we cannot etch more than 0.8% of the thickness—i.e., the maximum removal is limited to 0.4% of the thickness on each side. Thus for a 10-MHz device we can etch only about 0.6 μm from each face.

(d) The temperature: common choices range up to 75°C. Apparent activation energies for fluoride-based etchants range from 23 to 44 kJ mol^{-1} . Thus rates of etching at 55°C can range from 2.5 to 5 times the rates at 25°C. With ammonium bifluoride, excess etchant is often added, so that the etching temperature will also fix the concentration.

(e) The amount of surface damage: damaged material etches more rapidly than undamaged material, so that the rate of etching of a lapped blank is initially high and then falls and finally becomes constant (see Fig. 23).

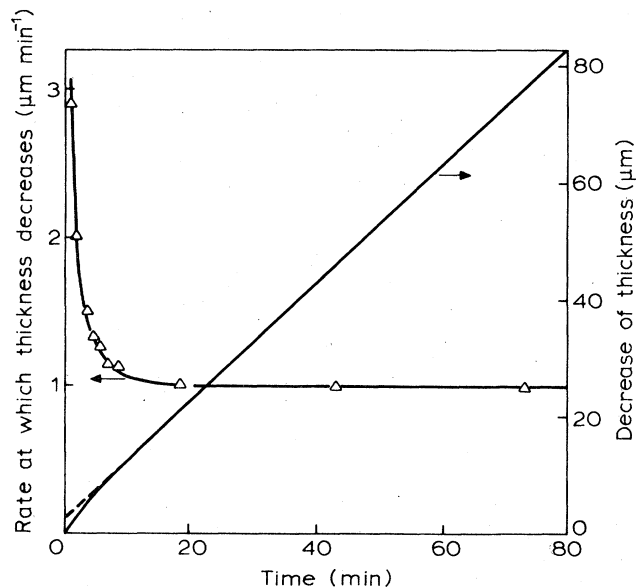


FIG. 23. Etching rate and amount removed as a function of time. The etchant used was a saturated aqueous solution of ammonium bifluoride at 80°C. Unpublished data produced by J. R. Cox (Philips, Redhill).

(f) The nature of the face being etched (i.e., its orientation): for example, rates of etching for a 5.4 molar solution of ammonium bifluoride at 25°C are $0.015 \mu\text{m h}^{-1}$ (on an X face and a Y face), $1.1 \mu\text{m h}^{-1}$ (Z face), and $0.48 \mu\text{m h}^{-1}$ (AT blank face). Faces more than 5°–10° from a natural (singular) face etch at about the same rate as the Z face. With many etchants the final form of an AT face is stepped with (0111) trends and risers which appear to be Y and X faces. The ratio of step length to riser height depends on many parameters but ratios of about 20 are common. The mean face orientation changes slowly with etching time.

(g) Additives: sugar, glycol, and various detergents are often added to "improve" the performance of an etch. There appears to be a real advantage in adding a detergent: perhaps it removes small amounts of grease which would otherwise make the etching less uniform. As a percentage of blanks unbroken after cutting, the yields of blanks after lapping and etching are very similar to the cutting yields in Table XXXVII. Thus there is a very clear economic advantage in using high- Q material.

When thin wafers are needed, the problem of "etch tunnels" linking both faces can be serious. As already mentioned, low dislocation density material can be used to give reasonable yields. It is also found that in "swept quartz" (i.e., material which has been subjected to solid-state electrolysis) there are fewer channels. Sweeping is known to remove some impurities, particularly alkali metals, so that perhaps only decorated dislocations give rise to deep pits.

As far as obtaining an accurately oriented blank is concerned, it is clear that each of the necessary processing

steps causes a loss of accuracy and that the batch of blanks produced will have an appreciable spread. (In some cases a histogram of number in a particular angular range can even have two maxima.) However, at the stage of the nearly finished blank the manufacturer can recover a lot of the loss by remeasuring the orientation and classifying the blanks into angular ranges.¹¹ The blanks nearest the target orientations are then used for the most critical applications. Inevitably this wastes some blanks which can perhaps be reprocessed for use in higher-frequency devices but which are mostly sent for scrap. Remeasuring and classifying with the scrapping of out-of-tolerance blanks is cheaper than making out-of-specification devices.

B. Electrodes

Electrode materials are usually applied by evaporation but sputtering is occasionally used. Evaporation has the advantage that the electrodes contain no gases. (We have already seen that changes in the electrode weights are extremely undesirable.) The most popular electrode material is silver. Gold is used in some high-quality devices. Other materials, e.g., evaporated aluminum or copper and sputtered chromium, have been used. It has been reported that aluminum and chromium cause some problems. The oxides of both elements have free energies of formation which exceed that of quartz, and they might therefore reduce the surface of the quartz. However, it is likely that the poor results obtained by some workers are due to strains. Aluminum is commonly used for high-frequency devices, for which its low density is an advantage. Electrodes are usually applied in two stages. First a keyhole-shaped basecoat is applied to both faces. The shaft of the key is used as an electrical connection. The second stage is to apply a circular coat over the central region. This is done with the device operating, and the deposition is stopped when the frequency falls to the target value.

C. Mounting and encapsulation

The quartz plate is held in some mount which serves as a mechanical holder and also provides the electrical connection. Often the blank is held in the clips by a cement (silver-loaded epoxy resins or water glass are common choices but polyimides have some advantages). The type of mount used depends on the application of the device. Two-, three-, and four-point mounts are used. The positions of the mounts can be optimized to minimize the effects of the inevitable tensile or compressive forces or the twisting and bending moments which can be applied. Ballato *et al.* (1977), EerNisse *et al.* (1978), and Fletcher

and Douglas (1979) gives résumés of the theory and practice in this field. See also Mingins *et al.* (1963) and Lee *et al.* (1976).

Finally, the device is sealed in a case, which can be made of glass, ceramic, or metal. The metals used include stainless steels, plated mild steel, copper, and nickel. The final seal can be made by soldering, cold welding, or resistance welding. Ceramic cases have given excellent results but are uncommon. It is possible to compare the other enclosures in terms of long-term stability, but it should be noted that very large variations can occur. The following results are widely quoted: if solder-sealed enclosures have unit stability, resistance-welded devices will be four times better, cold-welded devices will be eight times better, and glass enclosures will be ten times better. The results obtained in practice depend on the final stages of treatment. For example, baking the components in vacuum before use always increases long-term stability. Similarly, the ambient in the enclosure is important. The best results are obtained in a high vacuum, but some manufacturers use dry nitrogen, hydrogen, or helium. The use of a gas ensures that the blank heats rapidly to its operating temperature. For fairly small enclosures the time constants range from about 80 sec for an evacuated glass enclosure down to about 10 sec for a helium-filled metal enclosure.

D. Manufacturer's and user's responsibilities

Most of the important device properties have now been introduced and the factors to which they are sensitive have been mentioned. Here I collect these two sets of parameters and introduce a few additional ideas necessary for the discussion in Sec. VII. I also introduce some new evidence to illustrate relations not previously demonstrated adequately.

The first parameter always specified is the device frequency. To a first order of approximation this is fixed by the thickness of the quartz blank. It depends also of course on the blank orientation, but, as we have seen, the device manufacturer does not usually measure the thickness directly; instead he measures the resonant frequency, and with reasonable technology at the lapping stage a spread of resonant frequencies after lapping should be about $\pm 0.4\%$. After etching, because of the spread of etching rates the spread of resonant frequencies will be larger, but not enormously larger: a spread of $\pm 0.5\text{--}0.6\%$ is a reasonable target.

To a second order of approximation, the device frequency is fixed by the mass of the electrodes. As we have seen, the manufacturer trims the frequency by adding a little extra mass. At this stage any reasonable device should be within 50 ppm of the target at the adjustment temperature, and a good device should be within about 5 ppm of the target. Note that at this stage the target may differ from the device's operating frequency to allow for the difference in temperature and ambient pressure, and a good manufacturer may well set this target to allow for other factors so that when the device is delivered it will be

¹¹Before electrodes are applied, a light etch is desirable.

within the target range specified by the customer. Note that the customer's target must allow for the load capacitor. Figure 24(a) shows a typical variation of frequency with load capacitor for an *AT*-cut device. Other cuts can have smaller changes. Note that Fig. 24(b) shows that the pullability

$$S = \frac{1}{f_L} \frac{d(\Delta f)}{dC_L} \quad (40)$$

falls as C_L increases. Thus, since C_L will vary, there is an advantage in using a large value of C_L .

So far, the technological factors involved are only the obvious ones of quartz size and electrode mass. We now turn to the third-order approximations for the device frequency and look at some of the more subtle effects.

The customer will specify an allowable frequency variation with temperature, either in terms of a temperature coefficient or the position of an extremum in the frequency-temperature plot. To a first approximation these factors are fixed by the blank orientation, so that the spread of, say, temperature coefficients is strongly correlated with the spread of orientation. However, the mass of the electrodes and the value of the load capacitor

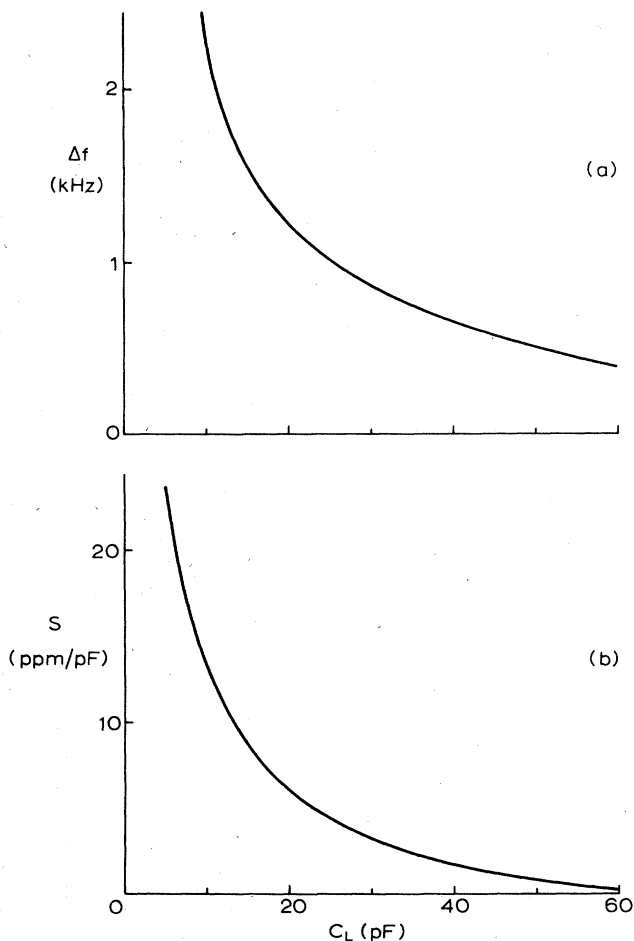


FIG. 24. Frequency change Δf as a function of C_L and pullability [$S = (1/f_L)(d\Delta f/dC_L)$] as a function of C_L .

also have significant effects. The value of the load capacitor is controlled by the user, and in attaining the target frequency, the device maker has already made use of the electrode mass. Thus to attain a target behavior the only free parameter is the spread of orientations. Thus if the manufacturer cannot achieve the desired behavior by controlling the orientation, he must revise his targets for the blank thickness and surface curvature or electrode mass. Note that if the frequency-temperature plot is not smooth, poor technology has been used or an error made in the device design.

The next parameter fixed by the customer is the constancy of frequency with time, i.e., the aging characteristics of the device. Device aging is a subject which can lead to animated discussion among device makers. The main problem is that many factors are involved and that these factors are not independent so that it is possible to have present two or more factors which change the frequency in different directions as a function of time and thus obtain spuriously good aging over a particular time interval.

The study of aging is obviously time consuming and thus most aging studies make two assumptions. The first is that aging is temperature dependent in a predictable fashion. Although making presumptions without knowing the exact mechanisms involved is clearly dangerous, it is useful and in a large-scale manufacturing context (moderate technology) it works. For small-scale high technology operations it may not be valid. Typical assumptions are that about 25 days at 85°C is equivalent to a year at room temperature and that about 30 days at 110°C to 130°C is equivalent to a year at 85°C. The other assumption is that the rate of aging falls with time.

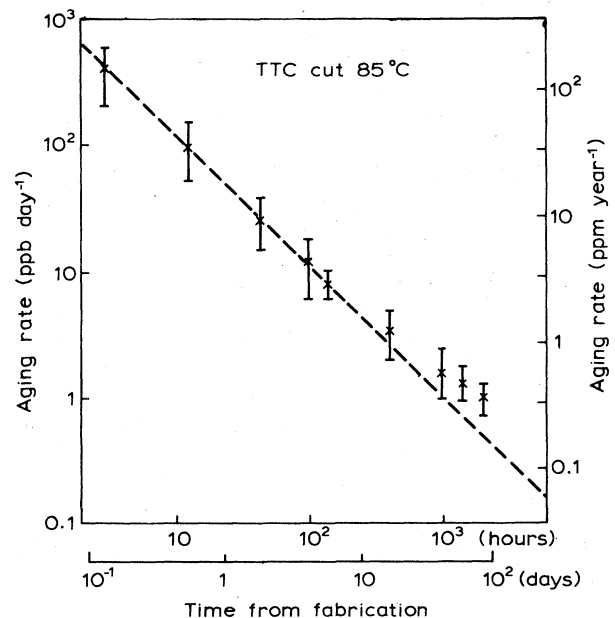


FIG. 25. Aging rate as a function of time from fabrication.

TABLE XXXVIII. Data on diffusion of electrode materials into quartz. The measurements were made using Rutherford back scattering.

Annealing temperature (°C) ^a	Copper ^c		Penetration (Å) ^b		Silver ^c		Gold ^c	
	polished	lapped	polished	lapped	polished	lapped	polished	lapped
400	1000	1400	1200	2200				
300	160	500	250	1200	250		1000	
200	60	130	100	300	80		250	

^aThe samples were annealed for 6 h.

^bAbsolute accuracy probably a factor of 2. Relative accuracy $\pm 25\%$.

^cPolished samples were finished on Syton. Lapped samples were finished on 15- μm alumina.

Two mathematically equivalent forms are used. The first states that the frequency change in each time decade is constant—i.e., with times measured from the time of manufacture the measured change from day 1 to day 10 is equal to the change from day 10 to day 100, which in turn is equal to the change from day 100 to day 1000, and so on. The second form is to say that the logarithm of the rate of aging is inversely proportional to time. Figure 25 shows that this second form is only an approximation, and indeed many plots for individual devices show that devices which initially show an increase of frequency with time can, after some time has elapsed, show a decrease of frequency with time.

With regard to aging, it is generally agreed that two factors are of prime importance (Hafner and Blewer, 1968), but these can be subdivided (Besson *et al.*, 1982). The first factor is changes in mass distribution and the second is changes in strains. These are not always completely independent.

Consider first changes in mass distribution. We have already seen that adding or removing one monolayer from the electrodes changes the frequency very significantly. Thus any volatile material on or in the electrodes or on the case and able to reach the electrodes can change its location (particularly when the device's temperature changes: during heating the case is hotter than the electrodes, and during cooling the case is cooler). Hafner and Blewer (1968) have shown the excellent results which can be attained by high vacuum processing, eliminating all contact with fingers and similar greasy sources of contamination. Because contamination with organic materials is so common, Vig (1976) developed a method involving exposure in air to short-wavelength ultraviolet light which locally creates ozone and literally burns away organic material. Most manufacturers submit blanks to rigorous cleaning and the use of vacuum baking of all components before final assembly has been mentioned earlier. Similarly, particulate matter must be removed, e.g., by ultrasonic cleaning. (Failure to do this can lead to step changes in frequency, as discussed later.)

Changes in the mass distribution can occur which do not involve mass transfer between the blank plus electrodes and the case of the ambient gas. Many electrode materials can move into quartz by diffusion which is greatly enhanced by surface damage (see Table XXXVIII). Movement from the electrodes can be

enhanced by electric fields which can also move impurities in the quartz. Brice and Metcalf (1982) report reversible time-dependent effects due to the movement of lithium in devices exposed to electric fields. This is a different effect to the instantaneous frequency change due to a field which can produce changes of a few ppb per volt (Hruska, 1980). Thus the device manufacturer must produce devices with undamaged surfaces on pure quartz blanks, but the user has a responsibility for not exposing devices to electric fields, particularly changing ones. Note that the dc resistance of a typical quartz resonator is greater than or comparable to the dc resistance of most capacitors, so that a simple blocking capacitor is not ade-

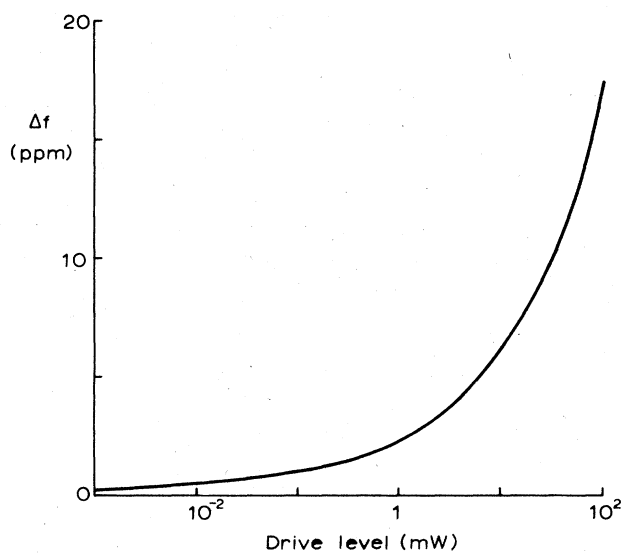


FIG. 26. The variation of frequency with power level for a typical AT device. Data from Philips (1982). At low powers, the frequency change Δf is probably a result of the variation of elastic constants with strain. This effect will also be noticeable at high power levels when there can also be effects due to heating. The rate of loss of heat from a typical quartz blank is 10–100 mW cm^{-2} per degree by which the blank temperature exceeds the case temperature. Thus with a power input of 100 mW the temperature of the blank can be 1°C to 10°C above the case. This is why large devices are needed at high power levels.

quate protection. A resistor (say, 10^6 or $10^7 \Omega$) in parallel with the resonator and a blocking capacitor in series with this parallel combination should not affect the behavior of the circuit but will protect the device from electric fields.

Jaroslavsky and Lavrentsov (1982) have shown that aging rates rise at high power levels, and here *high* indicates $100 \mu\text{W}$ or more. Thus crystal users have a responsibility for minimizing the power level if good aging characteristics are required. Note in any case that frequency changes with power level (see Fig. 26).

Turning now to strain related effects, we can note first that electrode or impurity migration can be enhanced by strain. Impurities cause lattice-constant changes and these changes can cancel elastic strains. Even if material migration and other long-term stress relaxation processes cause no mass distribution effects, the relaxation of stress causes frequency changes. Some cuts of quartz are more sensitive to strains than others. The *SC* and *TTC* cuts were developed with this in mind. With moderate technology these cuts are typically a factor of 5 better than *AT* devices made using identical technology. For example, Brice and Metcalf (1982) report aging rates of 1 ppb day⁻¹ for *TTC* devices and 6 ppb day⁻¹ for identically processed *AT* devices. Thus the device manufacturer has a responsibility for optimizing electroding and mounting to minimize strain or for choosing cuts which show small strain effects. However, the user also has some responsibilities in this field: acceleration, vibration,¹² temperature gradients, and temperature changes all produce stresses in the active region of the device and even power level changes can produce frequency changes (Fig. 26) so that the user must either eliminate these effects or specify (and be prepared to pay for) a device which will withstand them.

Users would like devices with good short-term stabilities or noise performance. The factors which govern these parameters have not been completely isolated. Obviously, the electrical Q of the device is involved. Cuts which show small strain effects give better performance. Devices which are superficially the same but come from different suppliers differ in performance so that technological factors must be involved. Low-noise devices can be made but it seems likely that the sophisticated technology used is more elaborate and expensive than necessary. Besson *et al.* (1982) discuss these problems and make it clear that both circuit and device parameters are involved.

Table XXXIX summarizes the circuit design factors which must be taken into account when high performance is needed.

¹²A frequently discussed parameter is the response of the device to low-frequency vibration (microphony). Appropriate choices of cut, mounting orientation, and mounting methods and materials can significantly reduce microphony.

TABLE XXXIX. Design factors for high-performance circuits.

- (1) Use the specified value of C_L to attain the desired frequency and frequency-temperature variation.
- (2) Specify a large value of C_L to reduce variations caused by changes in C_L . (Note that C_L is the total capacity seen by the device, not just the capacitance of the component labeled *load capacitor*.)
- (3) Use as low an operating temperature as possible to reduce aging but remember that at low temperatures hysteresis may occur.
- (4) Maintain a constant operating temperature (even small rapid temperature excursions affect some devices).
- (5) Use a low power level to reduce aging, but remember that at low power levels the noise performance can be severely degraded.
- (6) Use a constant power level (frequency is a function of power level).
- (7) Minimize the dc voltage across the device to eliminate frequency changes caused by electromigration.
- (8) Keep the dc voltage across the device constant (frequency depends on voltage).
- (9) Specify a high device Q for good noise performance.

VII. THE RESULTS OBTAINED USING REAL CRYSTALS

A. The measurement of infrared Q

Quartz is usually specified in terms of an infrared Q which is sometimes called a material Q or more often just Q . This quantity is the electrical quality factor (Q_e) of as nearly as possible an ideal device, which is specified as follows.

Frequency: 5 MHz \pm 5 kHz, 5th overtone.

Cut: *AT* 2°51' \pm 2' from the *z* (minor rhombohedral) face rotated in the direction of the *Y* cut.

Quartz: cut from the *Z* zone.

Crystal Element: 14 mm diameter, planoconvex, radius of curvature 50 mm, finished to a polish.

Electrodes: 8.5 mm diameter, silver or gold, plate back $2kz$ (i.e., the mass of the electrodes decreases the resonant frequency by $2kz$).

Supporting points: at the intersections of the *Z* axis with the periphery.

Seal: in vacuum $< 10^{-3} \text{ N m}^{-2}$.

The Q_e value of these or similar devices can be correlated with infrared absorption in the quartz, as was shown by Sawyer (1972), Fraser and Dodd (1966), Rudd and Houghton (1966), Toyo (1975,1977), and others. Brice and Cole (1978,1979) have studied the measurement of the infrared Q which is well correlated with the hydrogen content of the crystal. Indeed, the general belief is that the important parameter is that part of the infrared absorption which depends on the hydrogen content.

The parameter actually measured is an extinction coefficient α , which is defined so that with a sample of thick-

ness t , the fraction of the incident light transmitted is

$$T = \frac{(1-R)^2 10^{-\alpha t}}{1-R^2 10^{-2\alpha t}}, \quad (41)$$

where R is the reflection coefficient of the surface. For quartz R is about 0.04 but depends on the surface finish. The coefficient α is a function of frequency (usually quoted as a wave number ν). From the work of Kats (1962a,1962b) and others it is known that the frequencies of interest are 3585, 3500, and 3410 cm^{-1} . [See Brice and Cole (1978) for other possible frequencies.] In order to deduce α from a plot of T against ν (easily obtained using a double-beam spectrometer) it is apparently necessary to use more than one sample having different values of t . Doing this is time consuming and involves expensive sample preparation if the values of R are not to change between samples. However, since R is small and we can find a value of ν (ν_{ref}) with very low absorption, we can approximate to the formula defining α_ν by writing

$$\alpha_\nu = [\log_{10}(T_{\text{ref}}/T_\nu)]/t. \quad (42)$$

If, at ν_{ref} , α is exactly zero, the fractional error is $R^2 10^{-2\alpha_\nu t}$, which should be less than $(0.04)^2$. The usual values of ν_{ref} are in the range 3800–3900 cm^{-1} . Brice and Cole (1978) showed that at these frequencies there is a small absorption ($0.025 \pm 0.002 \text{ cm}^{-1}$) which has to be added to the value given by Eq. (42) so that the best easily measured value of α_ν is

$$\alpha_\nu = [\log_{10}(T_{\text{ref}}/T_\nu)]/t + 0.025, \quad (43)$$

when α_ν is in cm^{-1} . However, α_ν depends on polarization (and all spectrometers produce light which is slightly polarized). Brice and Cole (1979) showed that if two measurements of α_ν were made and the sample was rotated by 90° about the beam axis between the measurements, then the mean of these measurements was a constant depending only on the sample and not on the initial angle between the polarization and some reference direction (say, the optic axis) in the sample. If we write α_1 and α_2 for the α values deduced using (42), then from (43) we obtain a best estimate

$$\alpha_\nu = \frac{1}{2}(\alpha_1 + \alpha_2) + 0.025. \quad (44)$$

However, we do not wish to know α_ν ; we want only that part α_ν^* which is related to the hydrogen content. Direct absorption of energy by the lattice is likely and could be significant. Brice and Cole (1978) and Brice (1984) showed that comparing data at 3585 and 3410 cm^{-1} with results at 3500 cm^{-1} (on which most prior calibrations had been based) gave lattice absorptions of zero at 3585 cm^{-1} and 0.044 at 3410 cm^{-1} . (Note that these values are strictly extra contributions: we cannot be certain that there is no lattice absorption at 3500 cm^{-1} .) The value of the lattice absorption causes us to overestimate α^* . Thus the best estimates of α^* are

$$\alpha_{3500}^* = [\log_{10}(T_{\text{ref}}/T_{3500})]/t + 0.025, \quad (45)$$

$$\alpha_{3585}^* = [\log_{10}(T_{\text{ref}}/T_{3585})]/t + 0.025, \quad (46)$$

TABLE XL. Value of C in the relation $Q = C \times 10^5 / \alpha_{3585}^*$.

Spectrometer resolution (cm^{-1})	C
≤ 1.2	1.60
1.4	1.56
1.6	1.46
1.8	1.41
≥ 2.0	1.39

and

$$\alpha_{3410}^* = [\log_{10}(T_{\text{ref}}/T_{3410})]/t - 0.019, \quad (47)$$

and the various α_ν^* are related by

$$\alpha_{3410}^* = 1.25\alpha_{3500}^* \quad (48)$$

and approximately

$$\alpha_{3585}^* = 1.03\alpha_{3500}^*. \quad (49)$$

The second of these relations is approximate, because the measured value of α_{3585}^* depends on the resolving power of the spectrometer used. An empirical correction for this will be given. Using these data in the relations between Q and α_ν given by the previously quoted workers gives

$$Q = C \times 10^5 / \alpha_\nu^*, \quad (50)$$

where

$$C = 1.35 \text{ for } \nu = 3500,$$

$$C = 1.69 \text{ for } \nu = 3410, \quad (51)$$

and the values of C for 3585 cm^{-1} are given in Table XL. These relations have now been tested on several hundred samples in five establishments using a total of seven spectrometers (some of which were used in different modes, so that different resolutions in the range 0.6–4 cm^{-1} were obtained). On any one machine the Q values obtained at the various frequencies were the same to within on average about 7% in the range $0.3 < Q \times 10^{-6} < 3$.¹³ Measuring Q on the same sample on different instruments gave agreement to within an average 7–10%. These results are consistent with the expected experimental errors of 5–7% in the individual measurements. Thus we have a consistent method to produce a Q value but it should be noted that the scale given by (50) is not universally accepted. In the critical range (1.8–2.0 million) divergences between the scales are generally only 10% and at most 20%.

¹³Above an apparent Q of 2.5 million, the value of Q determined at 3585 cm^{-1} systematically exceeds the values determined at other wave numbers. This divergence reaches 7% at $Q = 3$ million when a spectrometer with a resolution of 1.7 cm^{-1} is used.

It should be noted that while the device Q of a nearly ideal device is well correlated with the infrared Q , the correlation is not perfect and the scatter of the data is larger than we would like to admit as being caused by experimental error. Thus some other factor may influence the device Q . One possibility is the dislocation density (see Sec. VIII.E).

B. Device properties affected by Q

We have already noted that on a statistical basis we expect that as the infrared Q falls, the concentrations of most impurities rise, dislocation densities increase, and the material becomes more fragile. Thus to separate effects caused by these parameters from ones due intrinsically to the material Q is likely to be difficult.

Obviously from the definition of Q (Sec. VII.A) the Q_e of a nearly ideal device will correlate well with material Q . Most resonators now manufactured are far from ideal: the majority of devices fabricated in large numbers have Q 's in the range from 20 000 to 200 000. If we write the electrical quality factor Q_e of the device in the form

$$\frac{1}{Q_e} = \frac{1}{Q} + \sum_i \frac{1}{Q_i}, \quad (52)$$

where the Q_i are related to the electrical and mechanical energy losses in the electrodes, at the quartz surface, and to the mounts, then for a constant processing schedule we might expect that the Q_i values would be constant. Consider now two cases calculated on this basis. We use first a material with $Q=1$ million and make devices with $Q_e=2.7 \times 10^4$. Without otherwise changing the process we substitute material with a Q of 2 million. We then expect Q_e to increase by about 2%. However, from the data in Fig. 27 we find an increase of about 17%. The second example involves using material with $Q=1$ million to make devices with Q_e about 2×10^5 . The expected change on substituting material with $Q=2$ million is about a 10% rise in Q_e . However, from the published data of Asahara and Taki (1972) our experimental finding is an increase of 20%. Thus we find that as the material Q rises, the quality factor of the devices (Q_e) rises faster than is consistent with Eq. (52) if all the Q_i terms are constant. Thus at least one of the terms Q_i must depend on Q or a parameter correlated with Q .

The fact that device yield falls with Q has already been illustrated (Table XXXVII), and Fig. 21 showed that the depth of damage increases as Q falls. A consequence of this is that a damage removal process which works well for a high- Q material may easily not be satisfactory for lower- Q materials.

Brice *et al.* (1981) carried out a systematic study of the influence of Q on device properties for $1.3 < Q \times 10^{-6} < 2.6$. They examined batches of identically prepared devices and looked at the equivalent series resistance R_1 , the variations of R_1 and resonant frequency with power level [using four parameters, Δf and ΔR , which are the differences between extreme values, and hf

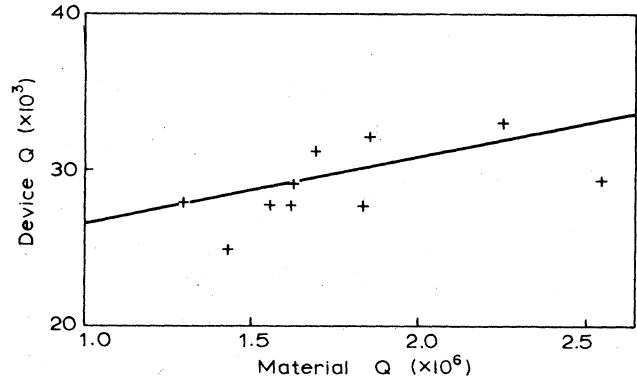


FIG. 27. Device Q as a function of material Q .

and hR , the maximum differences between values with power increasing and decreasing (see Fig. 28)], and the temperature coefficient. They also looked at the spreads of these quantities. Figures 28–32 outline their results. They also found that

$$hR_1 = (0.9 \pm 0.3) \Delta R_1, \quad (53)$$

$$hf = (0.9 \pm 0.6) \Delta f, \quad (54)$$

and

$$\Delta f = (9.5 \pm 6.0) \Delta R_1, \quad (55)$$

where Δf is in hertz and ΔR_1 is in ohms. Clearly Δf and hf are vital quantities. The power range (six decades) used is more than would be encountered in practice. Changes over one decade are typically factors of 6 and 3 less, respectively. These results show quite clearly that below $Q=1.8$ million, average values deteriorate and production spreads increase. It is also noticeable that at

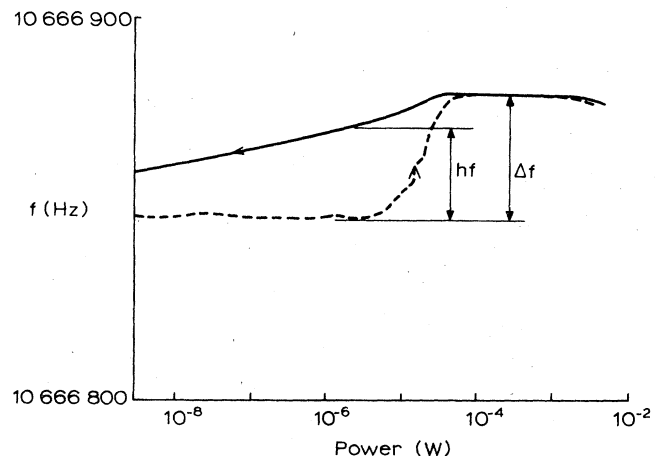


FIG. 28. The variation of frequency with power level for a device, showing drive-level dependence. Note that the power levels are low compared with those in Fig. 24. Note also that the parameter Δf is not the same in the two figures. In this figure Δf is the total frequency deviation, and hf is the maximum difference between values for power increasing and power decreasing.

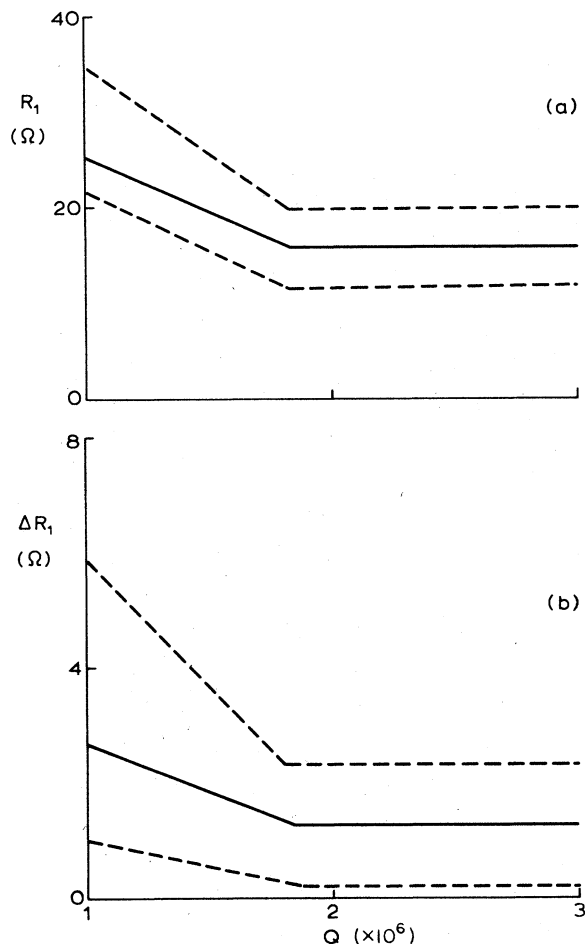


FIG. 29. The variation of R_1 and ΔR_1 with material Q . The solid lines are the median values and the dashed lines are the upper and lower quartiles.

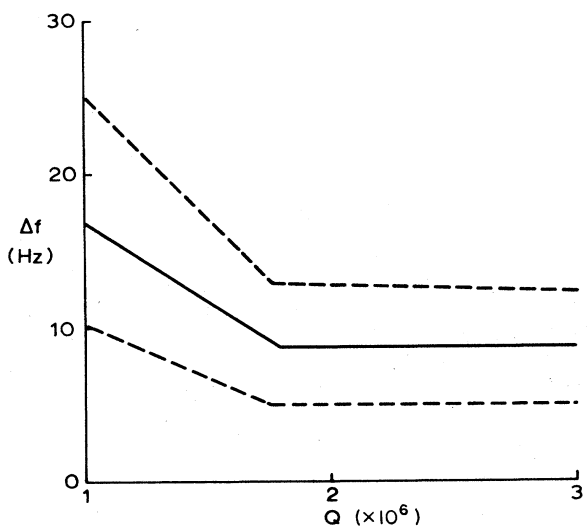


FIG. 30. The variations of Δf with material Q . The solid line is the median and the dashed lines are the upper and lower quartiles.

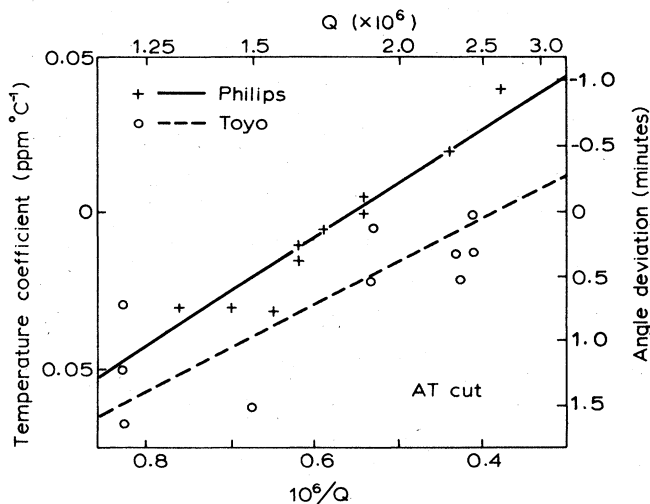


FIG. 31. The variation of temperature coefficients (left-hand axis) or the apparent deviation of angle from the expected (right-hand axis) as a function of Q . The differences between the two sets of data are probably not significant: the angles cut may well not have been the same.

high- Q values the distributions are symmetrical (probably Gaussian) but at low- Q values the spread of results is decidedly asymmetric. Clearly with any reasonable specification the production yields would deteriorate rapidly. Consider, for example, a specification calling for R_1 to be less than 25Ω . For $Q > 2$ million the yield would be about 90%. At $Q = 1.75$ million it is 75%. At $Q = 1.4$ million it is 50%, and for $Q = 1$ million it is 25%. As discussed earlier, the effect on R_1 is probably largely but not entirely due to the extra damping by low- Q material. The residual effects on R_1 could be attributed to strain or

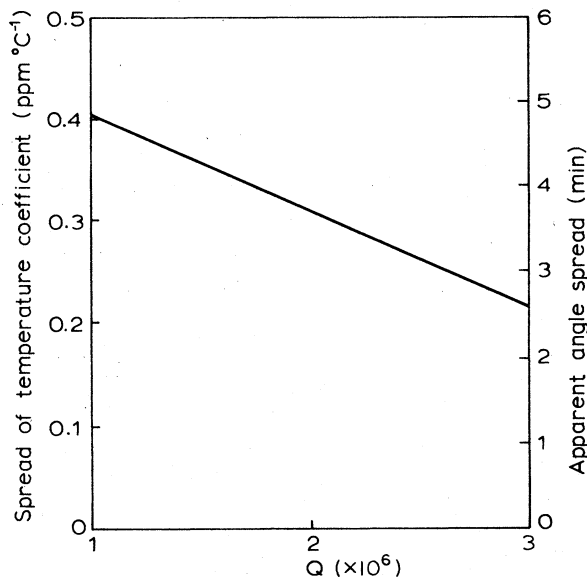


FIG. 32. The spread of temperature coefficients (measured as the standard deviation) as a function of material Q .

perhaps dislocations. The deterioration of ΔR_1 and hR_1 could reasonably be attributed to damage's leaving loose chips on the quartz surface. Note that after a device has been run at a high power, ΔR_1 is much less. Figure 28 refers only to the first cycle of power increase followed by power decrease. Subsequent cycling gives values of ΔR_1 and hR_1 which are much smaller. The degradation of Δf and hf found as Q falls can be directly accounted for by the changes in ΔR_1 and hR_1 (see Table XXXIV). These results are particularly marked because they refer to production techniques which are barely adequate. Better technology (particularly lapping and etching to ensure that all surface damage is removed) makes the effects much less marked although still discernible.

The results in Fig. 31 relating to temperature coefficients can be interpreted as showing a change in the effective value of the angle of cut θ . Similar data due to Asahara and Taki (1972) are plotted as circles and a dashed line. The differences between the two sets of data in terms of the mean parameter angle are not significant: they merely represent minor errors in target setting. However, the slopes of the trend lines are significant and strongly suggest that an angle change does occur and that over the Q range considered the angle change is of order 0.02° .

From the results given here and earlier, it is apparent that a material Q of about 1.8 million is in some way critical. The use of material with a much higher Q does not bring significant advantages, but the use of a material with a much lower one can bring very significant disadvantages which become more onerous as the Q falls. However, Q is not the only parameter involved, so we shall now consider others.

C. The effect of impurities

The effect of hydrogen has already been discussed. The only other impurities likely to be present at over 1 ppm relative to silicon are carbon, aluminum, lithium, and sodium (see Tables IX and X).

There appears to be no information about effects due to carbon or its location on the lattice. As a substitutional impurity it should be harmless (no charge compensation would be needed and it should diffuse slowly). As an interstitial impurity its small size and mass would allow rapid diffusion. Since crystals grown by the carbonate process contain much more carbon than ones grown by the hydroxide process, and since it seems no one has said that carbonate process material is markedly inferior to hydroxide process material,¹⁴ we can conclude that carbon is not likely to be a source of trouble.

Both lithium (Brice and Metcalf, 1982) and sodium (Iwasaki and Kurashige, 1982; Warner *et al.*, 1965) seem

to have deleterious effects—caused, apparently, by their high mobility in the devices [see Filler *et al.* (1984)].

It has been known for many years that the presence of aluminum degrades the behavior of quartz devices subjected to ionizing radiation. Other more mobile impurities may also affect performance, since it is known that swept quartz (see Sec. III.C) behaves better in high radiation fluxes. Taking the logarithm of the fractional frequency change per rad as a guide figure, for natural quartz we get -11 , for high-grade ($Q > 2.2$ million) synthetic quartz we get -11.5 , and for swept quartz about -12 .

Thus for most purposes using high-grade quartz we need only worry about the lithium and sodium contents, which in critical applications (low aging, high fields) may need to be well below 1 ppm. If high radiation fluxes are unavoidable, a more widespread purity specification may be needed.

D. The effect of inclusions

Asahara *et al.* (1975) have studied the effects of inclusions on device properties and have found that in material with $Q > 2.4$ million, inclusions in the active region of a device had little effect on any device parameter, even when the total volume of the inclusions was 0.2% of the volume of the sample. They recommend that for a wide range of applications densities in the size ranges > 100 , 70–100, and 30–70 μm should not exceed, respectively, 1, 4, and 8 cm^{-3} . However, it is noteworthy that their devices were plates about 200 μm thick and that the largest recorded inclusion size was 100 μm . Inclusions with sizes equal to the plate thickness almost certainly could not be accepted. In practice, significant inclusion densities are rare in the bulk of high- Q boules. High densities in the seed veil are more common and lead to dislocation formation. See Secs. III.B and III.D. Dislocations are undesirable, first intrinsically (see Sec. VII.E) and because they tend to be decorated with hydrogen, giving a low Q . Thus isolated crystals with prominent seed veils in a batch which gave high- Q values on a few test samples may be atypical and should probably be discarded.

E. The effect of dislocations

As mentioned earlier, heavily dislocated crystals machine differently from low-dislocation ones. Here *high* means of order 10^4 cm^{-2} and *low* means of order 10^2 cm^{-2} . Thus mixtures of high- and low-dislocation density boules could create problems in a production environment: the two types would require different cutting angles to accommodate the different changes in orientation during lapping. There is also some evidence to suggest that highly dislocated crystals crack at lower thermal shock values. See Fig. 33 but note that this correlation may be a consequence of the correlations on Figs. 4 and 6 between Q and dislocation density and between thermal shock and Q .

¹⁴My colleagues at Philips have looked for differences and failed to find them.

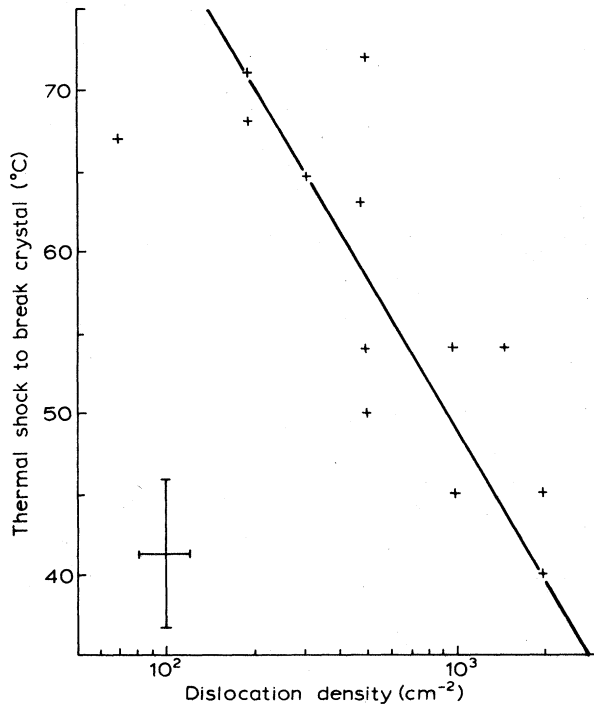


FIG. 33. The correlation between thermal shock necessary to break a boule and the dislocation density.

The material near a dislocation is strained and a high density of dislocations may change the etching characteristics. Again this could adversely affect a production line.

A single dislocation and its strain field should not appreciably affect the operation of a resonator, but arrays of dislocations may well do so, and Bye and Cosier (1979) list such arrays as defects affecting the Q of the device. They actually use the equivalent series resistance R_1 as the key parameter in their discussion of 1.4-MHz devices. Looking at their topographs¹⁵ shows that resonators with obviously low dislocation counts ($< 10^2 \text{ cm}^{-2}$) had R_1 values from 124 to 219 Ω and that ones with obviously high densities ($> 10^4 \text{ cm}^{-2}$) had R_1 in the range 209–614 Ω . Thus there does seem to be a significant effect.

If we assume that the increase in R_1 is due to energy scatter by the dislocations, we can propose that for efficient scattering the spacing between dislocations should be significantly less than the wavelength of the sound wave, say, by a factor of 4. Since the velocity of sound in quartz is about $3 \times 10^5 \text{ cm sec}^{-1}$, the wavelength at a frequency f (MHz) is $0.3/f$ (cm) and the critical density of dislocations should be about $80f^2$ (cm^{-2}). Since Bye and Cosier were studying 1.4-MHz devices, the critical concentration would be about 300 cm^{-2} in their case. See Brice (1984) for further discussion.

¹⁵Dr. Bye provided me with copies of all the topographs taken during the study.

F. Other parameters affecting devices

We have already shown that the resistance to fracture is an important parameter which affects performance and yield. This parameter depends on Q and possibly dislocation density and is therefore not an independent variable.

Bye and Cosier (1979) show that growth striations affect R_1 adversely. Growth striations are bands of strain resulting from variations in the growth rate of the crystals. Modern temperature control equipment makes this a rare phenomenon, which is most easily revealed by x-ray topography. Any batch of crystals giving consistently high R_1 values should be examined for this effect, which should not vary much from crystal to crystal in the batch. Thus one topograph of a Y -cut or an AT -cut sample should be sufficient to establish whether the effect is present. It is not currently possible to give an exact numerical value of the allowed strain, but from analogy with the effects of growth sector boundaries (Table XXXII) which are known to be harmful, we can suggest that strains of order 10^{-5} could produce significant effects. Certainly strains of this order affect R_1 [Bye and Cosier (1979) and Toyo (1975)]. Toyo (1975) also shows an effect on temperature coefficient. Thus further evidence exists that only Z -zone material should be used.

Similarly, as stated earlier, twinned material is not acceptable (Toyo, 1975).

G. The selection of suitable material

On the basis of the evidence given or cited here, we can draw up a specification for quartz which should give high yields of devices to technically high specifications with the minimum effort and waste. The same specification also allows the most economic production of devices to low technical specifications. The important points are as follows.

(a) An infrared $Q > 1.8$ million. (An even higher Q might be needed if a device $Q > 2$ million were required.)

(b) A dislocation density $< 80f^2$ (where the resonant frequency f is in MHz and the density is in cm^{-2}). The occurrence of etch tunnels (see Sec. VI.A) may impose a much lower limit to dislocation densities in high-frequency devices (fundamental mode devices at frequencies over 16 MHz or other devices with wafers $< 100 \mu\text{m}$ thick). For such devices densities of a few tens per cm^2 may be needed.

(c) Only Z -zone material to be used in the active region of a device and bulk lattice strains to be less than 10^{-5} .

(d) A lithium content of less than 1 ppm relative to silicon.

(e) No large inclusions in the bulk of the quartz. Here *large* is about the minimum device dimension.

(f) Ability to withstand a 50°C thermal shock (imposed by heating a boule in water at 70°C and, immediately after removal, plunging it into water at 20°C) is also a useful guide. See Brice (1984).

To enforce these specifications we need acceptance tests. The most important of these is the Q test discussed in Sec. VII.A. To avoid having to test an excessive number of samples I above suggest quoting a minimum Q about 0.2 million larger than that suggested by (a). Doing this permits a very small test sample, three to six specimens, measured in the regions which will be the active parts of the device should be adequate. Readers with statistical interest should note that the sampling situation is unusual: we have a good estimate of how the standard deviation of the population should vary with the mean Q value. This considerably reduces the sample size needed for any desired degree of confidence.

Once a small sample Q test is done, every boule must be examined visually for twins and pronounced seed veils. This inspection should also result in the discovery of any boules with large inclusions. The material manufacturer's quality control should eliminate crystals with obvious external defects (suggesting twins), large inclusions, or heavy veiling, but any batch may contain a few percent of boules which could give trouble.

Batches given a Q test and visually inspected should be satisfactory for most purposes, but cannot be guaranteed to reach the desired dislocation density, strain, level, and purity specifications. Thus it is recommended that in critical applications these quantities be measured directly. Testing for purity is most easily done with a solid-source mass spectrometer but other methods are possible. The purities of all the boules in a batch should be similar; thus small-sample testing is usually safe. As noted above, a small sample subjected to topographic measurements (using also the rocking-curve data) should give a safe estimate of the strain. However, dislocation densities (N_D) in a batch do vary significantly. The distribution of $\log N_D$ is roughly Gaussian, so that knowing the spread of Q values and the relation between Q and N_D discussed earlier allows us to estimate the expected spread of N_D values. For a batch mean Q of two million, the calculated and measured standard deviations of $\log N_D$ are about 0.3, i.e., equivalent to factor of 2 deviations.

When the samples are being visually inspected, it is not terribly laborious to do a thermal shock test on a 100% test basis. This should destroy only bad crystals. A 50°C shock seems a reasonable level for small crystals. The breaking strain involved with a particular shock can be calculated from the theory given by Timoshenko and Goodier (1951) and Carslaw and Jaeger (1959). If α is the mean expansion coefficient, the strain associated with a shock ΔT is of order $\pi\alpha\Delta T$ and variation with the size of the boule should be negligible if the boules are quenched in a water bath.

Details of specifications, sampling procedures, and test methods need to be agreed upon with the supplier of the quartz.

VIII. CONCLUSIONS

Quartz resonators are remarkable devices, offering at their best unparalleled stability and reproducibility.

While most of the physics of device design and performance is well understood, there are some gaps in our quantitative understanding. In particular, we can relate measurable material properties to the electrical quality factor and to device yield in only a qualitative manner.

The main topic of this paper has been the effects of using less-than-ideal crystals (i.e., ones which can be obtained in large quantities) to fabricate devices. Attention has been concentrated on platelike devices using shear mode vibrations but the same general conclusions can be applied to other resonators or indeed to other devices made from quartz.¹⁶

The defects found in quartz include twins, inclusions, dislocations, and impurities of which the most important is hydrogen. The presence of twins makes any boule unsuitable for use. The presence of inclusions leads to dislocation formation, and high dislocation densities degrade device performance either directly or by facilitating hydrogen incorporation during growth. Hydrogen (probably as hydroxyl ions) can degrade device performance directly (low device Q), but more usually it is the weakening of the quartz which causes problems which are both economic (low yields, large spreads of properties, etc.) and technical (drive-level-dependent effects, poor aging, etc.). Lithium and sodium can degrade device properties, because they migrate easily. Other impurities affect radiation hardness. On a statistical basis all impurity concentrations and dislocation densities rise with the hydrogen content—i.e., they increase as the infrared Q falls. For a Q below about 1.8 million, decreasing the Q tends to have understandable catastrophic effects on performance and yield. Thus for both technical and economic reasons the most important factor in a specification is that the infrared Q exceed 1.8 million. Because of the spread of Q in a batch, a 1.8 million minimum level probably implies a batch mean Q of 2 million or more. This level would in any case be desirable, because it allows only a small sample to be tested. In some applications it may also be worthwhile specifying a maximum dislocation density (which might in critical cases be less than 10^2 cm^{-2}). Similarly, in critical cases a maximum level of some impurities might need to be specified (e.g., < 1 ppm lithium, < 0.5 ppm aluminum). The specification should also allow for the rejection of twinned boules and ones with high inclusion contents.

Armed with our current understanding of device theory, process technology, and the relevant materials science, we can already mass produce resonators which give day-to-day stabilities of about 5 ppb in favorable situations, and this figure could be reduced. Special devices can be made at present in small numbers which in com-

¹⁶Within the Philips Concern we have shown that the materials specifications given in Sec. VII.G are necessary and sufficient for material to be used in surface wave and optical components.

mercially available oscillators give day-to-day stabilities of 0.1 ppb.

It is not possible to predict the future accurately, but current laboratory results suggest that improvements by at least a factor of 10 are possible in the professional market. Crystals for consumer use are only a little less stable (≈ 10 ppb on a day-to-day basis) than the ones used at the lower end of the professional market. However, they tend to have less favorable temperature dependences, so that their performance in inexpensive systems is appreciably worse. However, improvements are possible and will be implemented if demanded, so that if a popular application is found we can expect that inexpensive devices will be produced with properties similar to the ones now used in professional equipment.

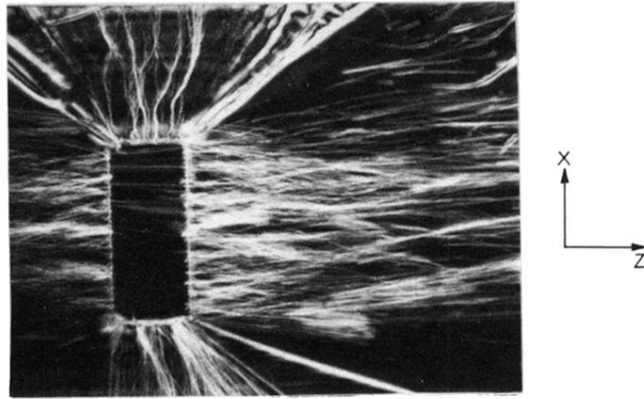
ACKNOWLEDGMENTS

This paper is one product of a very fruitful collaboration with Dr. E. D. Fletcher (Philips, Redhill), Mr. D. J. Grevink (Philips, Eindhoven), Mr. W. Koelewijn (Philips, Doetinchem), and Mr. J. Dowsett (Cathodeon Crystals, Linton, U.K.). Many of the illustrative data are taken from unpublished work by colleagues in various parts of the Philips Concern. Some of these are acknowledged in figure captions and tables. Many manufacturers of quartz crystals cooperated by supplying quartz to non-standard specifications and in providing information. Dr. J. Asahara (Toyo), Dr. D. R. Kinloch (Sawyer), and Dr. R. W. T. Rabbetts (STC) were particularly helpful.

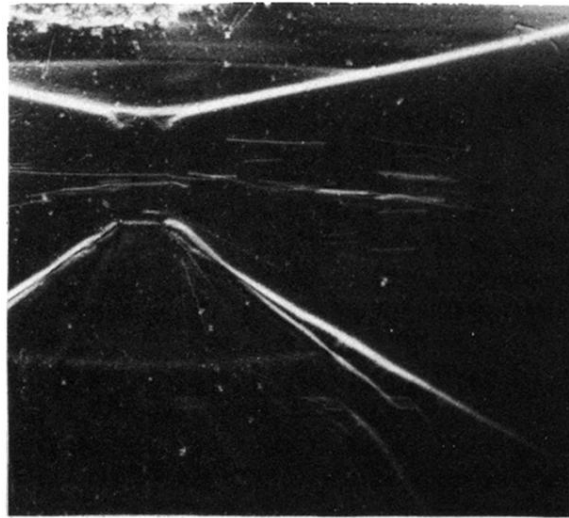
REFERENCES

- Ackermann, R. J., and C. A. Sorrell, 1974, *J. Appl. Crystallogr.* **7**, 461.
- Anderson, T. L., R. E. Newnham, L. E. Cross, and J. W. Laughner, 1976, *Phys. Status. Solidi A* **37**, 235.
- Asahara, J., E. Yazaki, K. Takazawa, and K. Kita, 1975, *Proc. Ann. Symp. Freq. Contr.* **29**, 211.
- Asanuma, N., and J. Asahara, 1980, *Proc. Ann. Symp. Freq. Contr.* **34**, 120.
- Ballato, A., 1977, in *Physical Acoustics*, edited by W. P. Mason (Academic, New York), Chap. 5.
- Ballato, A., 1978, *IEEE Trans. Sonics Ultrason.* **SU-25**, 107.
- Ballato, A., 1979a, *IEEE Trans. Sonics Ultrason.* **SU-26**, 299.
- Ballato, A., 1979b, *IEEE Trans. Sonics Ultrason.* **SU-26**, 186.
- Ballato, A., E. P. EerNisse, and T. J. Lukaszeh, 1977, *Proc. Ann. Symp. Freq. Contr.* **31**, 8.
- Ballato, A., T. J. Lukaszeh, and G. J. Iafrate, 1982, *Ferroelectrics* **43**, 25.
- Ballman, A. A., and R. A. Laudise, 1983, in *The Art and Science of Growing Crystals*, edited by J. J. Gillman (Wiley, New York), Chap. 13.
- Bechmann, R., 1958, *Phys. Rev.* **110**, 1060.
- Bechmann, R., A. Ballato, and T. J. Lukaszeh, 1962, *Proc. IRE* **50**, 1812.
- Bennett, R. E., 1960, *Quartz Resonator Handbook: Manufacturing Guide for AT Type Units* (Comptometer Corp., Niles, Illinois, for the Department of the Army).
- Besson, R. J., J. M. Groslander, and F. L. Walls, 1982, *Ferroelectrics* **43**, 57.
- Bond, W. L., 1976, *Crystal Technology* (Wiley, New York), Chap. 4.
- Bond, W. L., and J. A. Kusters, 1977, *Proc. Ann. Symp. Freq. Contr.* **31**, 153.
- Bottom, V. E., 1972, *J. Appl. Phys.* **43**, 1493.
- Bottom, V. E., 1981, *Proc. Ann. Symp. Freq. Contr.* **35**, 3.
- Bottom, V. E., 1982, *Introduction to Quartz Crystal Unit Design* (Van Nostrand, New York).
- Brice, J. C., 1973, *The Growth of Crystals from Liquids* (North-Holland, Amsterdam).
- Brice, J. C., 1975, *J. Cryst. Growth* **28**, 249.
- Brice, J. C., 1977, *Rep. Prog. Phys.* **40**, 567.
- Brice, J. C., 1980, *J. Mater. Sci.* **15**, 161.
- Brice, J. C., 1981, *Phys. Educ.* **16**, 162.
- Brice, J. C., 1984, *Proc. Ann. Symp. Freq. Contr.* (in press).
- Brice, J. C., and A. M. Cole, 1979a, *Proc. Ann. Symp. Freq. Contr.* **32**, 1.
- Brice, J. C., and A. M. Cole, 1979b, *J. Phys. D* **12**, 45.
- Brice, J. C., J. Dowsett, and E. D. Fletcher, 1981, *Proc. Ann. Symp. Freq. Contr.* **34**, 312.
- Brice, J. C., and W. S. Metcalf, 1982, *Philips Tech. Rev.* **40**, 1.
- Brown, R., D. K. Martin, and R. K. Potter, 1926, *Proc. IRE* **14**, 57.
- Cady, W. G., 1922, *Proc. IRE* **10**, 83.
- Clastre, J., C. Pegeot, and P. Y. Leroy, 1978, *Proc. Ann. Symp. Freq. Contr.* **32**, 310.
- Darces, J. F., and H. Merigoux, 1978, *Proc. Ann. Symp. Freq. Contr.* **32**, 304.
- Dodd, D. M., and D. B. Fraser, 1965, *J. Phys. Chem. Sol.* **26**, 673.
- EerNisse, E. P., 1976, *Proc. Ann. Symp. Freq. Contr.* **30**, 3.
- EerNisse, E. P., T. J. Lukaszeh, and A. Ballato, 1978, *IEEE Trans. Sonics Ultrason.* **SU-25**, 132.
- Euler, P., P. Ligor, A. Kahan, and P. Pellegrini, 1978, *Proc. Ann. Symp. Freq. Contr.* **32**, 24.
- Evans, R. C., 1966, *Crystal Chemistry* (Cambridge University Press, Cambridge), p. 187.
- Filler, R. L., J. A. Kosinski, V. J. Rosati, and J. R. Vig, 1984, *Proc. Ann. Symp. Freq. Contr.* (in press).
- Fletcher, E. D., and A. J. Douglas, 1979, *Proc. Ann. Symp. Freq. Contr.* **33**, 346.
- Flickstein, J., and M. Schieber, 1971, *J. Cryst. Growth* **8**, 157.
- Flickstein, J., and M. Schieber, 1974, *J. Cryst. Growth* **24/25**, 603.
- Frischat, G. H., 1970, *J. Am. Ceram. Soc.* **53**, 357.
- Frondel, C., 1962, *The System of Mineralogy* (New York, Wiley), Vol. 3.
- Gerber, J., 1979, *Proc. Ann. Symp. Freq. Contr.* **33**, 569.
- Gray, D. E., 1972, *The American Institute of Physics Handbook* (McGraw-Hill, New York).
- Griggs, D., 1974, *J. Geophys. Res.* **79**, 1655.
- Hafner, E., and R. S. Blewer, 1968, *Proc. IEEE* **56**, 336.
- Hart, M., 1981, *J. Cryst. Growth* **55**, 409.
- Heising, R. A., 1946, *Quartz Crystals For Electrical Circuits* (Van Nostrand, New York); reprinted 1978 (Electronic Industries Association, Washington).
- Holland, R., and E. P. EerNisse, 1969, *Design of Resonant Piezo-electric Devices* (MIT, Cambridge, Mass.).
- Homma, S., and M. Iwata, 1973, *J. Cryst. Growth* **19**, 125.
- Hruska, C. K., 1980, *IEEE Trans. Sonics Ultrason.* **SU-27**, 87.
- Hruska, C. K., 1983, *IEEE Trans. Sonics Ultrason.* **SU-30**, 324.
- IRE, 1949, *Proc. IRE* **37**, 1379.
- Iwasaki, F., and M. Kurashige, 1982, *Ferroelectrics* **43**, 43.

- James, J. A., and R. C. Kell, 1975, in *Crystal Growth*, edited by B. R. Pamplin (Pergamon, Oxford), Chap. 14.
- Kahan, A., 1982 Proc. Ann. Symp. Freq. Contr. **36**, 159.
- Key, P. L., E. D. Kolb, R. A. Laudise, and E. E. Bressnahan, 1974, J. Cryst. Growth **21**, 164.
- Keyes, R. W., and F. W. Blair, 1967, Proc. IEEE **55**, 565.
- King, J. C., 1959, Bell System. Techn. J. **38**, 573.
- Klapper, H., 1972, Phys. Status Solidi A **14**, 99.
- Klapper, H., 1975, Acta Crystallogr. Sect. A **31**, S212.
- Knowles, J. E., 1975, Proc. Ann. Symp. Freq. Contr. **28**, 230.
- Kobayashi, Y., 1978, Proc. Ann. Symp. Freq. Contr. **32**, 317.
- Koga, I., M. Argua, and Y. Yoshinaki, 1958, Phys. Rev. **109**, 1467.
- Kusters, J. A., and J. G. Leach, 1977, Proc. IEEE **65**, 282.
- Lamb, J., and J. Richter, 1966, Proc. R. Soc. London Ser. A **293**, 479.
- Landolt-Bornstein, 1966, *Numerical Data and Functional Relationships in Science and Technology*, New Series Vol. 111/1 (Springer, Berlin).
- Landolt-Bornstein, 1977, *Numerical Data and Functional Relationships in Science and Technology*, New Series Vol. 111/11 (Springer, Berlin).
- Lang, A. R., and V. F. Miuscov, 1967, J. Appl. Phys. **38**, 2477.
- Laudise, R. A., 1970, *The Growth of Single Crystals* (Prentice-Hall, Englewood Cliffs).
- Laudise, R. A., and J. W. Nielsen, 1961, Solid State Phys. **12**, 149.
- Lee, P. C. Y., and Y. K. Yong, 1983, Proc. Ann. Symp. Freq. Contr. **37**, 200.
- Lias, N. C., E. E. Grudenski, E. D. Kolb, and R. A. Laudise, 1973, J. Cryst. Growth **18**, 1.
- Ludanov, A. G., A. A. Fotchenkov, and L. A. Yakovlev, 1976, Akust. Zh. **22**, 612 [Sov. Phys.—Acoust. **22**, 343 (1976)].
- Lushnikov, V. G., and V. E. Khadzhi, 1967, Dok. Akad. Nauk SSSR **172**, 1072 [Sov. Phys.—Dokl. **12**, 116 (1967)].
- Mason, W. P., 1950, in *Piezoelectric Crystals and their Applications to Ultrasonics* (Van Nostrand, New York).
- Mason, W. P., 1951, Bell Syst. Tech. J. **30**, 366.
- McLaren, A. C., 1971, Phys. Status Solidi **4**, 235.
- McSkimin, H. J., P. Andreatch, and R. N. Thurston, 1965, J. Appl. Phys. **36**, 1624.
- Mortley, W. S., 1969, Nature **221**, 359.
- Okano, S., T. Kudama, K. Yamazaki and H. Kotake, 1981, Proc. Ann. Symp. Freq. Contr. **35**, 166.
- Pamplin, B. R., 1980, *Crystal Growth* (Pergamon, Oxford).
- Passaret, M., and A. Regreny, 1974, J. Cryst. Growth **22**, 80.
- Philips, 1982, "Piezoelectric quartz devices," *Philips Data Handbook, Components and Materials* (Philips, Eindhoven), Part 9.
- Ralph, J. E., 1982, J. Phys. E **15**, 722.
- Rosenberger, F., 1979, *Fundamentals of Crystal Growth I* (Springer, Berlin).
- Rudd, D. W., and N. C. Lias, 1967, High Press. Techn. **63**, 32.
- Samsonov, G. V., 1973, *The Oxide Handbook* (IFI/Plenum, New York).
- Sawyer, B., 1976, J. Cryst. Growth **36**, 345.
- Sequin, CH.H., 1971, Solid-State Electron. **14**, 417.
- Shannon, R. D., and C. T. Prewitt, 1969, Acta Crystallogr. Sect. B **25**, 925.
- Shevel'ko, M. M., and L. A. Yakovlev, 1977, Akust. Zh. **23**, 331 [Sov. Phys.—Acoust. **23**, 187 (1977)].
- Sinha, B. K., and H. F. Tiersten, 1978, Proc. Ann. Symp. Freq. Contr. **32**, 150.
- Sinha, B. K., and H. F. Tiersten, 1979, J. Appl. Phys. **50**, 2732.
- Sosin, A., 1973, Proc. Ann. Symp. Freq. Contr. **27**, 136.
- Suchanek, J., 1982, Ferroelectrics **43**, 17.
- Takagi, M., 1974, J. Cryst. Growth **24/25**, 541.
- Thurston, R. N., H. J. McSkimin, and P. Andreatch, 1966, J. Appl. Phys. **37**, 267.
- Tiersten, H. F., 1969, *Linear Piezoelectric Plate Vibrations* (Plenum, New York).
- Touloukian, Y. S., 1967, *Thermophysical Properties of High Temperature Materials* (MacMillan, London).
- Toyo, 1975, Toyo Technical Bulletin C-5.
- Toyo, 1977, Technical Paper 77-10.
- Toyo, 1979, Technical Paper 79-11.
- Toyo, 1980, "Crystal Growth of High Quality Synthetic Quartz," Toyo Technical Paper.
- Vangheluwe, D. C. L., and E. D. Fletcher, 1981, Proc. Ann. Symp. Freq. Contr. **35**, 157.
- Vig, J. R., 1976, IEEE Trans. **PHP-12** 365.
- Ward, R. W., 1984, Proc. Ann. Symp. Freq. Contr. (in press).
- Warner, A. W., D. B. Fraser, and C. D. Stockbridge, 1965, IEEE Trans. Sonics Ultrason. **SU-12**, 52.
- Weast, R. C., 1964, *Handbook of Chemistry and Physics* (Chemical Rubber Company, Cleveland).
- Weil, J. A., 1973, Proc. Ann. Symp. Freq. Contr. **27**, 153.
- White S., 1968, Nature **219**, 1248.
- Wilke, K. T., 1973, *Kristal Zuchtung* (VEB, Berlin).
- Wyekoff, R. W. G., 1960, *Crystal Structures* (Interscience, New York), p. 312.
- Yamashita, S., A. Shinomiya, and H. Kumasaki, 1975, J. Cryst. Growth **30**, 27.
- Young, T. J., D. R. Koehler, and R. A. Adams, 1978, Proc. Ann. Symp. Freq. Contr. **32**, 1978.
- Zelenka, J., and P. C. Y. Lee, 1971, IEEE Trans. Sonics Ultrason. **SU-18**, 79.



(a)



(b)

FIG. 3. X-ray topographs of sections from two crystals. Note in (a) that the dislocations (white lines) originate from the included area around the seed.